The Use of Epidermal Growth Factor Receptor Activity Biosensing to Understand Cancer Gene Network Sensitivity and to Monitor Intratumoural Heterogeneity.

Cheung, Anthony; Cheung, Anthony

Awarding institution:
King's College London

Title: The Use of Epidermal Growth Factor Receptor Activity Biosensing to Understand Cancer Gene Network Sensitivity and to Monitor Intratumoural Heterogeneity.

Author: Anthony Cheung

The Use of Epidermal Growth Factor Receptor Activity Biosensing to Understand Cancer Gene Network Sensitivity and to Monitor Intratumoural Heterogeneity.

A thesis submitted to the King's College London for the degree of Doctor of Philosophy

By

Anthony Cheung

The Richard Dimbleby Laboratory

Division of Cancer Studies and

Randall Division of Cell and Molecular Biophysics

School of Medicine

King's College London

2013

Dedicated to My Wonderful Grandmother

who meant so much to her friends, her families, and me for so many years.

We all love you and miss you dearly.

Acknowledgments

This project received generous funding from Cancer Research UK, Engineering and Physical Science Research Council (EPSRC) and the Comprehensive Cancer Imaging Centre (CCIC), collaborated between University College London and King's College London. I would like to thank every member of the Dimbleby department and Randall Division for their help and support throughout the past few years. The calibre of education, the multidisciplinary teams and the availability of learning resources have greatly impressed me.

Dr Gregory Weitsman has been hugely helpful and I would like to say many many thank-yous for his constant source of guidance and patience. I would also like to thank all the kind people around me for their help - Dr Gilbert Fruhwirth, Dr Rachel Evans, Dr James Monypenny of Pitmilly, Dr Elena Ortiz-Zapater, Dr Fabian Flores-Borja, Dr Oana Coban, Dr Hanna Milewicz, Dr Jody Barbeau, Dr Tai Kiuchi, Dr Melanie Goodison, Mr Adrian Brock, Ms Dora Jonsdottir, Dr. Maria Lioumi, Dr Michel Eisenblatter, Dr Wahyu Wulaningsih, Dr Ruhe Chowdhury and Ms Appitha Arulappu; in addition, Professor Boris Vojnovic, Dr Paul Barber, Dr Mieke Van Hemelrijck, Dr Katherine Lawler, Dr Simon Ameer-Beg and Dr Simon Poland for their help with the microscope and software. I am also grateful to Professor Alethea Tabor, Professor Helen Hailes, Dr Tammy Kalber and Dr Nick Mitchell, who contributed a big part on this project with their supplies on liposome solution.

I especially wish to thank Dr Gargi Patel and future doctor Anjalika Mallick for their moral support, patience with my whining and all the good laughs making the work-hours enjoyable. Love, kisses and gratitude to another unbelievably talented doctor, Sheeba Irshad, who joined this group with me on the same day back in 2010. I wish her well in continuing her project.

Most of all, I would like to give my whole-hearted appreciation to **Professor Tony Ng**, who gave me this career-changing opportunity to join his research group; provided me with countless advice and experience on a variety of cancer research topics with encouraging enthusiasm. Thank you for believing in that little boy I once was (and probably still am) and giving me the opportunity to achieve something special, for myself and my family.

Lastly, I would like to thank my parents, my aunt and my cousins, who give me all the freedom to explore the world and to pursue my own path in the past ten years... but ensuring that there is always a warm home to return to.

SPECIAL ACKNOWLEDGEMENT OF SUPPORT FROM MISS MARIANNE BLAKE

''In April 2010, Miss Marianne Blake ran the London Marathon in a time of 4 hours 24 minutes, despite having breast cancer metastasised to both her brain and liver. As a result of Marianne's determination, friends and family has donated more than £17000, which was used to purchase the genome library for the Dimbleby Laboratories''

http://www.dimblebycancercare.org/news/marianne-blake-a-tribute

Abstract

The epidermal growth factor receptor (EGFR) plays a pivotal role in cellular proliferation, differentiation and migration and is found to be overexpressed in a variety of tumours including the basal-like subtype of breast cancer. Despite decades of basic research in the HER signalling field, and many EGFR-targeted anti-cancer drugs are used clinically, the success rate for these agents is low, particularly in terms of improvement of overall survival. In breast cancer, the clinical response rates vary between clinical studies, ranging from 6-49%, in part, depending on the type of breast cancer, the stage of the disease, and the treatment used. These marginal benefits are mainly due to insufficient patient selection, and potentially also due to an inadequate inhibition of HER signalling and tumour escape via alternate signalling routes (such as HER2/3/4/c-Met).

The first objective of this work was to use an in-house semi-automated protein activity sensing/imaging technique, to interrogate the EGFR-centric subnetwork of proteins, in order to obtain better understanding of molecular factors influencing the therapeutic sensitivity of the EGFR network.

To monitor EGFR activity in cells we use a CrkII-based biosensor (CrkII protein flanking with eGFP and mRFP1), which undergoes conformational changes upon phosphorylation of tyrosine-221 by EGFR and other receptor tyrosine kinase (RTK)s including c-Met and PDGFβR. This changes are detected by fluorescence lifetime

imaging microscopy (FLIM) combined with fluorescence resonance energy transfer (FRET). Using the sensor, we have conducted a high-content FLIM screen utilising a library of short interfering (si)RNA consist of 533 genes interconnected with EGFR directly or indirectly, chosen from the Human Protein Reference Database. Genes that modulate the EGF-induced biosensor conformational changes were identified. Including EGFR, we identified 22 possible targets (4.1% from the siRNA library) and have selected a few for further validation to establish the biological importance of the genes identified as primary hits.

The same biosensor was also transfected using a liposome-based delivery system into murine models of basal-like breast cancer; and demonstrated a significant degree of intratumoural heterogeneity in EGFR activity, as well as the effect of EGFR inhibitors *in situ*.

In the long term, the knowledge obtained in this thesis can potentially be translated to biomarkers that are based on a better understanding of tumour cell sensitivity to EGFR inhibition and may thereby suggest new combination treatments.

Abbreviation

AR	Amphiregulin
BTC	Betacellulin
Cbl	Casitas B-lymphoma
CFP	Cyan fluorescent protein
DEP1	Density-enhanced phosphatase-1
DNA	Deoxyribonucleic acid
dsRNA	Double stranded RNA
ECL	Enhanced Chemiluminescence
eGFP	Enhanced green fluorescent protein
EGF(R)	Epidermal growth factor (receptor)
EPN	Epigen
EPR	Epiregulin
ER	Estrogen receptor
FBS	Fetal Bovine Serum
FLIM	Fluorescence lifetime imaging microscopy
FRET	Forster (or fluorescence) resonance energy transfer
GAP	GTPase-activating protein
GEF	Guanine nucleotide exchange factor
GFP	Green fluorescent protein
Grb-2	Growth factor receptor-bound protein-2
HB-EGF	Heparin binding EGF-like growth factor

HCS	High content screening
HER	Human epidermal growth factor receptor
HGF	Hepatocyte growth factor
HPRD	Human Protein Reference Database
HTS	High throughput screening
JAK	Janus kinase
MAPK	Mitogen-activated protein kinase
miRNA	MicroRNA
mRFP1	Monomeric red fluorescent protein 1
mRNA	Messenger ribonucleic acid
MVB	Multivesicular bodies
NRG1	Neuregulin/Heuregulin 1
NSCLC	Non small cell lung cancer
PBS	Phosphate buffered saline
PCR	Polymerase chain reaction
PEG	polyethylene glycol
PET	Positron emission tomography
PI3k	Phosphatidylinositol-3-kinase
Picchu	Phosphorylation Indicator of Crk Chimeric Unit
PKC	Protein kinase C
PKR	Protein kinase R
PLC	Phospholipase C
PR	Progesterone receptor

PTB	Phosphotyrosine binding domain
PTP	Protein tyrosine phosphatase
RFP	Red fluorescent protein
RISC	RNA-induced silencing complex
RNase-III	Ribonuclease-III
RNA	Ribonucleic acid
RNAi	RNA interference
SDS	Sodium Dodecyl Sulfate
SDS-PAGE	SDS-Polyacrylamide Gel Electrophoresis
SEM	Standard Error of the Mean
SH	Src-homology
shRNA	Short hairpin RNA
siRNA	Small interfering RNA
Sos	Son-of-sevenless
STAT	Signal transducers and activator of transcription
SUV	Standard uptake value
TBS(T)	Tris-buffered saline (Tween-20)
TCSPC	Time-correlated single-photon counting
TGFα	Transforming growth factor-α
TKI	Tyrosine kinase inhibitor
TNBC	Triple negative breast cancer
RTK	Receptor tyrosine kinase
YFP	Yellow fluorescent protein

Table of Contents

Table of Figures

Table of Result Figures

CHAPTER 1: Introduction

1.1 Overview on breast cancer

Despite continuing research and advances in treatment, breast cancer remains the most common female cancer worldwide and the second leading cause of all cancer deaths (Ferlay, Shin et al. 2010; Malvezzi, Arfe et al. 2011). One-in-eight women develop breast cancer at some stage in their lifetime (Hayat, Howlader et al. 2007). Each year in the United Kingdom, over 47,000 women are diagnosed with breast cancer and the incidence rates are increasing slowly (Malvezzi, Arfe et al. 2011). With the improved medical management of patients, survival rates in England are high; with 83.3% of women diagnosed with breast cancer survive for five years (Statistics 2013). In 2010, women breast cancer caused 1031 deaths in the under-50 age group reported in England and Wales, while 9259 deaths was reported for the over-50 age group. Breast cancer is much less common among men (10290 deaths (99.4%) in women comparing to 62 deaths (0.6%) in men in 2010 (Statistics 2011)), but often has a very high mortality rate due to late detection.

Development of breast malignancy is strongly associated with certain risks such as age, genetic predisposition, hormonal and lifestyle factors. Breast cancer is staged by tumour sizes, local metastases to lymph nodes and distant metastases beyond the breast area (Cooper, Meng et al. 2011). Early breast cancers are treated primarily with surgery followed by radiotherapy. Adjuvant treatments such as hormone therapy (e.g. Tamoxifen), cytototoxic chemotherapy (e.g. Anthracycline), or molecularly targeted treatments (e.g. Trastuzumab) are often prescribed to avoid recurrence from micrometastases (Duffy, O'Donovan et al. 2011).

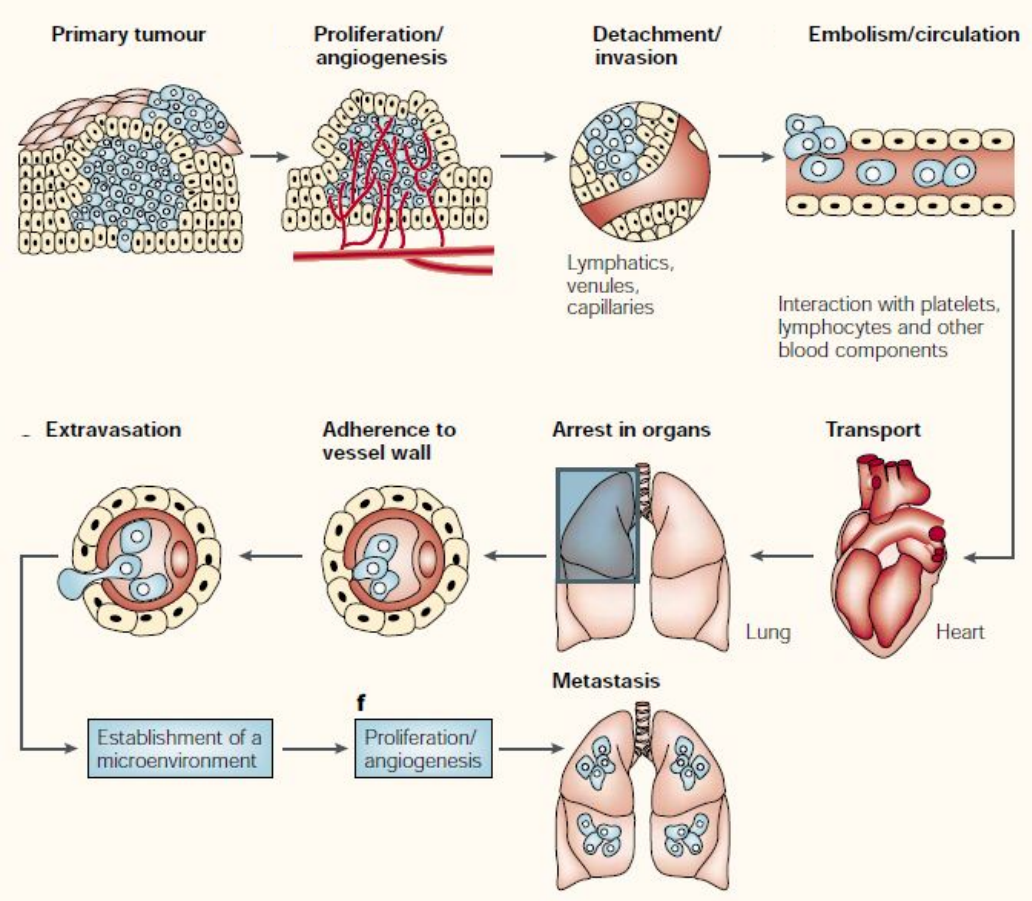

Figure 1: Metastasis formation.

Cellular transformation allows tumour growth and angiogenesis, follows by cell migration through the lymphatic channels or blood capillaries. Most circulating tumour cells are rapidly destroyed, but some of them survived and become trapped in the capillary beds of distant organs, such as lungs or liver. Extravasation followed by tumour proliferation within the organ parenchyma completes the metastatic process. To continue growing, the micrometastasis must develop a vascular network and evade destruction by host defences. The cells can then invade blood vessels, enter the circulation and produce additional metastases.

Modified from Fidler, I. J. (2003). Nat Rev Cancer 3(6): 453-458.

The genetic changes of a single or a small number of cells allow uncontrollable growth and proliferation leading to tumour formation, followed by angiogenesis and metastasis via the lymphatic system or the bloodstream to distant organs (**as illustrated in Figure 1**)

Metastatic breast cancer is the most advanced stage of breast cancer where cancer cells have spread past the breast and axillary (underarm) lymph nodes to other areas of the body, where they continue to grow and proliferate. The majority of cancer-related deaths are due to the growth of secondary metastatic tumours (Fidler 2003; Hunter, Crawford et al. 2008; Cooper, Meng et al. 2011). Tumour cells may also spread into the bloodstream without being detected in the lymphatic system. The most common region is the bone followed by the lung, and less frequently the liver and brain (Kang, Siegel et al. 2003; Minn, Gupta et al. 2005; Minn, Kang et al. 2005). Advanced/metastatic breast cancer is linked to a significant decrease in five-year survival (approximately 20%) compared with localised forms of the disease (Hayat, Howlader et al. 2007).

In order to gain new insights into the pathological evidences behind different stages of breast cancer and to improve survival rates, it is important to identify the gene expression signature and molecular mechanisms that contribute to the development of the disease (van de Vijver, He et al. 2002).

1.2 Basal-like breast cancer

Breast cancer is traditionally divided into three major subtypes by its histopathological features based on the expression of hormone-receptors (estrogen receptor (ER) and progesterone receptor (PR)), human epidermal growth factor receptor 2 (HER2) and grading with Ki67 staining, a nuclear marker of cell proliferation (Cheang, Chia et al. 2009). The subtypes are ER-PR positive luminal (luminal A - low proliferation; luminal B – high proliferation), HER2 amplified and triple-negative breast cancer (TNBC) with the absence of ER, PR, and HER2 (Cooper, Meng et al. 2011; Bertucci, Finetti et al. 2012).

The introduction of molecular classification of breast cancer subtypes based on gene expression profiles and biomarker studies have yielded new prognostic and therapeutic information to achieve more favourable clinical outcomes (Corkery, Crown et al. 2009). In 2000, five molecular subtypes of breast cancer were recognised based on the gene expression patterns. The subtypes included normal-like, HER2-amplified, luminal-A (low proliferation rate), luminal-B (high proliferation rate) and basal-like breast cancer (Perou, Sorlie et al. 2000).

In addition to the gene expression differences between these subtypes; according to the breast cancer genomic analysis performed by Molecular Taxonomy of Breast Cancer International Consortium (METABRIC) which has produced a novel molecular classification of breast cancer population into 10 subgroups based on the

integrated analysis of copy number and gene expression in a discovery and validation set of 997 and 995 primary breast tumours, respectively, with long-term clinical follow-up. The basal-like tumours were found to be associated specifically to a chromosomal deletion event (on chromosome 5) which may account for changes involving cell cycle, DNA damage repair and apoptosis (Curtis, Shah et al. 2012).

These molecular features are strongly related to cancer development and progression. (Kao, Salari et al. 2009; Vuoriluoto, Haugen et al. 2011). Due to the absence of identified targets for therapies, basal subtype has a less favourable prognosis than the others, particularly luminal-A subtype, which has the highest survival rates. Basal subtypes are usually high-graded tumours, with more than 75% being grade III (Bertucci, Finetti et al. 2012). They are also associated with aggressive phenotype characterised by high cell proliferation, relatively younger patient age, high probability of early relapse and high risk of deaths after relapse (Hudis and Gianni 2011; Ishikawa, Horiguchi et al. 2011; Toft and Cryns 2011).

Basal subtypes account for about 15-20% of all breast cancer and they are often triple-negative for ER, PR, and HER2 (Irshad, Ellis et al. 2011). These characteristics represent a major challenge to the survivorship care for the patients. The frequent triple-negativity of basal-like breast cancers does not render them candidate to hormonal and anti-HER2 therapies (Bertucci, Finetti et al. 2012). However, many basal subtypes overexpress epidermal growth factor receptor (EGFR) and intermediate filament cytokeratins 5/6 (CK5/6) (Nielsen, Hsu et al. 2004). Some

triple-negative basal-like breast cancers are also negative for both basal CK5/6 and EGFR, and will not respond to endocrine therapy or any available targeted agents (Reis-Filho, Milanezi et al. 2006). Given that EGFR is frequently (up to 57%) overexpressed in basal-like breast cancers (Nielsen, Hsu et al. 2004; Irshad, Ellis et al. 2011), a subset of breast cancer patients might demonstrate benefits from therapeutic approaches designed to target EGFR overexpression.

1.3 EGFR signalling

EGFR (a.k.a. ErbB1 or HER1) is a 170kDa transmembrane glycoprotein that straddles the cell membrane. It was first discovered on the cell membrane of fibroblast in 1975; thereafter, it became the most thoroughly studied receptor among all the known receptor tyrosine kinases (RTKs).

EGFR belongs to the HER family of RTK, namely HER1/EGFR, HER2/*neu*, HER3 and HER4, all have frequently been found to be overexpressed in epithelial tumours. They share the typical RTK molecular architecture, with a ligand-binding extracellular domain, a transmembrane helix, juxtamembrane regulatory regions, a cytoplasmic tyrosine kinase domain and a carboxy-terminal tail (Inamura, Ninomiya et al. 2010).

All receptors of the HER family have a highly conserved intracellular tyrosine kinase domain, although HER3 contains substitutions of critical amino acids in this kinase domain and therefore lacks of kinase activity; while the extracellular domains are less conserved among the four receptors, suggesting that they have different specificities in ligand binding. In addition, there are no known growth factors that bind to HER2 but HER2 is the preferred dimerisation partner for the other activated HER receptors (Normanno, De Luca et al. 2006; Lemmon and Schlessinger 2010).

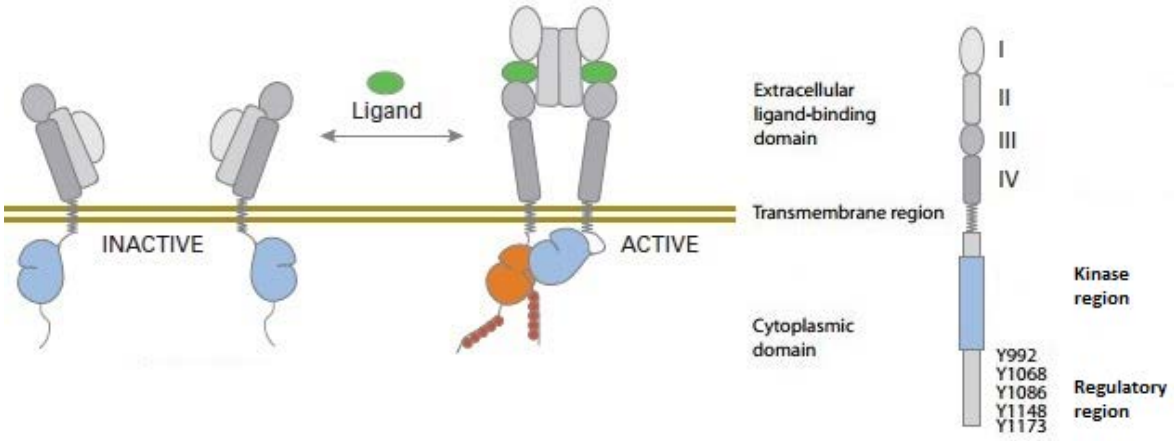

Figure 2: Ligand induced conformational changes in the EGFR ectodomain.

Upon ligand binding, the rotation of domains I/II above the axis of domain II/III junction activates tethered EGFR ectodomain into active EGFR dimers.

Modified from Kumar, A., E. T. Petri, et al. (2008) J Clin Oncol 26(10): 1742-1751.

The extracellular domain of EGFR is comprised of four domains (I–IV). The unliganded monomer is held in closed conformation by an intra-molecular tether formed by loops in cysteine-rich domains I and III. The many cysteine residues form 22 disulfide bonds (Pedersen, Meltorn et al. 2001). When specific ligand binds to the cell surface extracellular domain of EGFR, the intra-molecular tether is broken and the receptor is opened into an extended conformation which interacts back-to-back with another monomer (**as illustrated in Figure 2**). This promotes receptor homo- or hetero-dimerisation and phosphorylation on the tyrosine residues in the intracellular portion of the receptor (Roskoski 2004; Kumar, Petri et al. 2008). Domains I and III of HER2 interact directly with one another and this stabilise the

extended configuration of HER2 extracellular region. This close proximity of domain I and III explains the absence of natural ligands for HER2 (Ferguson 2008).

Ligand-induced EGFR dimerisation is thought to be the key stimulatory step, leading to transactivation of downstream kinase targets and initiation of signalling cascades. There are eight known EGF agonists: EGF, transforming growth factor α (TGFα), amphiregulin (AR), betacellulin (BTC), epigen (EPN), epiregulin (EPR), heparin binding EGF-like growth factor (HB-EGF) and neuregulin 2-β (Ferguson 2008; Henriksen, Grandal et al. 2013). Furthermore, a 140kDa mutated version of EGFR was found in 1988, referred to as EGFRvIII. This mutation lacked the ligand binding domain but demonstrated constant activation without any ligand binding, and was able to activate downstream signalling cascades. EGFRvIII mutation was found in a subset of patients with breast, gliomas, prostate and ovarian tumours (Pedersen, Meltorn et al. 2001).

The juxtamembrane region, which is between the membrane and the tyrosine kinase domain, plays a role in receptor downregulation and sensitation. Three serine/threonine phosphorylation sites are present in this region: Thr654, Thr669 and Ser671. It was known that Protein kinase C (PKC) phosphorylates Thr-654 and inhibits the kinase activity as well as ligand binding to EGFR. Phosphorylation of EGFR at Tyr845 in the kinase domain is implicated in stabilizing the activation loop, while Lys721 participates in ATP-binding activity (Pedersen, Meltorn et al. 2001).

1.4 EGFR-targeted therapy

Epidermal Growth Factor Receptor (EGFR) Expression in Various Tumor Types	
Tumor Type	**Tumors Expressing EGFR, %**
Head and neck	80–100
Renal	50–90
Lung	40–80
Breast	14–91
Colon	25–77
Ovarian	35–70
Prostate	39–47
Glioma	40–63
Pancreas	30–50
Bladder	31–48

Table 3: The expression of EGFR in various tumour types.

EGFR expression has been detected to varying degrees in a wide range of solid cancers. Reported values are 14 to 91% for breast carcinomas.

Inamura, K., H. Ninomiya, et al. (2010) Arch Pathol Lab Med 134(1): 66-72.

Clinical interest in the EGFR gene has been heightened with the FDA approval of specific EGFR tyrosine kinase inhibitors (e.g. Gefitinib). EGFR protein overexpression has been reported to occur in 14–91% of breast cancers (**see Table 1**) and a various type of tumours. EGFR gene amplification generally results in increased protein expression (Marquez, Wu et al. 2004; Bhargava, Gerald et al. 2005; Shia, Klimstra et al. 2005; Dacic, Flanagan et al. 2006). EGFR protein overexpression without gene amplification occurred in only 2% in breast carcinomas (Bhargava, Gerald et al. 2005). The data for the relationship between the presence of EGFR gene amplification and responses to EGFR tyrosine kinase inhibitors are still limited. Other mechanisms such as gene mutation and transcriptional or post-transcriptional factors might also have a role in the expression of EGFR protein.

There are a number of approaches designed to target EGFR. Patients might demonstrate benefits from treatment with one of the following agents, either alone, or in combination with standard chemotherapy.

Therapeutic antibody against EGFR

Cetuximab (also known as Erbitux and IMC-C225), is a humanised mouse monoclonal antibody that binds to the receptor with higher affinity than EGF or TGFα, preventing receptor dimerisation (Roskoski 2004). Although Cetuximab is used as monotherapy or in combination with chemotherapeutic agents for some patients with colorectal (Cunningham, Humblet et al. 2004; Saltz, Meropol et al. 2004), head and neck (Baselga, Trigo et al. 2005), and non-small cell lung cancer (Fischer, Griesinger et al. 2012), the response rates were modest (Dancey and Sausville 2003; Roskoski 2004).

For breast cancer, the clinical response rates vary between clinical studies, ranging from 6-49%, in part, depending on the type of breast cancer, the stage of the disease, and the treatment used (Modi, D'Andrea et al. 2006; Dickler, Rugo et al. 2008; Hudis and Gianni 2011). A recent phase II study by Carey et al. reported a poor response (in fewer than 20% of patients) to combination Cetuximab plus Carboplatin among the metastatic TNBC patients (Carey, Rugo et al. 2012). Modi et al. reported a withdrawal of a phase I trial using the combination of chemotherapeutic agents Paclitaxel and Cetuximab, due to the high level of dermatologic toxicity and disappointing efficacy (Modi, D'Andrea et al. 2006).

Small molecule tyrosine kinase inhibitors of EGFR

Most frequently mutated gene coding for the intracytoplasmic tyrosine kinase domain of EGFR occurs from exon 18 to 24. Particularly, 90% of these mutations occur with the deletion in codons 746 to 750 of exon 19 (del746_A750) in the catalytic site and transversion of T to G in codon 858 of exon 21 (L858R) in the activation loop. Both cause conformational change of the tyrosine kinase domain, resulting in constant activation of EGFR without ligand binding (Pao and Miller 2005; Inamura, Ninomiya et al. 2010).

Two examples of the reversible small molecule for EGFR inhibition are Gefitinib (also known as Iressa, or ZD1839) (Baselga 2002; Dancey and Sausville 2003) and Erlotinib (also known as Tarceva, or OSI-774) (Baselga and Hammond 2002). Both tyrosine kinase inhibitors (TKIs) are advanced in clinical development for a broad range of solid tumours. These small molecules competitively inhibit ATP binding to EGFR, thereby hindering the receptor autophosphorylation and kinase activation (Pedersen, Meltorn et al. 2001).

Corkery et al. have demonstrated the combination of Gefitinib with chemotherapy enhanced cell cycle arrest in basal-like breast cancer cell-lines, with reduced phosphorylation of ERK and Akt protein kinases (Corkery, Crown et al. 2009). Gefitinib has also been shown to induce inactive unphosphorylated EGFR/HER2 heterodimers resulting in anti-proliferative effect in EGFR and HER2 expressing breast cancer cell-lines (Anido, Matar et al. 2003).

Gefitinib has been used in clinical trials for EGFR-expressing cancers, such as head and neck and non–small-cell lung cancer (NSCLC) (Cappuzzo, Gregorc et al. 2003; Cohen, Rosen et al. 2003; Fukuoka, Yano et al. 2003). Mok et al. have demonstrated the use of Gefitinib for the treatment of pulmonary adenocarcinoma was significantly more effective in patients harbouring EGFR mutation that those that were negative for the mutation (Mok, Wu et al. 2009).

It has been reported that mutations in the tyrosine kinase domain of EGFR were associated with Gefitinib sensitivity in patients with NSCLC and the tumours were highly responsive to EGFR tyrosine kinase inhibitors (Lynch, Bell et al. 2004; Paez, Janne et al. 2004; Inoue, Kobayashi et al. 2009; Sugio, Uramoto et al. 2009). Such mutations were also associated with sensitivity of Erlotinib, with over 80% of patients marked clinical improvement on Gefitinib or Erlotinib have been shown to contain mutations in the exons encoding the EGFR tyrosine kinase domain (Pao, Miller et al. 2004; Pao and Miller 2005).

Gefitinib has been used in combination with Trastuzumab as a potential combination for treating Trastuzumab-resistant HER2 positive metastatic breast cancer (Somlo, Martel et al. 2012). Gefitinib has demonstrated a median duration of clinical benefit of 10.9 months (Dennison, Jacobs et al. 2007). Erlotinib has been used in a number of clinical studies for EGFR-expressing cancers (Perez-Soler, Chachoua et al. 2004; Dickler, Rugo et al. 2008; Britten, Finn et al. 2009), but also demonstrated limited clinical benefits. It was shown that patients with positive

EGFR expression have a higher response rate (11.3%) compared to patients with negative EGFR expression (3.8%), with overall survival rate of 6 months (Shepherd, Rodrigues Pereira et al. 2005).

Other strategies

Other antibody entities against EGFR were investigated for anti-tumour activity, such as Panitumumab (ABX-EGF) (Yang, Jia et al. 2001; Peeters, Price et al. 2010) or bispecific antibody MDX-447 which targets EGFR as well as the high affinity Fc receptor (FcγRI) and enhances immune-based killing by antibody-dependent cellular cytotoxicity (ADCC) (Pedersen, Meltorn et al. 2001; Fury, Lipton et al. 2008). Alternative tyrosine kinase inhibitors (both reversible and irreversible inhibitors) are in preclinical or early clinical development, which have different specificities for HER family members (Baselga and Hammond 2002).

Casamassimi et al. reported a gene therapy strategy using antisense oligonucleotides to decrease EGFR ligands and EGFR expression *in vitro*, and therefore inhibit the proliferation of tumour cells (Casamassimi, De Luca et al. 2000). The antisense oligonucleotides targets cells by hybridising to complimentary messenger RNA (mRNA) sequences, preventing of the translation of the mRNA and inhibit gene expression (Wagner 1994).

In summary, despite strong preclinical data, only a subset of cancer patients shows clinical response to these therapies. In addition, patients who demonstrated initial response can become refractory to continuous treatment. However, it is likely that the true prognostic significance of the EGFR has been underestimated as the published studies only assessed total cellular EGFR levels, rather than the activated form of the receptor, and were not standardised with regard to patient selection or assay methods.

This lack of clinical efficacy of EGFR-targeted treatments indicated the use of a compensatory mechanism by cancer cells for bypassing the therapeutic effect of EGFR-specific agents. The inadequate inhibition of EGFR pathway and its downstream signalling components or alternate signalling escape routes, such as HER2/3/4, c-Met and fibroblast growth factor receptor (FGFR) (Sharpe, Pearson et al. 2011), might also contribute to the resistance to the therapeutic treatments.

In order to select the most beneficial treatments and combinatorial strategies, it is important to obtain a better understanding of what molecular factors, or biomarkers, which may influence the therapeutic sensitivity of the EGFR network and their roles in cancer development.

1.5 EGFR and signalling proteins

Ligand binding to EGFR on the cell surface induced EGFR auto-dimerisation and cross-interaction with other HER partners. A transient signalling complex composed of adaptor and effector proteins was then assembled. The dissociation of this complex led to a cascade of signalling events, followed by gene activation and cellular response.

Tyrosine kinases are enzymes that transfer the ϒ phosphate of ATP to specific tyrosine residues (Baselga and Hammond 2002). There are several tyrosine phosphorylation sites that are phosphorylated upon ligand binding: Tyr992, Tyr1068, Tyr1086, Tyr1148 and Tyr1173, which serve as binding sites for signalling molecules to transmit signals for the phosphorylation and activation of downstream targets (**as illustrated in Figure 2**) (Roskoski 2004). After auto-phosphorylation or trans-phosphorylation by other kinases such as Src and Jak-2, the intracellular tyrosine residues of EGFR can serve as docking sites for various transducers and adaptor proteins that contain Src-homology-2 (SH2) or phospho-tyrosine-binding (PTB) domains. Signalling molecules that associate directly with EGFR included adaptor proteins Grb-2, Nck, Shc, Crk and Dok-R, as well as phosphatases PTB-1B and SHP-1, and tyrosine kinase Abl; while Cbl, Pl3K-C2b and Stat5b are thought to have an indirect association with EGFR (Olayioye, Neve et al. 2000; Jorissen, Walker et al. 2003).

Downstream targets often include serine/threonine kinases such as the mitogen-activated protein kinase (Ras/Raf/MAPK) protein kinase cascade, which is recruited via Grb-2 and Son-of-sevenless (Sos), and involved in cell proliferation; the phosphatidylinositol-3-kinase (Pl3K)-activated Akt pathway, which induces cell motility and invasion; and the Janus kinase (JAK)-dependent signal transducers and activator of transcription (STAT) pathway which enhances cell migration (**see Figure 3**) (Jorissen, Walker et al. 2003; Andl, Mizushima et al. 2004).

Genetic dysregulation in any of the individual molecules involved in EGFR signalling might promote development of cancers. For example, KRas is a small G protein that acts as a transducer linking ligand-dependent receptor activation to downstream of EGFR. The gain-of-function mutations in KRas codons 12 and 13 can lead to constitutive signalling and activation of MAPK- and PI3K-dependent pathways (Bardelli and Siena 2010). It has been showed that patients with mutant KRAS codon 12 or 13 in metastatic colorectal cancer were unlikely to benefit from EGFR-targeted therapy (Van Cutsem, Kohne et al. 2009; Peeters, Douillard et al. 2013). However the effects of somatic mutations are often manifested through the complexity of the interaction between proteins expressed by aberrant genes; the aberrant function at a protein level must therefore be assessed even in the presence of these genetic changes. Protein complex formation, conformational change and post-translational modifications such as receptor phosphorylation can also alter the functional outputs of the cell (e.g. migration and proliferation) (Citri and Yarden 2006).

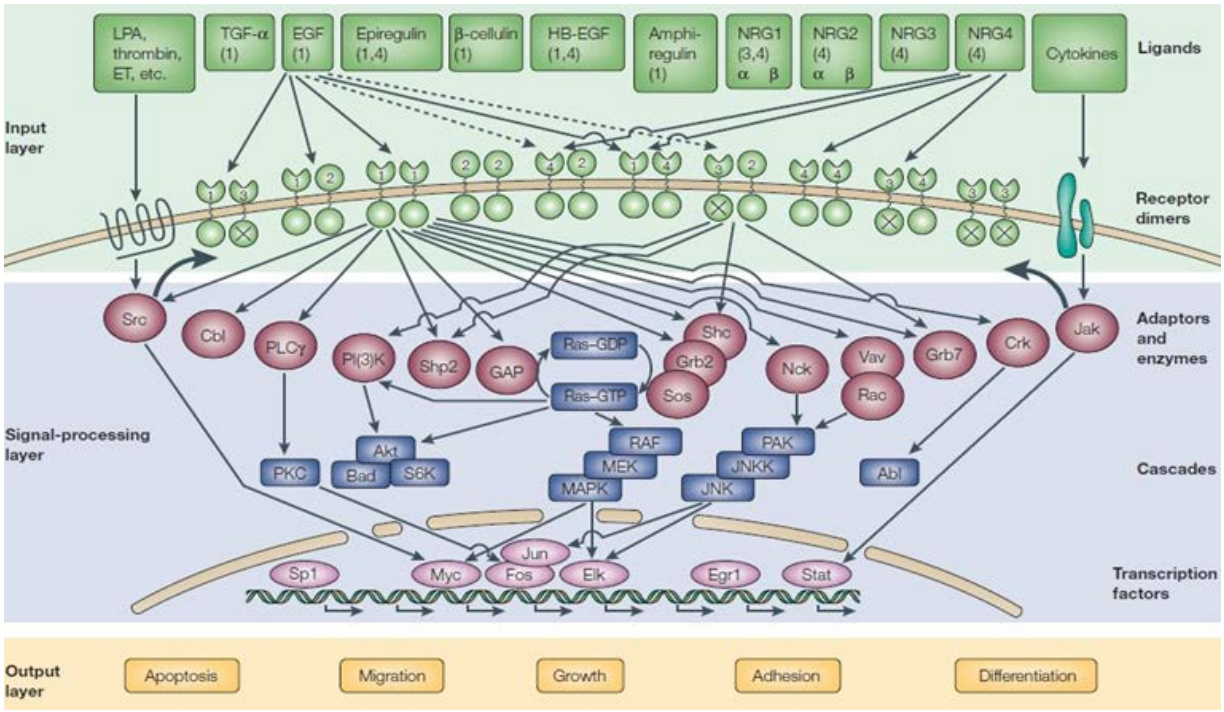

Figure 4: Schematic illustration of the EGFR and downstream signalling pathways.

There is a rich cross-talk among the HER family. In the input layer, specific ligand such as EGF binds to EGFR leading to receptor dimerisation (homo- or hetero-dimers with other HER receptor members). Binding of ligand to the EGFR ectodomain triggers the interaction with a number of protein kinases such as adaptor protein (Shc, Grb2 and Crk), Ras-specific GTPase-activating protein (GAP), PI3K, second-messenger-generating enzyme PLCγ, and ubiquitin ligase (Cbl). Activation of these protein kinases initiates signalling cascades and translates in the nucleus into distinct transcriptional programmes in regulation of a host of cellular function, including cell growth, migration and survival.

Modified from Roskoski, R., Jr. (2004) Biochem Biophys Res Commun 319(1): 1-11

1.6 Negative regulatory mechanisms for EGFR signalling

A transient signalling complex composed of adaptor proteins and effectors is assembled following the activation of EGFR. For the regulation of signal output, this process is carefully coordinated by negative regulatory mechanisms by promoting receptor internalization, intracellular trafficking, and subsequent ubiquitination and degradation of both ligand and receptor molecules (Henriksen, Grandal et al. 2013).

During signal termination, activated receptor-ligand complexes are endocytosed in clathrin-coated pits and ubiquitin ligase Casitas B-lymphoma (Cbl) is recruited to target the receptors for ubiquitination (Marmor and Yarden 2004). Early endosomes merge and mature to form multivesicular bodies (MVB) and late endosomes.

Two distinct processes have been identified to determine the fate of the internalised receptors (Sorkin and Goh 2009) (**see Figure 4**). First process involves the continuous association with Cbl, which interacts with Tyr1045 on EGFR and targets the receptors to the lysosomal compartment and catalyzes ubiquitination and intracellular degradation. The second process occurs with the uncoupling of Cbl in early endosome; EGFR may remain associated with EGF in the early endosomes and retain the capacity to continue signalling, or it may release the EGF into the acidic environment and the ligand will get degraded by the accumulated hydrolytic enzymes. Receptors are instead recycled to the plasma membrane (Lenferink,

Pinkas-Kramarski et al. 1998; Marmor and Yarden 2004). It has been shown that endocytosis of the receptor is required for pro-angiogenic vascular endothelial growth factor receptor (VEGFR) to activate ERK1/2 in endothelial cells (Gourlaouen, Welti et al. 2013).

EGFR activity can also be downregulated by tyrosine specific phosphatases, such as density-enhanced phosphatase-1 (DEP1), which dephosphorylates EGFR and decreases the signal outputs (Yarden 2001; Dikic and Giordano 2003; Bublil, Pines et al. 2010; Lemmon and Schlessinger 2010; Avraham and Yarden 2011). Other EGFR phosphatases include PTP1B (Haj, Verveer et al. 2002; Reynolds, Tischer et al. 2003) and the protein tyrosine phosphatase TCPTP (Mattila, Pellinen et al. 2005).

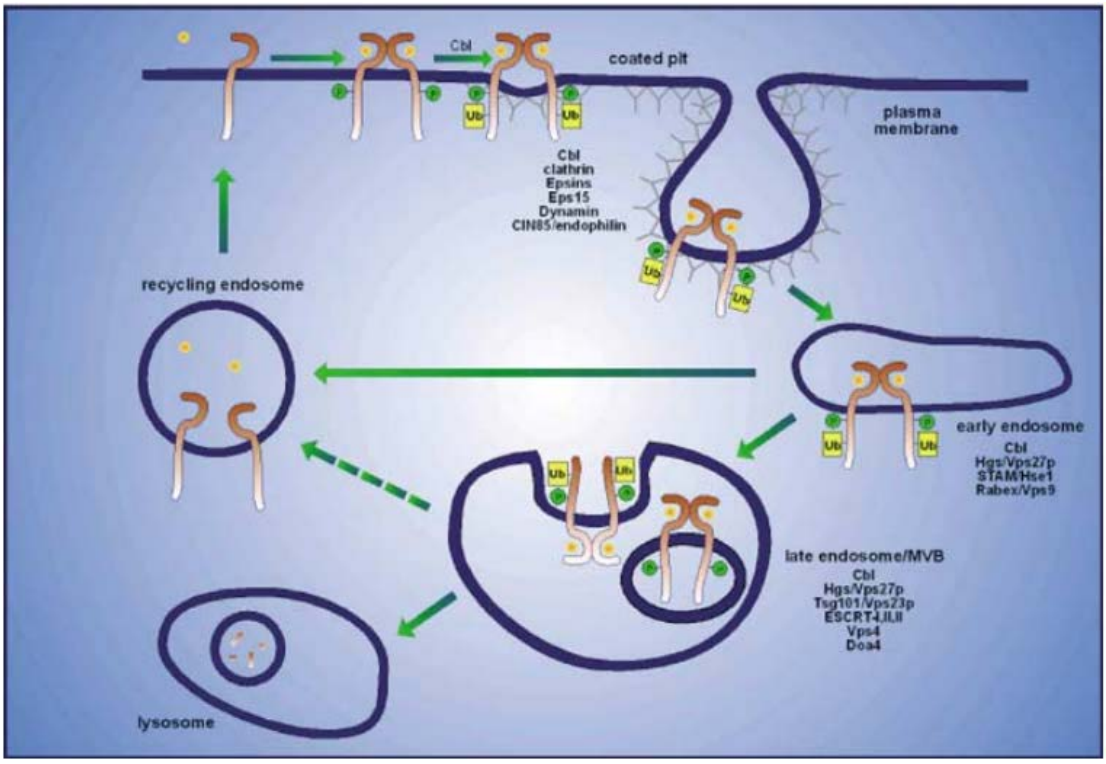

Figure 5: HER family receptor internalisation and intracellular trafficking.

Ligand binding induced phosphorylation of EGFR and recruitment of Cbl, which targets the receptors for ubiquitination. Receptors are then sorted into clathrin-coated pits by a multiprotein complex that includes coat adaptors such as Epsin and Eps15. Fission of clathrin-coated vesicles is mediated by GTPase dynamin. Ligand is released when the internal pH of early endosomes decreases. With the accumulation of hydrolytic enzymes that degrade the ligands, receptors are allowed to travel back to the surface. Trafficking from early to late endosomes/MVB is dependent on its continued association with Cbl. MVB sorting is regulated through recognition of ubiquitylated cargo by Hgs/Vps27p, Tsg101/Vps23p and other components of ESCRT complexes. Fusion of the MVB with the lysosome results in degradation of the contents of the internal vesicles.

Modified from Marmor, M. D. and Y. Yarden (2004) 23(11): 2057-2070

1.7 c-MET tyrosine kinase receptor

In recent years, oncology therapeutics development has started to pay more attentions on the role of c-MET and its relationship with EGFR. (Karamouzis, Konstantinopoulos et al. 2009)

Similar to EGFR, c-MET is also a proto-oncogene tyrosine kinase receptor, which drives the malignant progression of several types of cancer such as colorectal cancer, head and neck squamous cell cancer (Knowles, Stabile et al. 2009; Liska, Chen et al. 2011) and HER2 overexpressing breast cancer (Shattuck, Miller et al. 2008), whereas the c-MET signalling pathway activity was up-regulated after targeted inhibition of the HER family of tyrosine kinase receptor.

In tumour, several cytokines such as TGFβ induce transcriptional upregulation of both c-MET and its ligand hepatocyte growth factor (HGF). Besides transcriptional control, the levels of c-MET expression at the cell surface can also be finely regulated by proteolytic cleavage and ubiquitin-mediated degradation. Functionally, a direct shedding of the c-Met ectodomain from tumour cells following proteolytic cleavage may provide an alternate mechanism for producing circulating c-Met and was shown to be an indicator of malignant potential and overall tumour burden (Athauda, Giubellino et al. 2006).

Constitutive activation of c-MET is depended on two mechanisms: ligand-dependent activation due to elevated level of HGF, or ligand-independent activation due to gain-of-function mutation of c-MET, overexpression and loss of negative regulators, which promotes c-MET dimerisation and auto-phosphorylation on tyrosine residues Tyr1234 and Tyr1235 at the catalytic kinase domain. This leads to further phosphorylation on the docking tyrosines for the recruitment of scaffolding transducer and adaptor proteins, leading to activation of downstream oncogenic effectors such as ERK protein kinase and PI3K lipid kinase. In addition, phosphorylation of Tyr1003 promotes internalization and degradation of c-MET through Cbl interaction (Trusolino, Bertotti et al. 2010).

The major c-MET-regulated pathways are very similar to those of the EGFR network which control cell cycle progression, cell growth and survival. It has been suggested potential crosstalk between c-MET with EGFR, although it is not fully understood how they mediate each other (Guo, Villen et al. 2008). c-MET may render cancer cells resistant to EGFR-targeted therapies, possibly via its hetero-dimerisation with EGFR or by re-stimulating important signalling pathways (Mueller, Hunter et al. 2008; Mueller, Yang et al. 2010; Dulak, Gubish et al. 2011; Liska, Chen et al. 2011).

Clinical benefit of targeting the c-Met receptor has been reported in many types of human solid tumours, including non-small-cell lung cancer (NSCLC), breast, prostate, liver and renal cancers, for which the degree of c-Met expression correlates with poor patient prognosis (Nakajima, Sawada et al. 1999; Gherardi, Birchmeier et al.

2012). Notably in patients with NSCLC, combining EGFR (Erlotinib) and c-MET (MetMAb) inhibitors increased progression-free survival in patients with high levels of c-MET expression compared with the group receiving Erlotinib alone (Gherardi, Birchmeier et al. 2012). Preclinically, similar synergy has been seen between Foretinib (c-MET TKI) and Lapatinib (EGFR-HER2 dual TKI) (Liu, Shi et al. 2011). Either targeting alone or in combination with an anti-EGFR therapeutic, c-MET is undoubtedly a valuable target for cancer therapy.

1.8 Molecular imaging: FRET-FLIM technology

The interactions between the vast number of membrane receptors and secondary messenger molecules are the keys to determine cell behaviour. Methods of cancer prognosis estimation rely on clinical data, anatomical staging and histopathological features based on existing markers. Molecular fluorescence imaging of the spatial-temporal expression/interaction of protein complexes *in situ* allows us to obtain better understanding of the cancer proteome that might translate to potential clinical benefits.

Fluorescence is a result of a three-stage process. Each electronic energy state has several energy levels as represented by the closely packed horizontal lines shown in **Figure 5**. The resting state of a fluorophore is in the lowest level of energy, ground state (S0). Photon energy, supplied by an external source, such as a laser, can be absorbed by the fluorophore, creating an excited electronic singlet state (S1). The excited state exists for a finite time followed by relaxation into the lowest level of the excited singlet state. The average length of time spent in the higher electronic state is termed as fluorescence lifetime (tau or τ).

Energy is then dissipated either via radiative or non-radiative processes. Radiative transfer results in the fluorescent emission and the excited molecule will return to the ground state; whilst Förster (or fluorescence) resonance energy transfer (FRET) is a non-radiative, dipole-dipole coupling process where energy from a donor

fluorophore molecule is transferred to an acceptor fluorophore that are presented in close proximity (less than 10 nm). The first step of a FRET process is the absorption of photon energy by the donor molecule, which is then excited from ground state to the excited electronic singlet state. When the excited donor is in close proximity with an acceptor fluorophore, the energy is transferred from the excited donor to the acceptor, which generate an excited acceptor that in turn release the energy by emitting photon and returning to its ground state.

FRET efficiency is inversely proportional to the sixth power of the molecular distance between donor and acceptor and the fluorescence life-time of the interacting fraction by:

$$\eta_{fret} = \left(\frac{R_0^{\,6}}{R_0^{\,6} + r^6} \right) = 1 - \frac{\tau_{fret}}{\tau_d}$$

Where R_0 is the Förster radius (at which 50% of the excitation energy is transferred to the acceptor); r is the separation between the fluorophores; τ_{fret} is the lifetime of the interacting fraction and τ_d is the lifetime of the donor in the absence of acceptor. FRET can only be observed when the two fluorophores are within nanometre range, indicating interaction between the molecules (Peter and Ameer-Beg 2004).

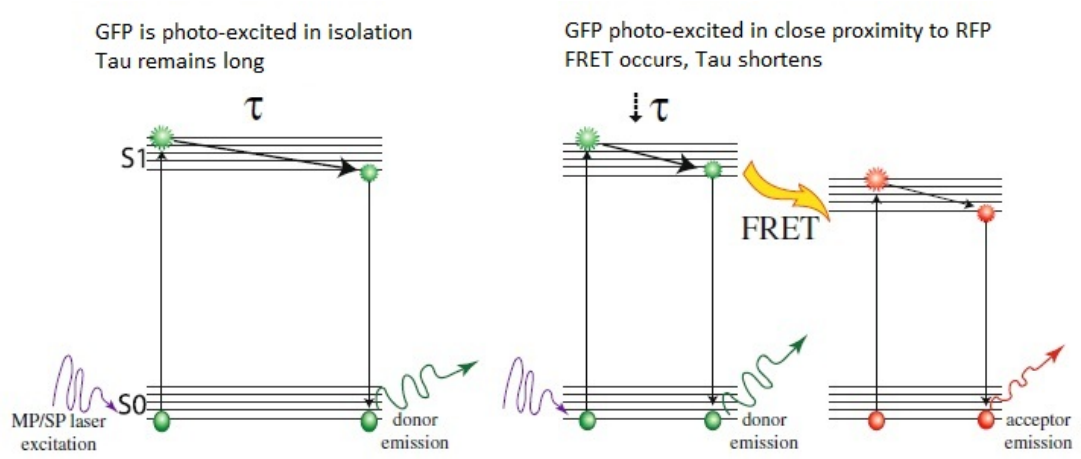

Figure 6: Jablonski representation of FRET

FRET is the process of energy transfer from an excited donor fluorophore to an acceptor fluorophore in close proximity. (Left) The donor fluorophore, GFP, is excited in isolation. (Right) When donor and acceptor (GFP and RFP) are in close proximity, energy is transferred from the excited donor fluorophore to the acceptor, generating an excited acceptor that in turn can emit fluorescence by reverting to its ground state.

Modified from Kelleher, M. T., G. Fruhwirth, et al. (2009) Target Oncol 4(3): 235-252.

A few methods have been established to detect FRET, for example acceptor photobleaching, fluorescence polarization imaging and fluorescence lifetime imaging microscopy (FLIM) (Beutler, Makrogianneli et al. 2008). FLIM is a state-of-the-art technique that provides a high resolution and sensitive readout of the fluorescence signals, which avoids potential artefacts, such as the destructive of fluorophore signal and low signal-to-noise ratio that can be inherent using other FRET measurement techniques (Peter and Ameer-Beg 2004). FRET-FLIM studies have received increased attention in recent years driven by the availability of FRET-based molecular probes, advanced quantitative analysis methodologies and the increasingly sophisticated microscopy and computer systems (Festy, Ameer-Beg et al. 2007).

The two principal ways to measure fluorescence lifetime are frequency domain and time domain-based methods. This project measured fluorescence lifetime by using time-correlated single-photon counting (TCSPC) method, where an optical pulse of light from the laser source is used to excite the donor fluorophore (Beutler, Makrogianneli et al. 2008). The decay of the intensity of fluorescence signal is then measured as a function of time (**see Figure 6 for an illustration of the system set up**). Once the FLIM data acquisition has been completed, the fluorescence lifetime is then calculated by fitting exponential fluorescence decay models to the measured intensities. The main advantage of using donor FLIM is that this method is independent of fluorophore concentration and donor-acceptor stoichiometry. It also does not require corrections for donor emission crosstalk in the acceptor

channel, direct acceptor excitation at the donor excitation wavelength, nor knowledge of detection-correction (which involves quantum yields, donor and acceptor detection efficiencies and varies with conditions such as pH and optical alignments) (Bastiaens and Squire 1999; Wouters, Verveer et al. 2001; Festy, Ameer-Beg et al. 2007).

The development of TCSPC FLIM combined with two-photon microscopical techniques has proven to be a powerful technology to study three-dimensionally sectioned cellular data. These advantages result from the use of intense near-infrared light to induce non-linear absorption in the probe fluorophore, whereby photobleaching and photodamage are greatly reduced. The intensity dependence of the non-linear absorption confines the excitation to a small volume in focal plane of the imaging lens and allows very high spatial (angstrom) and temporal (nanosecond) resolution for studying molecular interactions between two proteins. These techniques are used to study the functional and structural aspects of inter/intra-molecular mechanisms such as protein-protein interaction, conformational change and in applications such as high-throughput screening (Peter and Ameer-Beg 2004; Wallrabe and Periasamy 2005; Piston and Kremers 2007).

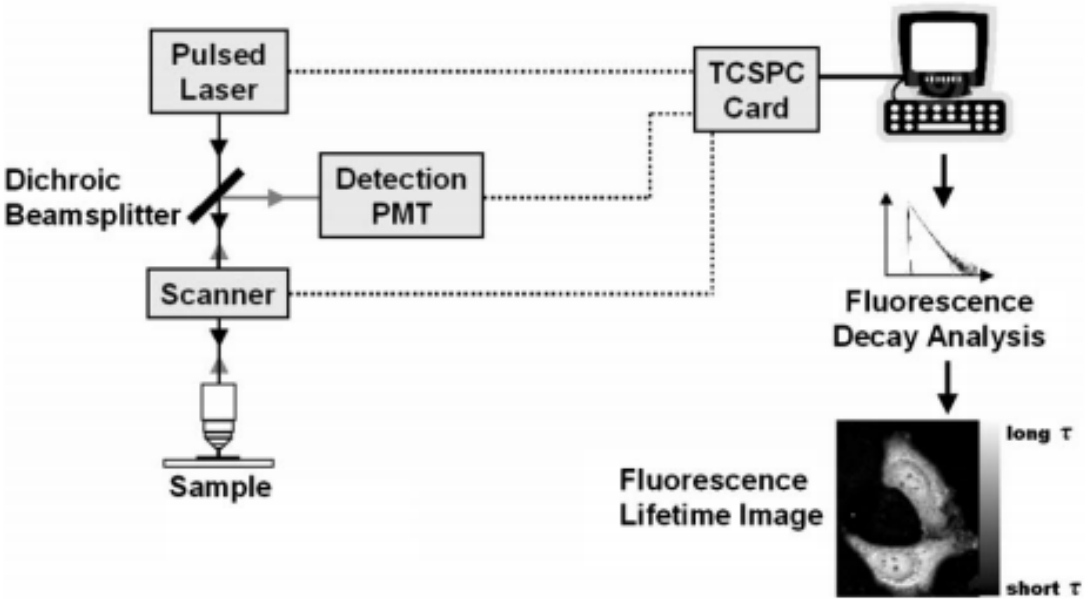

Figure 7: A schematic of a TCSPC FLIM set up.

A pulsed laser (black arrows) excites the sample at a MHz repetition rate, and the fluorescence (grey arrows) is detected with a photomultiplier detection system. The electronic signals for the detected photons and for the beam scan synchronisation (…) are fed into a TCSPC card in a PC. The time delay between the laser excitation pulse and the arrival of the fluorescence photon is measured many times, and a histogram of photon arrival times is built up in each pixel, which represents the fluorescence decay in each pixel. Subsequent data analysis allows the extraction of fluorescence lifetime from the decays, and its visualisation in a FLIM map.

Modified from Festy, F., S. M. Ameer-Beg, et al. (2007) Mol Biosyst 3(6): 381-391.

1.9 CrkII-based probe for monitoring EGFR activity in cells

PHOGEMON Project

In 2001, Phosphorylation and Guanine-nucleotide Exchange Monitoring Project (PHOGEMON Project) was established in Miki Matsuda's laboratory in Kyoto University, aimed to develop monitors for kinases and G proteins, the two key players of the signal transduction, using molecular fluorescence imaging. (http://www.lif.kyoto-u.ac.jp/labs/fret/e-phogemon/phomane.htm)

Integrated biosensors have been developed in based on intra-molecular FRET where the FRET donor and acceptor are fused in the opposing ends of the same protein molecule, avoiding the complication of variable stoichiometry between inter-molecular FRET pairs. FRET-based biosensor can be used to visualize spatiotemporal changes of protein activity as a consequence of stimulation or drug treatment in live/fixed cells, tissues or the deep tissue measurement in pre-clinical tumour models (Festy, Ameer-Beg et al. 2007).

eGFP/mRFP1 biosensor pair

CFP/YFP pair has been widely used in ratiometric FRET experiments (Kurokawa, Mochizuki et al. 2001; Yoshizaki, Ohba et al. 2003; Yoshizaki, Aoki et al. 2006; Aoki, Kiyokawa et al. 2008; Nishioka, Frohman et al. 2010; Kunida, Matsuda et al. 2012), but it carries a number of disadvantages such as substantial emission cross-talk due to spectral overlap (**see Figure 7**) and CFP alone may exhibit bi-exponential decay

kinetics, making quantitative analysis of an interacting FRET population difficult (Peter, Ameer-Beg et al. 2005).

The introduction of enhanced GFP (eGFP) and the monomeric variant of DsRed (mRFP1) provided a better suitable pair for donor FRET-FLIM assays, whereas mRFP1 has lower aggregation problems to form oligomers and has little or no green component in its fluorescence emission (Fruhwirth, Fernandes et al. 2011). This solved the problem of emission cross-talk, since eGFP can be excited at a wavelength beyond the excitation spectrum of mRFP1 (**see Figure 7**). In addition, eGFP is a photostable fluorophore that displays mono-exponential fluorescence decay, offering multiple advantages over the currently available CFP/YFP pairs (Peter, Ameer-Beg et al. 2005).

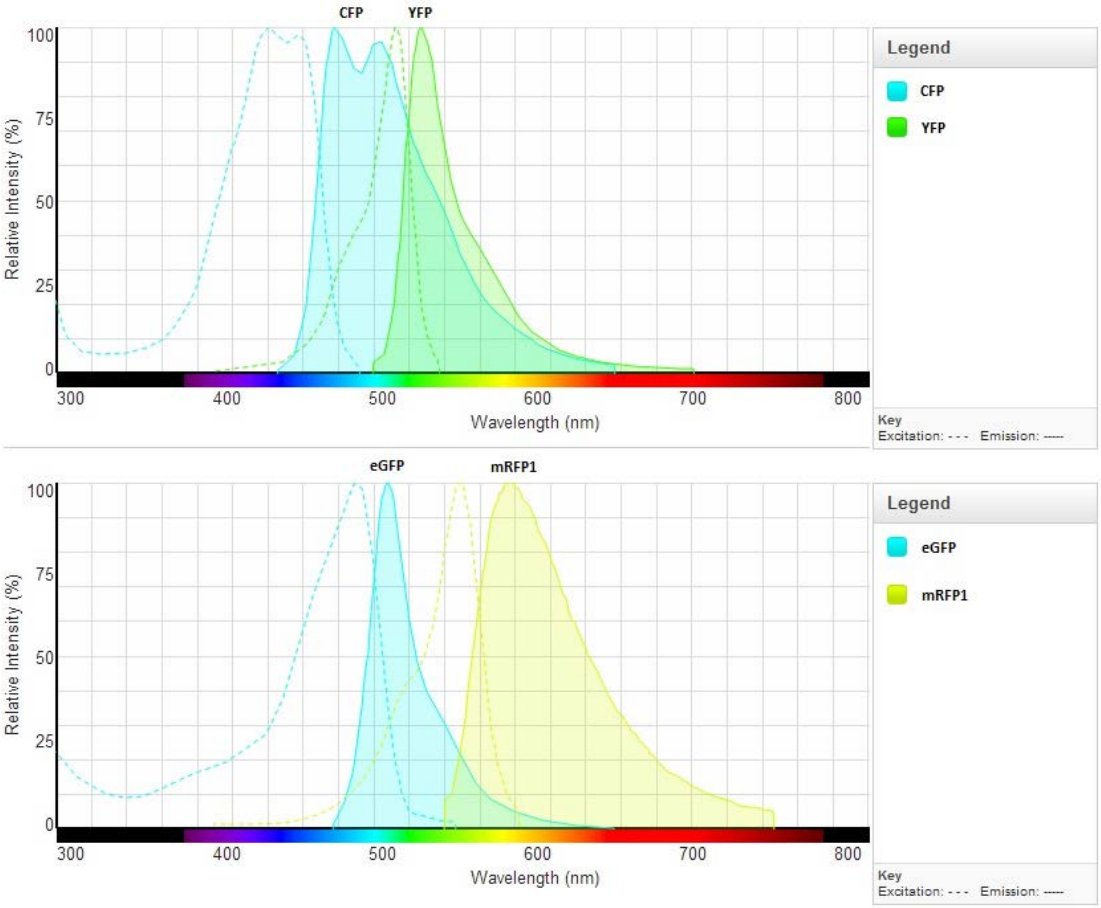

Figure 8: Emission spectra for CFP/YFP and eGFP/mRFP1 fluorophore pairs.

A large area of spectral overlap of cyan (CFP)/yellow (YFP) fluorescent protein pair was shown in the upper panel; compared to the low level of emission cross-talk of the enhanced green (eGFP)/monomeric red (mRFP1) pair in the lower panel. Spectra were created using online software Fluorescence SpectraViewer from Invitrogen.

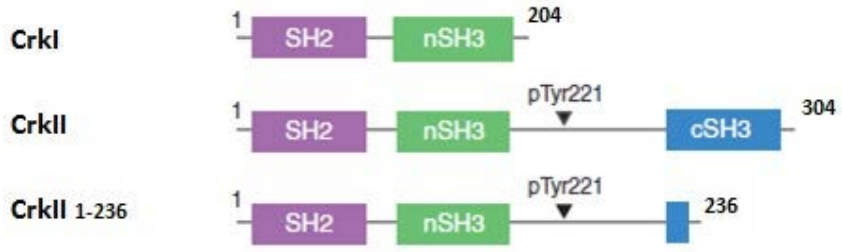

Figure 9: Domain structure of Crk proteins.

Adaptor protein Crk consists of SH2 and SH3 domain. CrkI contains a single SH3 domain while CrkII contains two. Phosphorylation site locates on Tyr221. The construction of Picchu-X sensor (amino acid 1-236) does not affect the phosphorylation of the protein.

Picchu-X biosensor

CrkII belongs to a family of adaptor proteins with Src-homology 2 (SH2) domain which contains a phospho-tyrosine binding site, and Src-homology 3 (SH3) domains connected with flexible peptide linkers that transmits signals from tyrosine kinases. Alternative splicing of the Crk transcript yields two different products, CrkI (SH2-SH3) and CrkII (SH2-SH3-SH3) (**Figure 8**) (Kobashigawa, Sakai et al. 2007).

The primary function of CrkII is to recruit phosphotyrosine-containing proteins (e.g. adaptor proteins paxillin and $p130^{cas}$) and growth factor receptors (e.g. EGFR), through SH2/p-Tyr221 interaction. The output from CrkII depends on the SH3-binding proteins, which recruit cytoplasmic enzymes such as C3G (guanine nucleotide exchange factor (GEF) for Rap 1), Sos (GEF for Ras), protein tyrosine phosphatase 1B (PTP1B) and c-Abl cytoplasmic tyrosine kinase in response to tyrosine kinase activation (Takino, Tamura et al. 2003). Only amino acids 1–236

were used in the construction of Picchu-X sensor. As part of the c-terminal SH3 was lacking, the output signals were reduced with the low affinity to target proteins (Kobashigawa, Sakai et al. 2007); however, the phosphorylation site Tyr221 remained for activity sensing.

Picchu, stands for 'Phosphorylation Indicator of Crk Chimeric Unit', is an example of eGFP/mRFP1 biosensor that has been extensively studied in this project. The use of this probe for reporting EGFR kinase activities in cells have been reported previously (Kurokawa, Mochizuki et al. 2001; Itoh, Kurokawa et al. 2005; Aoki, Kiyokawa et al. 2008). A flaw of the Picchu probe is that the diffusion of the probe is too fast to delineate the sub-cellular localization of tyrosine kinase activity. To overcome this flaw, Picchu was subcloned with carboxy-terminal CAAX tail of k-Ras as a plasma membrane-anchoring motif, generating the Picchu-X biosensor (Kurokawa, Mochizuki et al. 2001).

Picchu-X consists of YFP, spacer (Leu-Asp), CrkII protein (amino acids 1–236), spacer (Gly-Arg), CFP, spacer (Gly-Arg-Ser-Arg), and CAAX tail of K-Ras (amino acids 169–188). The new Picchu-X sensor was modified by the excision of the sensor module between YFP and CFP and insertion between the mRFP1 and eGFP. The resultant eGFP- and mRFP1-tagged Picchu-X constructs retain the original design of the CFP-YFP tagged version (Itoh, Kurokawa et al. 2005). Phosphorylation of CrkII protein occurs after activation of EGFR; hence FRET measurement of Picchu-X provides a sensitive means for monitoring EGFR activity.

Upon activation of tyrosine kinases, CrkII undergoes a change in intra-molecular folding, which promotes binding of SH2 domain to phosphorylated Tyr221 and brings eGFP in close proximity to mRFP1, thereby triggering fluorescence energy transfer (**as illustrated in Figure 9**) (Kurokawa, Mochizuki et al. 2001; Itoh, Kurokawa et al. 2005; Aoki, Kiyokawa et al. 2008).

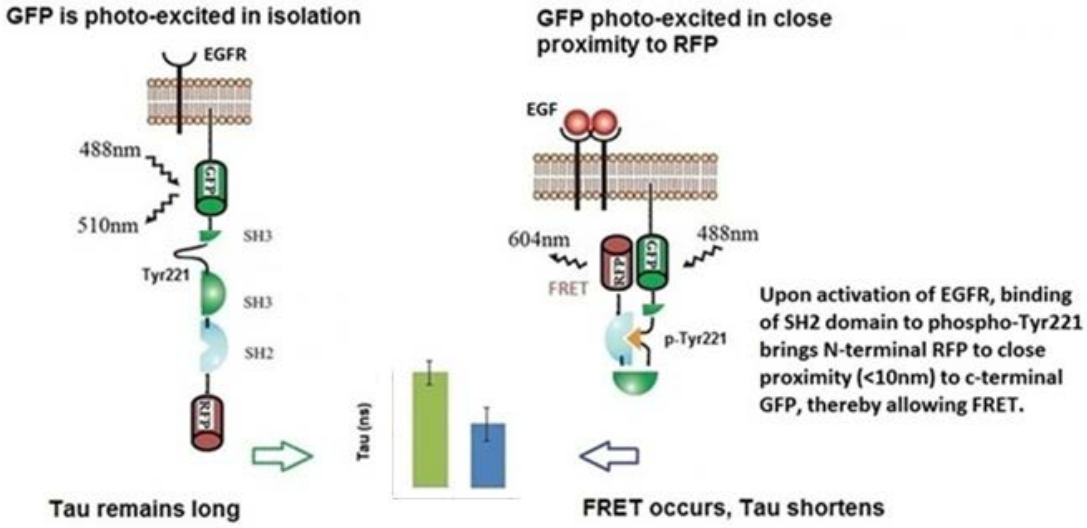

Figure 10: Schematic representation of Picchu-X.

Picchu, stands for 'Phosphorylation Indicator of Crk Chimeric Unit', is designed to monitor activity of the CrkII protein. Membrane anchoring domain, CAAX, is expressed at the C-terminal end generating the Picchu-X sensor. Upon stimulation of EGFR, binding of SH2 domain to phosphorylated Tyr221 brings eGFP in close proximity to mRFP1, thereby triggering fluorescence energy transfer.

Modified from Itoh, R. E., K. Kurokawa, et al. (2005) Exp Cell Res 307(1): 142-152.

1.10 Optical imaging for network screen

Constructing a protein interaction network map

The current trend in optical proteomic imaging of fluorescent protein *in situ* provides an excellent tool to understand the detailed molecular mechanism in various stages of cancer progression with better preservation of post-translational protein modifications or protein-protein interactions, especially on the sensitivity of detecting membrane events compared to biochemical extraction of membrane complexes. It is also useful to validate the treatment strategy for individuals with high risk of metastasis and disease relapse by correlating their profiles with multivariate proteomic signatures and using high content drug screens, thus sparing unnecessary and potentially toxic treatments (Kelleher, Fruhwirth et al. 2009). The availability of vast amount of clinical and biological literature databases, together with the technological and bioinformatics advancements in the past decades, protein activity sensing/imaging technique allow us to interrogate large-scale of protein network in order to obtain a better understanding of what molecular factors may influence the therapeutic sensitivity.

Data reported from a variety of experiments (e.g. yeast two-hybrid assays, mass spectrometry, immunohistochemistry, Western blot, coimmunoprecipitation, fluorescence microscopy, proteins chips, microarrays, ChIP-Seq, RNA-Seq) currently available from public datasets can be integrated and mapped into protein-protein interaction networks (interactomes) (Cusick, Yu et al. 2009; Fruhwirth, Fernandes et

al. 2011). These datasets are routinely updated based on collection of new functional and genomic information, to generate comprehensive and up-to-date resource for studying the human proteome.

Human Protein Reference Database

Human Protein Reference Database (HPRD) is a resource of curated proteomic information including protein-protein interactions, post-translational modifications and tissue expression (Keshava Prasad, Goel et al. 2009).

(http://www.hprd.org)

To date, this database has documented 8958 protein-protein interactions based on yeast two-hybrid analysis alone, 8827 interactions were based on *in vitro* and 7163 on *in vivo* experiments. Detection of 2410 interactions was confirmed by all three methods. In this project, HPRD was used to identify sets of ''seed proteins'', specific to metastatic phenotype, and generate interconnected network/subnetwork maps based on first order (direct partners) and second order (partners of partners) from seed proteins (Fruhwirth, Fernandes et al. 2011).

Cytoscape

Comprehensive map would be an invaluable asset for the understanding of biological processes and molecular mechanisms at the systems biology level. Such biomolecular interaction networks can be visualised using online software, Cytoscape, as a tool to filter and interpret selection of relevant subnetworks.

Each protein in the network is annotated as a node and its interactions with other proteins as edges. Another key feature of Cytoscape is its ability to set visual aspects of nodes and edges, such as shape, colour and size, based on attribute values. This data-to-visual attribute mapping allows multiple types of data to be visualised in a single network context (Shannon, Markiel et al. 2003; Cline, Smoot et al. 2007). Following this procedure, a subnetwork associated to EGFR was constructed and can be used to propose new experiments to interrogate the EGFR-centric subnetwork of proteins (**see Figure 10**) (Fruhwirth, Fernandes et al. 2011).

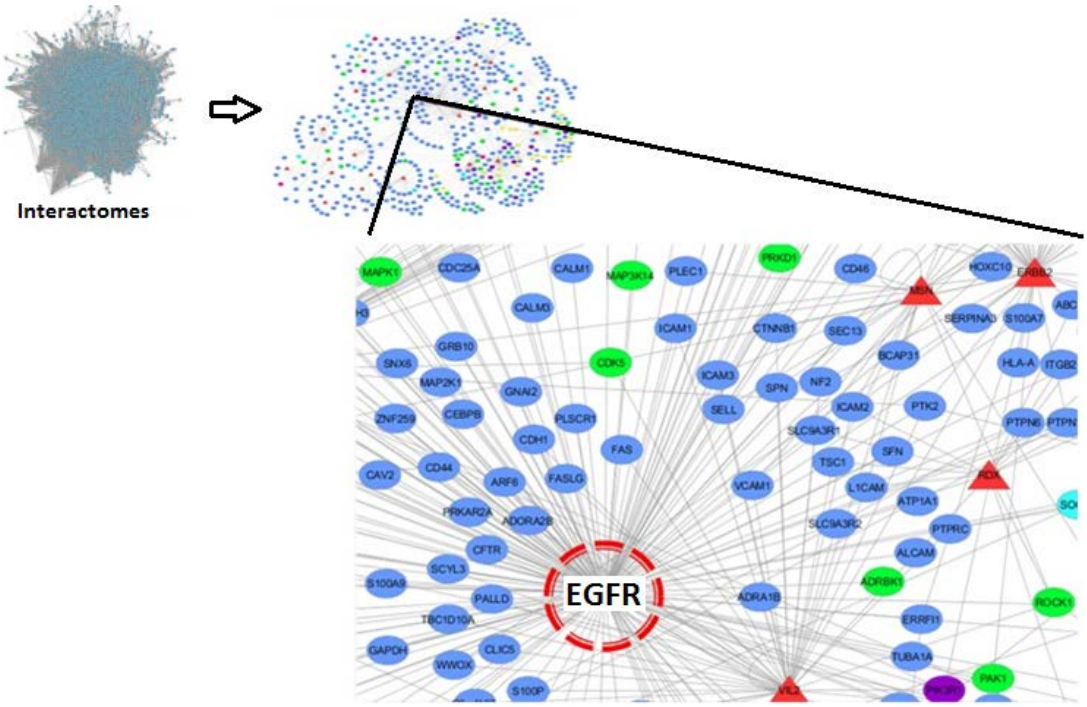

Figure 11: Signalling Network centred EGFR.

Large-scale map of protein-protein interactions (interactomes) was designed using the Human Protein Reference Database. An EGFR-centric subnetwork of proteins based on first and second order of interaction partners from the seed proteins (red triangles) was generated and visualised using the Cytoscape software.

Large-scale high content/high throughput screen

Many researches are now utilising compound libraries for drug screenings or genomic libraries for cellular studies, for which each compound/gene can potentially contribute to the cellular function or disease model. The developments in instrumentation and image analysis have made microscopy applicable to automated high content/high-throughput screening. High content screening (HCS) defined as multiparametric approaches for the simultaneous readout of spatiotemporally resolved context upon application of small molecule drug compounds or small interfering RNAs (siRNAs) at the single-cell level based on fluorescence imaging. In recent years, the term HCS is also applied to cell-based analysis techniques such as flow cytometry and other label-free assays (Gasparri 2009; Liang, Chang et al. 2012).

High throughput screening (HTS) can be defined as the automation of experiments such that large scale repetition becomes feasible, based on robotic microscopy for robust fluorescence intensity readout in combination with high-speed computing systems for quantitative analysis and storage of the data (Gonzalez and Negulescu 1998). Automation is a key to extract multiple parameter information from cells in order to improve productivity and to minimise measurement time, while decreasing the volumes of reagents required for the assays and maintaining the same experimental conditions when examining large number of samples.

HC/HTS approaches are increasingly being exploited in modern drug discovery (Giuliano, Chen et al. 2004), or use to study cellular mechanisms with imaging-based siRNA screen (Krausz 2007; Krausz and Korn 2008; Hutchins, Toyoda et al. 2010; Neumann, Walter et al. 2010). A few automated FRET approaches have been described using FLIM method (Esposito, Dohm et al. 2007; Grecco, Roda-Navarro et al. 2010).

1.11 RNA interference

RNA interference (RNAi) is a natural process of post-transcriptional silencing of individual gene, regulated by either microRNA (miRNA) or small interfering RNA (siRNA) that is homologous to the targeted messenger RNA (mRNA). RNAi has an important role in innate immune response against foreign long double-stranded RNA (dsRNA) from viruses or bacteria (Hannon and Rossi 2004). The enzyme dsRNA-dependent protein kinase R (PKR) is activated on binding to dsRNA and triggers sequence-independent destruction of RNAs. RNAi is also important in directing development as well as controlling gene expression (Hannon 2002).

siRNA is a 21-23 nucleotides dsRNA molecule that mediate RNAi mechanism of gene suppression. Ribonuclease-III (RNase-III) family enzyme, Dicer, cleaves up long dsRNAs in an ATP-dependent manner and delivers these small pieces of siRNA to a protein complex called RNA-induced silencing complex (RISC). Each siRNA is unwound into two single-stranded RNAs, namely the passenger strand and the guide strand. The passenger strand is targeted for degradation, while RISC uses the antisense guide strand of the siRNA to identify and degrade the complementary mRNAs, resulting in gene silencing and decrease in protein expression (Hannon and Rossi 2004; Morris 2005). Similar to siRNA, miRNA of approximately 21 nucleotides has also been identified to interfere with gene expression. However, the transcripts captured by miRNA-incorporated RISC complex are directed into a ribosome-free compartment, named P-body, resulting in translational repression (**see Figure 11**) (Yeung, Bennasser et al. 2005; Kim and Rossi 2007).

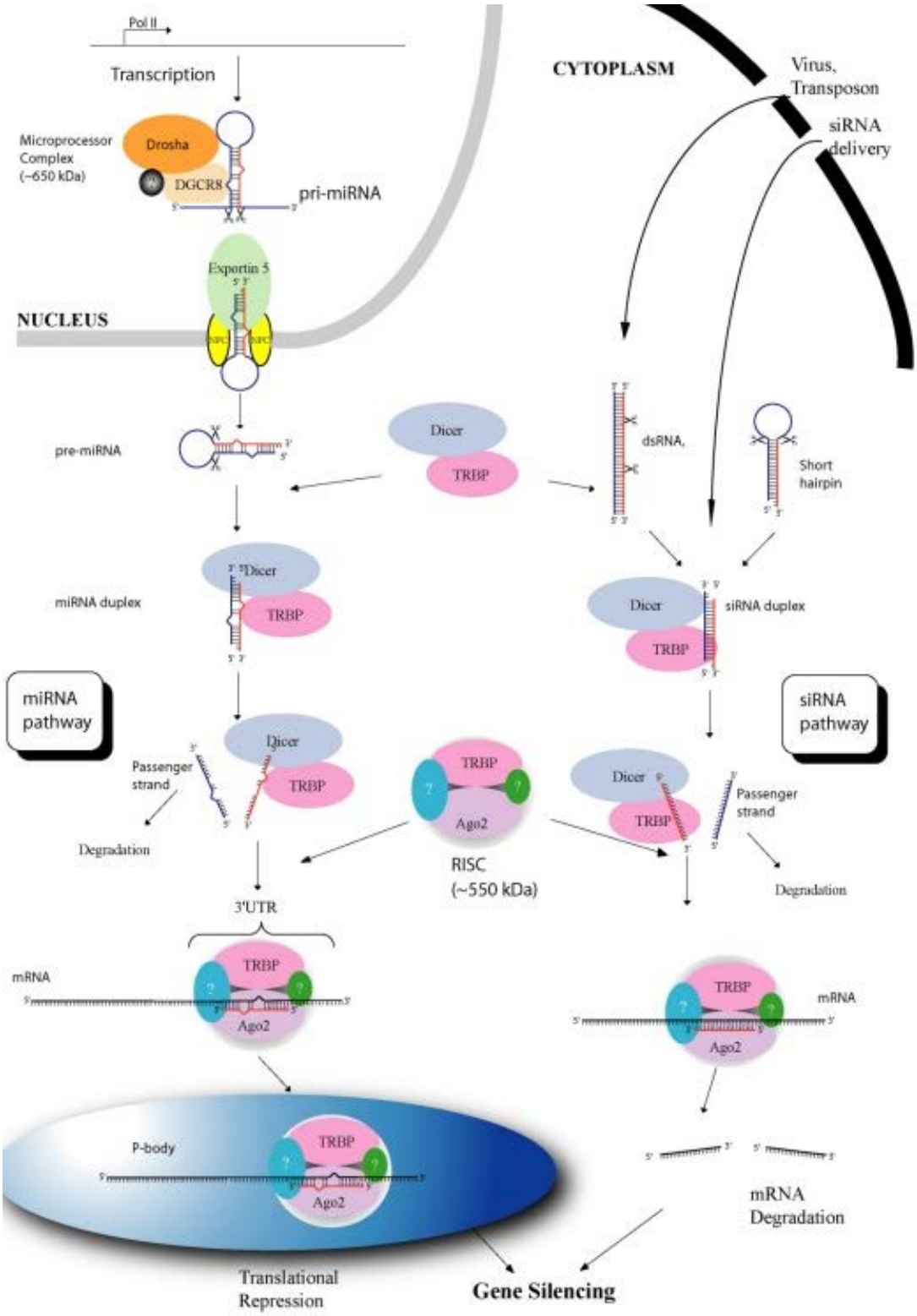
Pol II
Transcription
Microprocessor Complex (~650 kDa)
Drosha
DGCR8
pri-miRNA
Exportin 5
NUCLEUS
CYTOPLASM
Virus, Transposon
siRNA delivery
pre-miRNA
Dicer
TRBP
dsRNA,
Short hairpin
miRNA duplex
siRNA duplex
miRNA pathway
siRNA pathway
Passenger strand
Degradation
Ago2
RISC (~550 kDa)
3'UTR
mRNA
P-body
Translational Repression
mRNA Degradation
Gene Silencing

Figure 12: A model of RNA interference mechanism of the miRNA and siRNA pathways.

miRNAs are derived from pro-miRNAs transcribed by RNA Pol II in the nucleus. After cropping by Microprocessor, the primiRNAs are processed into pre-miRNAs and exported into cytoplasm. Both pre-miRNAs and dsRNA/short hairpins are trimmed by Dicer to generate miRNA and siRNA duplexes, respectively. The guide strand of the duplexes is incorporated into RISC for RNA silencing and the passenger strand is targeted for degradation. mRNAs with perfect complementary to the siRNAs are targeted to degradation, while transcripts captured by miRNA-incorporated complex are directed into the P-body resulting in translational repression.

Modified from Yeung, M. L., Y. Bennasser, et al. (2005) Cell Res 15(11-12): 935-946.

RNAi has now been adopted as a standard methodology for the silencing of gene expression in mammalian cells. The use of chemically synthesised RNA duplexes, consisting of two 21-nucleotides annealed together to form siRNAs, can be introduced into cultured cell to produce effective gene knockdown for the studies of protein functions. Synthetic siRNAs can induce RNAi by circumventing natural defence mechanism against long dsRNA (>30 nucleotides), bypass the dicing step and incorporate into RISC to facilitate the breakdown of homologous mRNA sequences (Elbashir, Harborth et al. 2001). However, the use of synthetic siRNAs are unable to produce stable gene knockdowns, whereas cells that are transfected with siRNAs typically recover from mRNA suppression within seven days or ten rounds of cell division.

Other strategy to interference gene expression is using short hairpin RNAs (shRNAs), which are expressed from vectors such as plasmids, retroviruses or adenoviruses. The main advantage of these vector constructs is that they can be stably transfected and amenable to long term studies. Promoter region in the vectors can ensure hairpin oligonucleotides are constantly expressed and maintain long-term mRNA inhibition (Hannon and Rossi 2004).

RNAi has revolutionised the study of functional definitions for every gene, and is being explored as a therapeutic tool (Dorsett and Tuschl 2004; Hannon and Rossi 2004). Landen et al. reported tumour growth *in vivo* was suppressed (with up to 91% reduction in tumour size when combining chemotherapy agent Paclitaxel) after

systemic delivery of siRNA-containing liposomal nanoparticles, which contained siRNAs targeting the overexpressed tyrosine kinase receptor EphA2 gene in ovarian cancer cell lines (Landen, Chavez-Reyes et al. 2005). RNAi has also been used to specifically target and prevent viral infections by human immunodeficiency virus type-1 (HIV-1) and Hepatitis virus (Yeung, Bennasser et al. 2005).

In this project, a library of siRNA targeting 533 genes encoding for proteins that interact with HER1-4 as seed proteins directly or indirectly, was chosen from the HPRD. This genome library was purchased from Ambion; three different siRNA sequences were available to uniquely silence each of these 533 genes. Combining with our in-house semi-automated FRET-FLIM-based HC/HTS imaging technology, this library allows us to interrogate the EGFR-centric subnetwork of proteins using the RNAi technique.

1.12 Delivery system – liposomal techniques

The other goal for this project was aimed to develop a synthetic nanoparticle delivery system to formulate serum-stable liposomes for *in vivo* delivery of the FRET-based probe to study the dynamics of EGFR activity and its modulation by known EGFR kinase inhibitors. This combination of therapeutics and diagnostics is referred as theragnostics (Lammers, Kiessling et al. 2010).

Several liposomal drug formulations have been approved for clinical applications, such as PEGylated liposomal Doxorubicin and Paclitaxel, for the treatment of solid tumours in patients with breast carcinoma metastases (Noble, Kirpotin et al. 2004; Yezhelyev, Gao et al. 2006) and refractory ovarian cancer (Gordon, Fleagle et al. 2001; Lawrie, Bryant et al. 2013).

Liposomes are very effective delivery carriers due to their physical and chemical structures and their biocompatibilities (Lian and Ho 2001). These artificially prepared small carrier vesicles are made of lipid bilayer composed of natural or synthetic cationic lipids such as phospholipids or cholesterols (Lian and Ho 2001; Kudsiova, Ho et al. 2011). Synthetic vectors for DNA/RNA delivery offers advantages over viral systems in term of their greater nucleic acid packaging capacity, lower immunogenicity and greater safety (Somia and Verma 2000).

Size, charge and surface properties of liposomes can be changed by modifying components of the lipid mixture (Torchilin 2005; Mustapa, Bell et al. 2007). Liposome surface modification, such as the attachment of targeting peptide, can direct liposomes to certain pathological areas in the body; while the attachment of fluorescence molecules or radionuclides may serve for diagnostic imaging (**see Figure 12**) (Torchilin 2005).

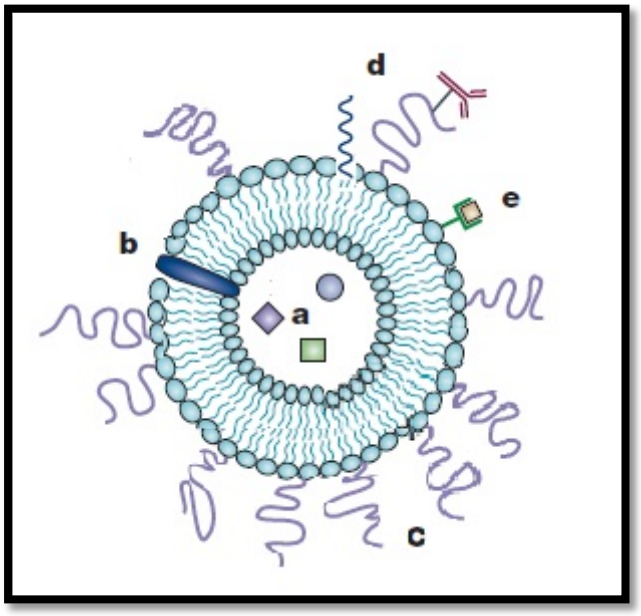

Figure 13: Overview of a liposomal vesicle.

Water-soluble drugs are entrapped into the aqueous interior of the liposomes (a); while water-insoluble drug can be incorporated into the liposomal membrane (b). Protective polymer PEG can shield and stabilize the liposome complexes (c). Surface modification with specific proteins and ligands can be applied for targeting delivery (d). Attachment of the diagnostic labels allows monitoring the fate of liposomes (e).

Modified from Torchilin (2005) Nat Rev Drug Discov. Volume 4, Issue 2, Pages 145-60

However, rapid clearance and degradation by the mononuclear phagocyte system, in particular those of the liver and spleen, is a major problem for the development of pharmaceutical nanoparticles (Cullis, Chonn et al. 1998). The flexible and hydrophilic polymer polyethylene glycol (PEG) can be incorporated into the lipid bilayer and stabilize the liposome structures, hence decrease their interactions with serum proteins and reduce inter-liposomes interaction to prevent aggregation. PEGylation of the liposomes prolongs *in vivo* circulating time compared to non-modified liposomes, which enhances the opportunity to target tumours (Varga, Wickham et al. 2000; Maruyama 2002; Grosse, Tagalakis et al. 2010).

The proliferation of new blood vessels and capillaries, referred as angiogenesis, is a common feature in rapidly growing tumour tissues and is necessary for the supply of fresh nutrients and growth factors. Liposomal nanoparticles with a size of several hundred nanometres could leak preferentially through the tumour vasculature as their sizes are close to that of vascular opening. Therefore liposomes could passively accumulate in the tumour region based on the 'enhanced permeability and retention effect', while passage is restricted by tight cellular junctions in normal tissue (Yuan, Dellian et al. 1995; Drummond, Meyer et al. 1999; Park and Yoo 2010).

Traditional small-molecule cancer therapies suffer from limited selectivity between tumour and healthy tissues. With surface modification, liposomes can selectively target certain receptors in the tumour cells and deliver molecules, and enhance the retention of the liposomes due to bio-molecular interactions. Small structural

differences in the selection of targeting peptides for receptor recognition or LPD (DOTMA/DOPE lipid (L), peptide (P) and DNA (D)) ratio can result in pronounced differences in transfection within each type of receptor-targeted nanocomplexes (Torchilin 2005; Mustapa, Bell et al. 2007; Grosse, Tagalakis et al. 2010; Kudsiova, Ho et al. 2011). Different strategies have been applied for EGFR-targeting studies that include antibody conjugation or small peptides that mimic the natural ligands to demonstrate specific interaction with the receptor (Sofou and Sgouros 2008; Beuttler, Rothdiener et al. 2009; de la Rica, Aili et al. 2012).

Moreover, the increase in size of the nanoparticles, due to for instance antibody-conjugation, may significantly affect the targeting efficiency of liposomes. This is because nanoparticles of small size have much longer circulation time *in vivo* than larger ones. Antibody-conjugation may also alter the surface charge, hydrophobic or hydrophilic properties of liposomes, which contribute greatly to the stability and biologic activity of liposomes. All these properties should be put into consideration when designing liposomal complexes (Beuttler, Rothdiener et al. 2009).

CHAPTER 2: Objective

Objective 1 – Characterisation of Picchu-X sensor

The primary objective of the project was to characterise the CrkII-based biosensor (Picchu-X) in cellular system of basal-like breast cancer for its sensitivity on monitoring EGFR activation and inhibition. **- see Chapter 4.1**

Objective 2 – High-content siRNA screen to identify regulators of EGFR signalling

The next objective was to interrogate, using this biosensor, the key molecular factors within the selected protein subnetwork that are involved in EGFR signalling. We discussed here an in-house development of a semi-automated high-content screening system, which incorporated FRET-FLIM high-throughput microscopy (Fruhwirth, Fernandes et al. 2011; Matthews, Fruhwirth et al. 2012), in combination with RNAi-based knockdown technique utilising a library of siRNA consisted of 533 genes. The aim was to identify genes that modulate EGF-induced biosensor conformational changes. **- see Chapter 4.2**

Objective 3 – Liposomal delivery of biosensor to cancer cells *in vivo*

Another vital aspect of this project involved the use of lipid-based nanoparticles to formulate serum-stable liposomes carrying EGFR-targeting peptides. These were used for *in vivo* delivery of the same biosensor, in order to study the intratumoural heterogeneity of EGFR activity and its modulation by known EGFR kinase inhibitor, in a murine model of basal-like breast cancer. **- see Chapter 4.3**

CHAPTER 3: Material and Method

3. 1: Reagents

Reagents for Cell Culture

Dulbecco's Modified Eagle Media - DMEM (Life Technologies Ltd)

RPMI Media 1640 (Life Technologies Ltd)

Minimum Essential Medium Eagle – MEME (Sigma-Aldrich)

Full medias contain 10% Penicillin/ Streptomycin (10,000IU Penicillin and 10,000µg/ml Streptomycin) (Life Technologies Ltd) 2mM L-Glutamine (Life Technologies Ltd), and 10% heat inactivated Foetal Bovine Serum (Sera Laboratories International Ltd)

Trypsin/EDTA (0.25% trypsin, 0.02% EDTA) (PAA)

Reagents for cellular transfection

Opti-MEM-1 (Gibco)

FuGene 6 (Roche Diagnostics)

FuGene HD (Roche Diagnostics)

Lipofectamine 2000 (Life Technologies Ltd)

Lipofectamine RNAiMAX (Life Technologies Ltd)

Reagents for Molecular Biology

DH5α bacterial cells (Invitrogen)

LB agar and LB broth (Sigma)

Ampicillin (Sigma) used at 100µg/ml

Kanamycin (Sigma) used at 50µg/ml

PureYield Plasmid Miniprep System Kit (Promega)

PureLink HiPure Plasmid FilterMaxiprep Kit (Life Technologies Ltd)

Ligands for receptors

EGF: recombinant human epidermal growth factor (PeproTech, USA) used at 10 or 100ng/ml

HGF: recombinant human hepatocyte growth factor (R & D Systems) used at 50ng/ml

Cell signalling inhibitors

PD168393 (Santa Cruz Biotech): anti-EGFR, used at final concentration of 10µM in DMSO

Morpholino-IPQA (described in (Pal, Glekas et al. 2006; Medina, Pillarsetty et al. 2011) synthesized in-house in the laboratory of Alethea Tabor at University College London): anti-EGFR, used at final concentration of 10µM in DMSO

SGX523 (Millipore): anti-CMET, used at final concentration of 5µM in DMSO

Lapatinib (LC labs, USA) was a kind gift from Professor Gyorgy Keri (Vichem Chemie Research Ltd Hungary): anti-EGFR and HER2, used at final concentration of 10µM in DMSO

Reagents for Western Blotting

Five-fold sample buffer: 100mM Tris (pH 6.8), 10% w/v SDS, 50% Glycerol; after protein determination in the sample, 100mM Dithiothreotol (DTT) and 0.002% w/v bromophenol blue were added

Gels: 30% Acrylamide/Bis solution 37.5:1 (BioRad) ammonium persulphate (Simga)

Precision Plus protein dual colour standard (BioRad)

Running buffer: 25mM Tris Base, 0.19M glycine, 0.1% SDS

Transfer buffer: 25mM Tris Base, 0.19M glycine, 20% w/v methanol

Wash buffer: Tris-buffered saline (TBS): 0.02mM Tris, 0.05M NaCl, 0.01M KCl, pH 7.4

TBS-Tween (TBST): TBS containing 0.1% Tween-20

Blocking solution: 4% Bovine Serum Albumin (BSA) (BioSera) made up in TBS-Tween

Amersham Hybond ECL nitrocellulose membrane (GE Healthcare)

Re-blot Plus (Millipore)

Pierce ECL Western Blotting substrate (ThermoScientific)

Coomassie stain: 0.25% w/v Coomassie brilliant blue R-250, 7% acetic acid, 40% methanol, made up to 1L in distilled water

Destain solution (7% acetic acid, 10% methanol, made up to 1L in distilled water)

Primary antibody:

Antibody	Target	Species	Size (kDa)	Company
pEGFR	Tyr 1173	rabbit	170	Millipore
EGFR		mouse	170	Cell signaling
HER2		mouse	185	Cell signaling
pc-MET	Tyr1234/1235	rabbit	145	Cell signaling
c-MET		mouse	145	Cell signaling
pCrkII	Tyr 221	rabbit	42	Thermo Scientific
CrkII		rabbit	42	Cell signaling
pERK1/2	Thr 188	mouse	44/42	Cell signaling
ERK1/2		rabbit	44/42	Cell signaling
XRCC6		rabbit	70	Epitomics
Tubulin		mouse	57	Sigma

Secondary antibodies: Goat anti-rabbit antibody, used in 1: 2000; goat anti-mouse antibody, used in 1:3000

Reagents for immunofluorescence staining

Primary antibody: Alexa Fluor-647 anti-mouse CD31 antibody (BioLegend), used in 1:200

Rat anti-mouse F4/80 antibody (Abcam), used in 1:250

Secondary antibody: Donkey anti-rat Cy5, used in 1:300

Mowiol: 10% (w/v) Mowiol 4-88, 25% glycerol, 100mM Tris-HCl pH 8.5 (Calbiochem)

DABCO: 2.5% (w/v) 1,4-diazabicyclo[2.2.2]octane (Sigma-Aldrich)

TBS: Tris-buffered saline (25mM Tris, 100mM NaCl, pH 7.5)

4% (w/v) paraformaldehyde (PFA) (Sigma-Aldrich)

Sodium Borohydride (Sigma-Aldrich)

Immersol 510 Immersion oil (Zeiss)

3. 2: Design and construction of Picchu-X biosensor

Yellow fluorescent protein-CrkII-cyan fluorescent protein (YFP-CrkII-CFP) (Phosphorylation Indicator of Crk Chimeric Unit, Picchu) probes for reporting EGFR kinase activities in cells have been reported previously (Kurokawa, Mochizuki et al. 2001; Itoh, Kurokawa et al. 2005; Aoki, Kiyokawa et al. 2008) and were obtained from M. Matsuda (Osaka University, Japan).

The new Picchu sensor was modified by the excision of the sensor module between YFP and CFP, then inserting this module between the mRFP1 and eGFP, in the pEGFP-N1 vector (Clontech) that has been modified in-house by the addition of mRFP1 and altering the multiple cloning sites). The membrane targeting CAAX sequence of k-RAS was cloned after the eGFP as a plasma membrane-anchoring motif and named as Picchu-X, with the resulting construct maintaining the same linkers as the original. The resultant eGFP- and mRFP1-tagged Picchu-X constructs retain the original design of the CFP-YFP tagged version (reference (Itoh, Kurokawa et al. 2005) and http://www.lif.kyoto-u.ac.jp/labs/fret/e-phogemon/picchu.htm). In additional, control sensor lacking mRFP1 acceptor fluorophore, named Picchu-X-GFP, was also constructed in the same manner. All constructs used in this project

were made by a prior member of my supervisor's laboratory, Dr Melanie Keppler, and were verified by sequencing before use.

3. 3: Plasmid purification and transformation

DNA construct was transformed into DH5α competent cells and plated on Luria-Bertani (LB) agar plates containing appropriate antibiotic (Ampicillin (1mg/ml) or Kanamycin (1mg/ml)). Bacterial colonies were incubated in LB medium (4ml for miniprep or 200ml for Maxiprep) and were allowed to grow overnight at 37°C. Miniprep and Maxiprep Kits were used to isolate plasmid DNA from bacterial cultures, following the manufacturer's protocol (Protocol overview: cells were harvested from bacterial cultures by centrifugation and cell pellets were resuspended in buffer containing RNase A; cells were lysed and mixed with precipitation buffer then flowed through an anion-exchange column fitted with the filtration cartridge unit; cell lysates were clarified and negatively charged phosphates of the DNA backbone interacted with the positive charges on the surface of the anion exchange resin; DNA was eluted under high salt condition and was desalted and concentrated by alcohol precipitation using 70% isopropanol prior to centrifugation; DNA pellets were washed with 70% ethanol and were air-dried after centrifugation; DNA was resuspended in nuclease-free water).

DNA extract was quantified and its purity was determined with NanoDrop 1000 spectrophotometer (Thermo Fisher Scientific). For quantity, absorbance was

measured at 260nm and purity was determined by the ratio of absorption at 260nm:280nm. Pure DNA has a ratio of between 1.8 and 2.0, while a ratio below 1.8 shows high protein contamination.

3. 4: Cell culture

MDA-MB-231 and 293T were cultured in DMEM, HCC1954 was cultured in RPMI Medium 1640 and BT20 was cultured in MEME. All media were supplemented with 10% foetal bovine serum (FBS), 2mM L-glutamine and penicillin/streptomycin antibiotics. The cell cultures were kept at 37°C in humidified air containing 5% CO_2. Media were changed frequently to remove dead cells and to refresh nutrients. The cells were split once they became 80-90% confluent.

3. 5: Transient transfection and cell treatments

Type of dish or plate	Surface area per well or plate (cm^2)	Total media volume per well or plate (ml)	Starting volume of FuGENE 6 Reagent (µl/well or plate)	Starting mass of DNA (µg/ well or plate)
60 mm	21	4	6.0	2.0
35 mm	8	2	3.0	1.0
6-well	9.4	2	3.0	1.0
12-well	3.8	1	1.5	0.5
24-well	1.9	0.5	0.6	0.2
96-well	0.3	0.1	0.15	0.05

To achieve 50–80% confluence required for transfection, cells were plated at 2 x 10^5 cells per 35mm culture dish (or 6-well-plate) for this cell density. FuGENE 6, FuGENE HD or Lipofectamine 2000 reagent were used for plasma DNA transfection. The number of cells for plating and the amount of DNA/reagent used were adjusted according to the table above. In occasions, to evaluate the cellular responses, cells were starved for 24hr before inhibitory or stimulatory treatments to retain cells in G_0 phase of cell cycle.

3. 6: Stable infection

Cells with stable knockdown of EGFR or c-MET were provided by Dr Gregory Weitsman. In brief, viral particles (transfer vector, packaging vector, enveloping vector and Rev expressing vector) with specific or non-targeting shRNA were generated by transfection into 293T cell cultures. The supernatants, which contained viral particles, were collected and added to target cells for infection. 48hr post infection, medium were refreshed daily with puromycin selection (2µg/ml) for

five days for the selection of antibiotic resistant cells due to expression of expression of resistance gene associated with shRNA.

3. 7: Protein expression- immunoblotting

The expression of proteins was tested by western blotting. 2 x 10^5 cells were seeded in 6-well-plates. At 80% confluence, the monolayer of cells was then exposed to biochemical treatment of inhibitors or ligands. The cells were washed twice with ice-cold PBS and protein extracts were prepared in 1 X SDS lysis buffer solutions. Protein concentrations were measured by the BCA protein assay kit using known concentrations of BSA protein as standards. For immunoblot, cell lysates were heated at 95˚C for 15min in 100mM DTT reducing agent, then electrophoresed on self-made 7.5% Tris-glycine SDS-polyacrylamide gels. Gels were run on an Invitrogen X-Cell mini-gel system, which were subjected to constant voltage electrophoresis at 200V until the blue loading dye reached the bottom of the gel.

After separation, proteins were electrophoretically transferred onto nitrocellulose transfer membrane at 300mAmp for 2hr on ice using the Invitrogen XCell II Blot Module. Membranes were blocked 45min in 4% BSA in TBS-Tween and then incubated with specific primary antibody overnight at 4^{O}C followed by appropriate secondary antibody for 45min at room temperature. The blots were visualised using the ECL Western Blotting Substrate kit. It was possible to re-use the transfer

membrane for a second incubation with different primary antibody. The protein bound to the transfer membrane were stripped off with Re-BLOT Plus Strong solution, diluted 1:10 with TBS-Tween, for 15min at 37^{o}C, followed by blocking and antibody incubation steps as above. Western blot results were analysed and normalised with Quantity One software (Bio-Rad Ltd).

3. 8: Fixation protocol

For cellular imaging experiments, cells that were seeded at 0.5 X 10^5 on glass coverslips were treated and fixed with 4% paraformaldehyde (PFA) in PBS for 15min then rinsed thrice with PBS over a five minute interval. Samples were then incubated with sodium borohyrate (1mg/ml) for 5min to reduce auto-fluorescence and nuclei were stained with Hochst33342 at concentration of 0.1µg/ml. Coverslips were then mounted on slides with mowiol mounting medium mixed with 2.5% DABCO as an antifading agent, and dried overnight at room temperature.

3. 9: *In vitro* liposomal transfection

Synthesis of lipids and preparation of liposomes were performed by Dr. Nick Mitchell in University College London, while all the cellular and animal experiments were performed in my supervisor's laboratory. 10µM liposome solutions, which contained 4µg of sensor plasmid DNA, were applied to cells at 60% confluence in 6-well-plates. After 4hr incubation at 37°C, cells were washed twice with sterile PBS

to remove unbound liposomes and then incubated with normal growth medium for 48hr to allow sensor protein maturation.

3. 10: Xenograft model

Four-week-old female Crl:CD1-Foxn1nu/nu mice were used for the experiments. Mice were kept in laminar flow isolators in the animal facilities at Guy's Campus. 1.5 X 10^6 cells were suspended in 50µl sterile PBS and were injected subcutaneously to the animals. Tumour volume was calculated using the formula v = l x (w) ^{2}/2, where v = volume, l = length and w = width of tumour. After three weeks, tumours reached volume of approximately 40mm^3 and 100µl liposome solutions in 5% glucose were injected into tail veins. Mice were monitored for 48hr post-administration. EGFR tyrosine kinase inhibitor, Morpholino-IPQA, was suspended in sterile and filtered water at pH 6.5 (at 10mg/ml) and 100ul was delivered intravenously to the mice (32mg/kg). All procedures were done in accordance with UK Home Office legislation.

4hr post-treatment of the inhibitor, solid primary tumours were dissected out and rapidly frozen in liquid nitrogen and stored at -80°C until further use. Frozen tumours were cut into 4µm sections with a cryostat for immunostaining and multiphoton (MP)-FLIM imaging experiments of the fluorescent biosensors as described previously (Festy, Ameer-Beg et al. 2007; Beutler, Makrogianneli et al.

2008; Makrogianneli, Carlin et al. 2009; Heasman, Carlin et al. 2010; Carlin, Evans et al. 2011; Matthews, Fruhwirth et al. 2012).

3. 11: Immunostaining for blood vessel and macrophage

Ex-vivo tissue samples were stained with Alexa Fluor-647 anti-mouse CD31 antibody to correlate Picchu-X activity to distance to blood vessels; while F4/80 antibody (secondary antibody: donkey anti-rat Cy5) were used for the staining of macrophages. Samples were fixed with 4% PFA in PBS for 15min then incubated with sodium borohydride (1mg/ml) for 10min to reduce auto-fluorescence. They were then blocked in 1% BSA for one hour then washed thrice before adding fluorophore-labelled CD31 antibody for an hour and placed in dark room (secondary antibody for F4/80 was needed and applied for an additional 45min). After washing, the solution of Hochst33342 was used for DNA staining and then samples were mounted in mowiol mixed with 2.5% DABCO.

3. 12: Confocal microscopy

Confocal fluorescence images were acquired on a confocal fluorescence laser-scanning microscope (model LSM 510; Carl Zeiss Inc.) equipped with 40X/1.3Plan-Neofluar and 63X/1.4Plan-APOCHROMAT oil immersion objectives, or a Leica DMIRE2 (Leica Microsystems, Germany). Confocal aperture was set to one Airy unit for the longest wavelength. The various colour filters that were used for detecting

the different fluorophores are as follow (excitation wavelength): DAPI (405-450nm), FITC (488- 510nm), Cy3 (543- 573nm) and Cy5 (633- 738nm). Images were analysed using the LSM Image Brower software.

3. 13: siRNA knockdown

Cells were transfected with 10nM of siRNA using Lipofectamine RNAiMAX according to the manufacturer's protocol. Control cells were treated with scrambled negative control siRNA sequence. Cells were grown and harvested 72 hours after the transfection.

3. 14: Preparation of high-content siRNA screen using automated liquid handling robot

For the high-content siRNA screen, JANUS Automated Workstation (PerkinElmer) was employed for the efficient automation of sample preparation. Its dual-arm system offered a 96-tip Modular Dispense Technology (MDT) Dispense Head or a 4-tip Dispense Arm for optimal precision pipetting, processing from tubes to vials to plates.

A library of siRNA targeting 533 genes encoding for proteins that interact with HER1-4 as seed proteins directly or indirectly; was chosen from the HPRD (please refer to (Fruhwirth, Fernandes et al. 2011) for a description of the bioinformatics techniques involved in selecting these genes). A set of three different siRNA

sequences were purchased for the targeted knockdown of each gene (Ambion). The primary 1nmol stock of the siRNA library was diluted 500 times in three steps for storage: ten times to create first-level dilution, then five times to create second-level and finally ten times to create third level dilution), which generated 2pmol/10µl/well in 96-well-plate format for third-level dilution plates that were used for cell transfection.

Lipofectamine RNAiMAX at the ratio 2:1 were robotically pipetted to third-level dilution plates and incubated with siRNA for 20min; meanwhile, cells were seeded into 384-well-plates (4000 cells/well). The transfection mixtures were added onto cells, each set of siRNA were aliquoted in duplicates (10nM final siRNA concentration) and the transfected cells were incubated at 37 ^{o}C. After 24hr, Fugene HD transfection reagent was used to transfect sensor plasmid DNA in 3:1 ratio. Cells were incubated for additional 48hr for sufficient gene knockdown and sensor protein maturation.

Prior to fixation, EGF (100ng/ml) was added to one of the siRNA replicate well, while the other replicate well left untreated. Plates were washed twice and fixed with 4% paraformaldehyde (PFA) for 15min then rinsed thrice with PBS. Samples were then incubated with sodium borohyrate (1mg/ml) for 10min to reduce auto-fluorescence. After further three washes, mowiol mounting medium mixed with 2.5% DABCO was added directly into the plates (50µl/well). Plates were stored at -20 ^{o}C until imaging.

3. 15: Single-photon FLIM/ epi-fluorescence microscope (automated systems were named Galileo and Hooke)

Lifetime and epi-fluorescence images of *in vitro* biosensor-transfected cells were captured on single-photon microscopy system that was developed and built in-house. The FLIM component of the system consists of a dual axis scanning system, a PMT detector (PMH-100, Becker and Hickl) and time-correlated single photon counting (TCSPC) detection (SPC830, Becker and Hickl). Fluorescence excitation is provided by a board spectrum Fianium laser which generates optical pulses with a duration of 40ps at a repetition rate of 80MHz. Single photon, time-resolved fluorescence is detected at 510±20nm using a photomultiplier tube (PMH-100, Becker and Hickl) with a 20x S-Fluor (NA 0.75) objective. The second mode of operation is a simple epi-fluorescence microscope, which consists of the output from lamp coupled into the microscope using a liquid light guide and a CCD camera for detection of fluorescence emission. Automated operation is achieved by incorporating a motorised microscope stage (Märzhauser GmbH, Wetzler, Germany), a closed-loop objective lens mount with a 500µm range of travel (Piezosystem Jena GmbH, Jena, Germany) and a motorised filter cube selector.

Semi-automated high-content SP-FLIM imaging

Five points on each well of the imaging plates were logged manually prior to data acquisition, and then imaged in a fully automated fashion. The automated system

saved operator marked x, y and z coordinates for each point. On completion of field of view marking, the system returned to each core and focussed using a high precision (auto-focus in 0.2µm lateral resolution) computer-controlled objective stage (Piezo-system), then imaged consecutively in the FITC cube for eGFP detection, the Cy3 cube for mRFP1 detection and the UV cube for auto-fluorescence or nuclear staining. The auto-exposure routine was also employed. The system saved all three images then switched automatically to laser-scanning mode to acquire the single photon data and save time-resolved images. FLIM images have 256 x 256 pixel resolutions and ADC was set to 64 time channels.

3. 16: Time-resolved multi-photon microscopy

Ex-vivo tissue section imaging was performed on multi-photon microscope system, comprising a solid-state pumped (8-W Verdi; Coherent), femtosecond self-modelocked Ti:Sapphire (Mira; Coherent) laser system, an in-house developed scan-head, and an inverted microscope (Nikon TE2000E, x40 oil objective) (Peter, Ameer-Beg et al. 2005; Barber, Ameer-Beg et al. 2009).

Imaging data comprised of 256x256 pixel resolution and 256 time channels. This arrangement facilitates analysis using multi-exponential decay models. FRET efficiency was calculated according to equation: FRET efficiency = 1- $\tau_{da}/\tau_{control}$, where τ_{da} is the lifetime of eGFP in cells that co-express mRFP1 and $\tau_{control}$ is eGFP lifetime measured in the absence of acceptor. Since sub-100 ps time resolution is

achieved with our instrumentation, for a $\tau_{control}$ value of 2.35 ns, FRET efficiencies as low as 3% can be determined accurately. Pixel-by-pixel lifetime determination was achieved using a modified Levenberg-Marquardt fitting technique (Barber, Ameer-Beg et al. 2005). For cases where sufficient reduction in the measured lifetime allows the separation of two distinct, spatially invariant, GFP lifetime subpopulations, i.e. non-interacting ($\tau_{control}$) and interacting (τ_{FRET}), an additional analysis was performed. Applying a bi-exponential fluorescence decay model and global analysis techniques to the data enables the determination of $\tau_{control}$ and τ_{FRET}, and their pre-exponential factors (or relative concentration) on a pixel-by-pixel basis (Barber, Ameer-Beg et al. 2009). The FRET population F_2 is the fraction of interacting molecules that exhibit τ_{FRET} according to the equation τ_{FRET} = FRET Eff/[1 - ($\tau_{FRET}/\tau_{control}$)], since $\tau_{da} = F_2 \times \tau_{FRET} + (1 - F_2) \times \tau_{control}$.

3. 17: Analytical Methods

FRET-FLIM Analysis

The fluorescence lifetime was calculated by fitting exponential fluorescence decay models to the images. The FLIM images obtained with the lifetime microscope were batch analysed by a PC workstation running in-house exponential fitting software (TRI2) written in CVI by Dr Paul Barber (Barber, Ameer-Beg et al. 2009). The program outputs files where all the fitting parameters were recorded for each image. These files were then analysed to produce a distribution of lifetime and an average lifetime. The analysis has been made robust to noise and to low photon

counts, providing fast execution and amenability to automation and batch processing. All cellular lifetime data acquired with SP-FLIM was fitted with the single exponential decay analysis, while all tissue lifetime data acquired with MP-FLIM was fitted with bi-exponential decay model. Data were expressed as means ± SEM, statistical significance was analysed using unpaired two-tailed Student's t-test.

Statistical analysis

SPSS Statistics 19.0 was used to analyse the association between donor eGFP fluorescence lifetime (Tau), intensity, and EGF treatment for each siRNA knockdown using linear regression model, where Tau= slope*intensity + intercept. Pearson correlation coefficient (r) was reported for the association between tau and lifetime. To observe the effect of EGF towards this association, a linear regression model which included an interaction term with EGF (dichotomous values, where EGF=0 or EGF=1, resulting in two linear equations of individual lines) was used to determine whether the effect of intensity on Tau differed by EGF status. A T-test was reported for the association between EGF and Tau and intensity, if the p value was < 0.05 then there was a statistically significant interaction.

CHAPTER 4: Result

4.1: Characterisation of Picchu-X sensor

Chapter introduction - Characterisation of Picchu-X sensor

The primary objective of the project was to characterise a range of new FRET-based sensors by which the CFP and YFP in the original probes were cleaved and replaced with eGFP and mRFP1 as the donor and acceptor fluorophore pair.

Biosensors that report on the enzymatic activities of Akt (Yoshizaki, Mochizuki et al. 2007) and EGFR (section 3.2), or levels of PIP_2 and PIP_3 (Aoki, Nakamura et al. 2005), respectively, were validated in cell based system for their accuracy and sensitivity on the simultaneous detection of the activation for their specific signalling pathway(s). The CrkII-based sensor reporting EGFR activity, namely Picchu-X, was selected for further studies due to its robustness of reproducibility of monitoring EGFR activity under different conditions.

The biochemical and FLIM-imaging data to confirm the functional aspects of Picchu-X sensor in a variety of basal-like breast cancer cell-lines that overexpress EGFR are presented here in Chapter 4.1. The sensor was then used to conduct a high-content FLIM screen utilising a library of siRNA consist of 533 genes interconnected with EGFR (see Chapter 4.2); and was further used to test intratumoural EGFR activity using a liposomal delivery method in a murine model of basal-like breast cancer (see Chapter 4.3).

(A)

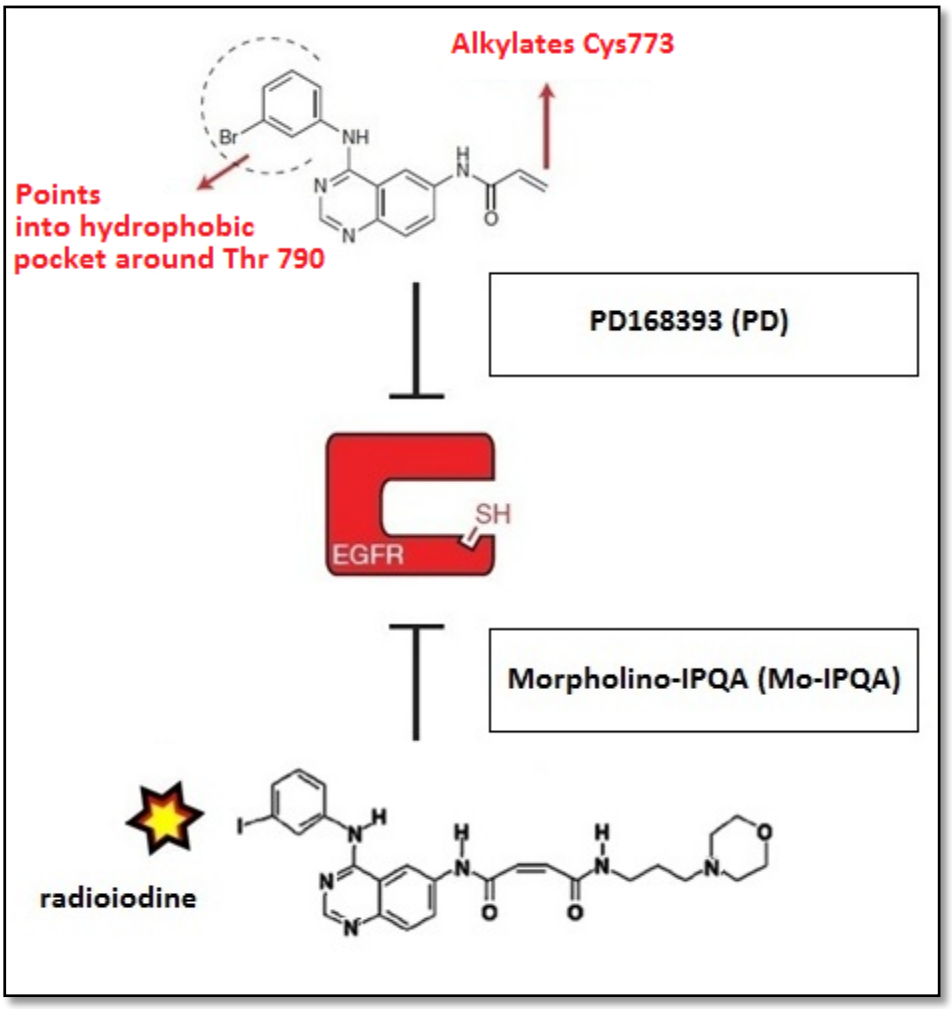

Result figure 4.1.1: Effects of specific EGFR tyrosine kinase inhibitor, Morpholino-IPQA and its precursor PD168393.

(A) EGFR tyrosine kinase inhibitors, Morpholino-IPQA (Mo-IPQA) and PD168393 (PD), interact irreversibly with the ATP-binding site of activated EGFR domain. The bromide group of PD168393 is replaced with an iodine group in Morpholino-IPQA, which can be replaced with radioactive iodine for molecular imaging.

(B)

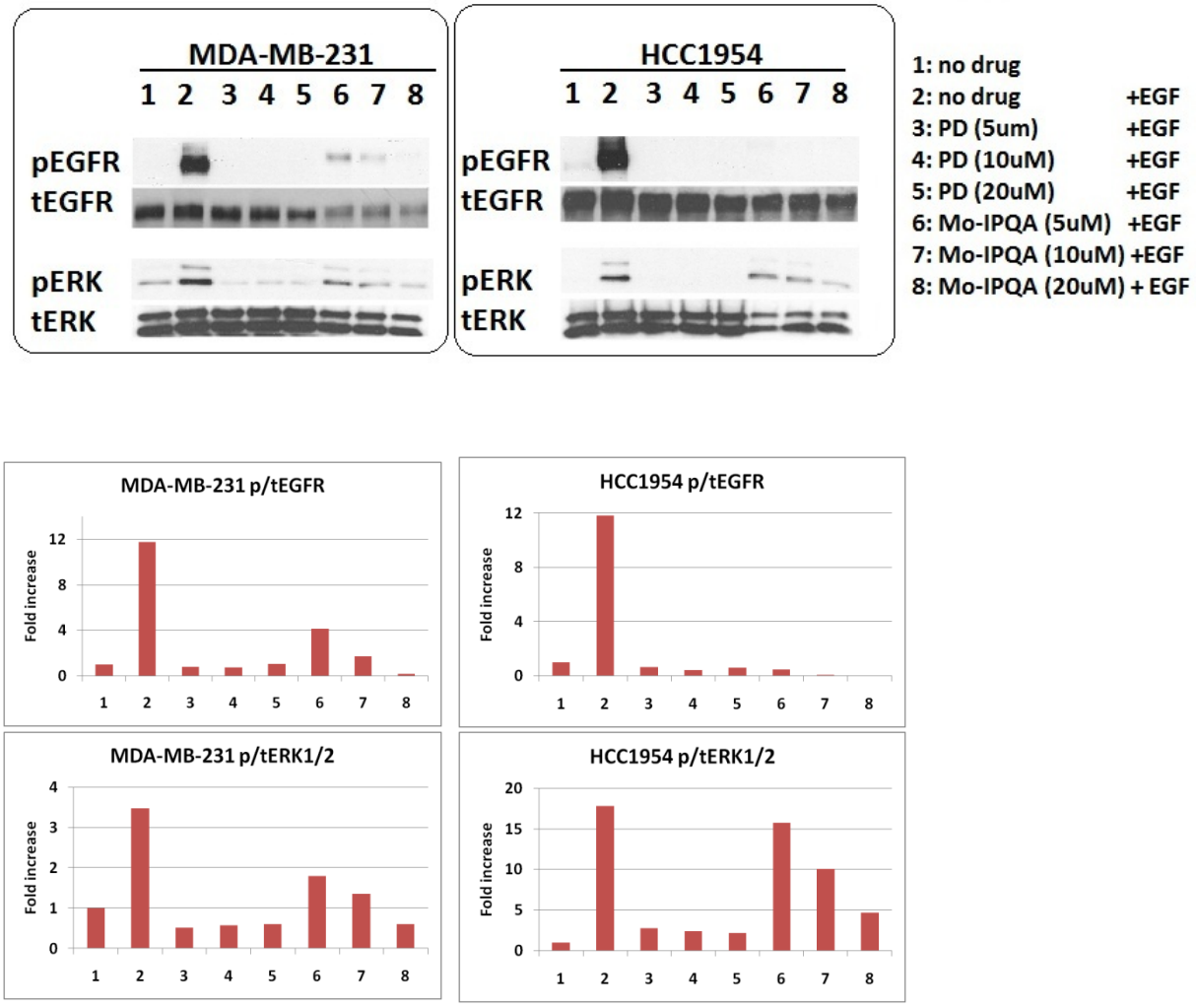

(B) MDA-MB-231 and HCC1954 cells were treated with 5, 10 or 20µM of PD168393 (PD) or Morpholino-IPQA (Mo-IPQA) for one hour before adding EGF (100ng/ml) for 30min, prior to lysis. Immunoblots were carried out using the antibodies indicated above. Histograms represent the phosphorylation level of EGFR and ERK1/2, normalised to total expression of the respective protein.

(A)

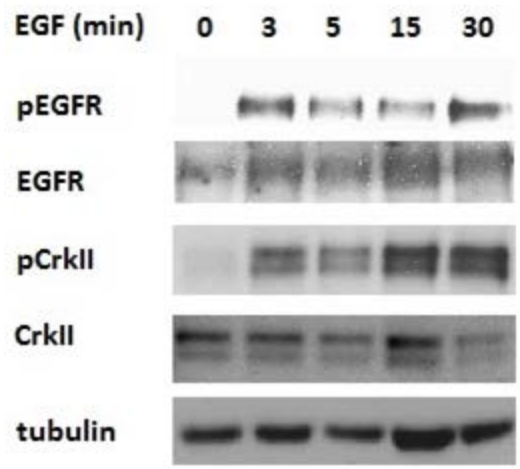

(B)

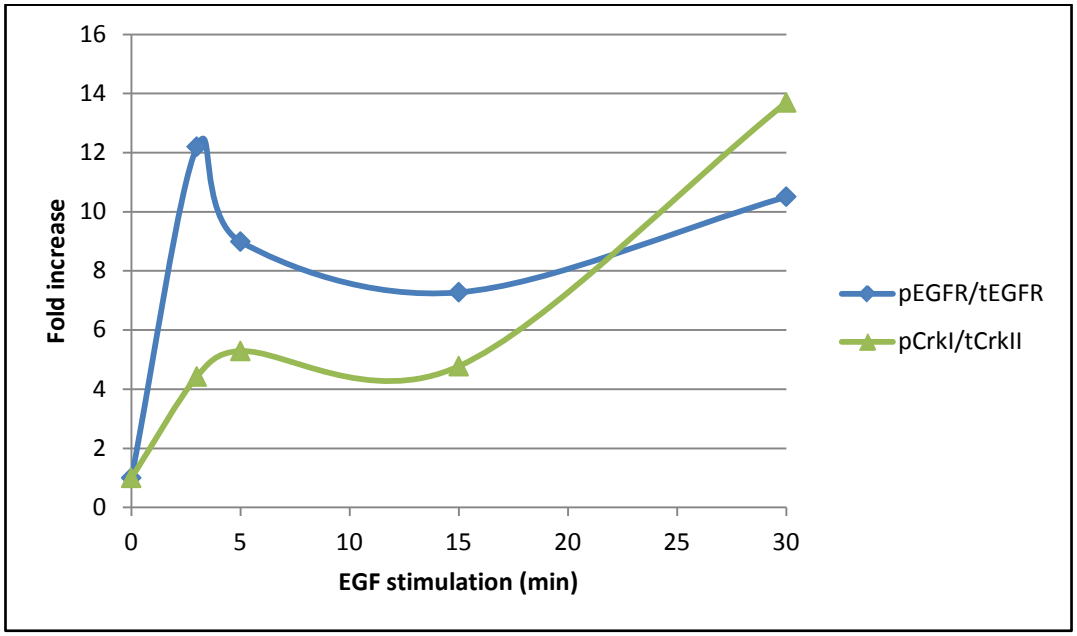

Result figure 4.1.2: EGF-induced activation of EGFR and corresponded Picchu-X activity.

(A) HCC1954 cells were seeded in 6-well-plate and transfected with Picchu-X plasmid DNA. After 48hr, cells were treated with EGF (100ng/ml) for up to 30min, prior to lysis. Immunoblots were carried out using the antibodies indicated above. (B) Western blot results were analysed and normalised with Quantity One software. Line graph represents the phosphorylation level of EGFR and CrkII, normalised to total expression of the respective protein.

Inhibition of EGFR activity using specific EGFR tyrosine kinase inhibitor

A number of EGFR over-expressing basal-like breast cancer cell-lines, MDA-MB-231, HCC1954 and BT20, were chosen for the study due to their abnormal EGFR tyrosine kinase activity, causing the aggressive cancer development and progression. We carried out inhibitory experiment using a specific, irreversible EGFR tyrosine kinase inhibitor, Morpholino-IPQA (Mo-IPQA) (Gelovani 2008) to investigate its EGFR inhibition ability compared to its precursor PD168393 (Fry, Bridges et al. 1998).

PD168393 is a cell-permeable and selective inhibitor of EGFR tyrosine kinase activity. It binds irreversibly to the catalytic domain of the activated EGFR domain with a 1:1 stoichiometry, alkylates the Cys773 group and blocks the binding of ATP by pointing its bromide group into the hydrophobic pocket of the ATP-binding pocket, hence prevents receptor activation (Fry, Bridges et al. 1998) (Gelovani 2008). The IC50 values of PD168393 for EGFR autophosphorylation were at approximately 11.1 nM (Chen, Kovar et al. 2005). The bromide group can be replaced with an iodine group, to form Morpholino-IPQA, which can interact irreversibly with the receptors **(Result figure 4.1.1A)**. This compound was synthesized in-house in the laboratory of Alethea Tabor at University College London (please see appendix for the synthesis and purification of Morpholino-IPQA). The iodine group in Morpholino-IPQA can be replaced with radioactive iodine and be explored as a potential radiotracer for the molecular imaging of EGFR overexpressing tumours (Pal, Glekas et al. 2006). This will be discussed further in the **Discussion Chapter**.

In the two basal-like breast cancer cell lines, MDA-MB-231 and HCC1954, inhibitors were applied at 5μM, 10μM or 20μM for one hour followed by EGF stimulation (100ng/ml).

A potent inhibitory effect was observed with the PD168393 treatment. At all three concentrations there were more than ten-fold decreases in the phosphorylation of EGFR comparing to EGF stimulation alone, confirming the blockade of ligand binding to the receptors **(Result figure 4.1.1B, lane 3, 4 and 5)**. For Morpholino-IPQA, immunoblot revealed small a dose-related increase in inhibition **(lane 6, 7 and 8)** and 10μM dose was selected for future experiments.

Interestingly, although the phosphorylation of EGFR was significantly inhibited in both cell-lines, the level of phosphorylated ERK1/2 remained high after the inhibition by Morpholino-IPQA as shown in **result figure 4.1.1B**. The inhibitor was washed away using sterile PBS before the stimulation of EGF, this indicated that the with the inhibition of Morpholino-IPQA, a small amount of receptors were still be able to get phosphorylated by the nature ligand, and only a small number of active receptors were required to activate a cascade of downstream signalling pathways, resulting in an increase of ERK1/2 activity. As demonstrated in Chen et al., the concentration of inhibitor required to inhibit the phosphorylation of downstream molecules such as ERK1/2 was usually much higher than needed for EGFR.

EGF-induced activation of EGFR and corresponded Picchu-X sensor activity

Result figure 4.1.2 demonstrated the tyrosine phosphorylation of the CrkII-based sensor upon EGF stimulation and its association with EGFR activity. The molecular weight for CrkII protein was 42kDa. A part of the C-terminal SH3 domain was cleaved by restriction enzyme for the construction of Picchu-X sensor (CrkII amino acids 1–236); however it would not affect the phosphorylation of Tyr221. The molecular weight of the CrkII-based sensor was expected to be approximately 90kDa (with eGFP and mRFP1 fluorescent proteins flanking on each terminal of the CrkII protein). However, instead of a single 90kDa band of the Picchu-X sensor, a double band was observed in the immunoblots in the region of 80kDa protein size. This was due to the partial fragmentation of the red fluorescent protein upon heating at 95°C for 15 minutes during sample preparation, which seems to be a common effect on DsRed-like fluorophores (Gross, Baird et al. 2000).

In HCC1954 basal-like breast cancer cells, EGFR phosphorylation peaked at 3min, followed by the activation of its downstream adaptor protein CrkII (as in Picchu-X sensor), which activity slowly increased over time and maximal by 30min after EGF stimulation (**Result figure 4.1.2)**. This result confirmed that the activity of Picchu-X sensor was corresponded to EGF-induced activation of EGFR in our basal-like breast cancer model.

(A)

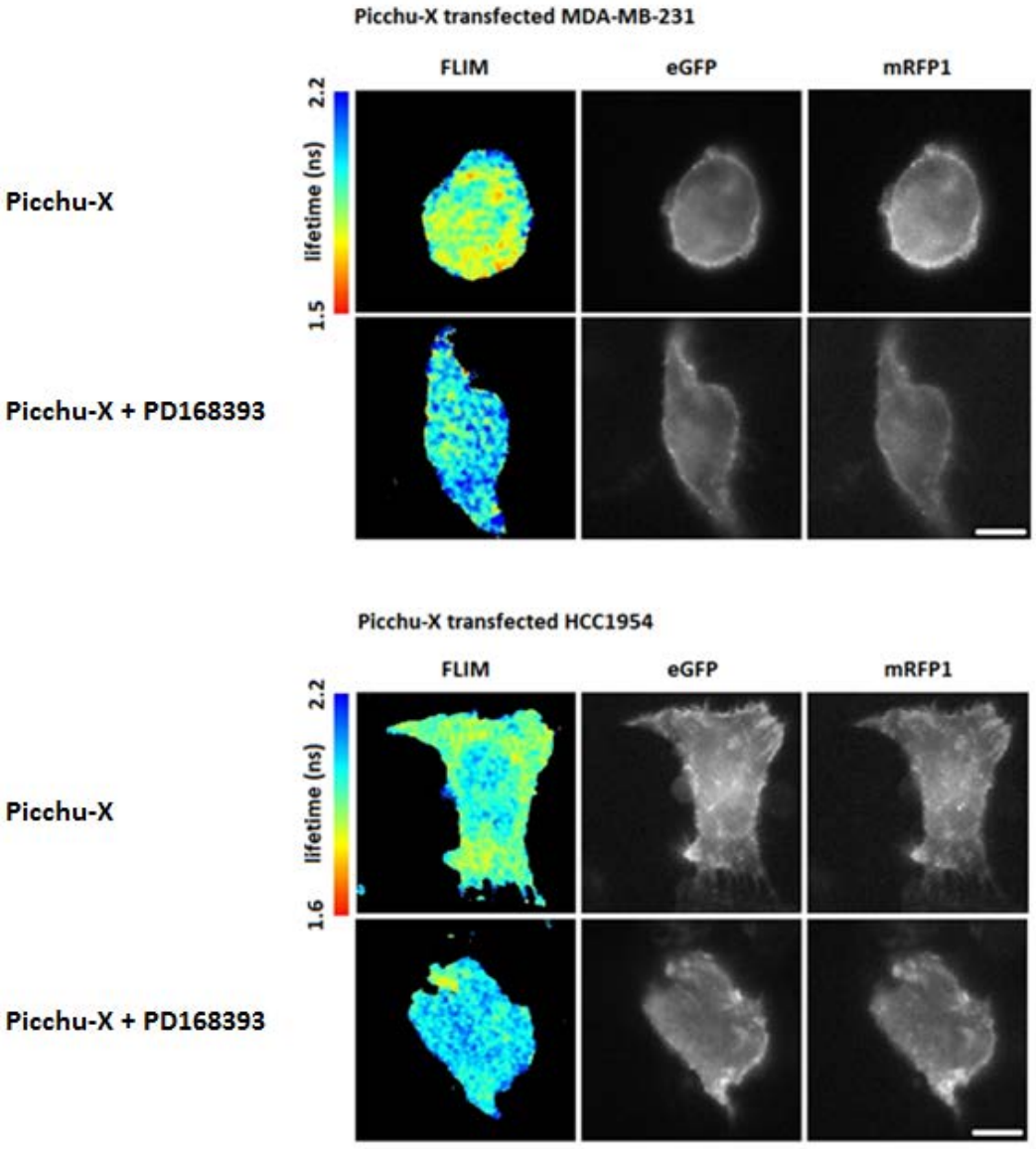
Picchu-X transfected MDA-MB-231
FLIM
eGFP
mRFP1
2.2
lifetime (ns)
1.5
Picchu-X
Picchu-X + PD168393
Picchu-X transfected HCC1954
FLIM
eGFP
mRFP1
2.2
lifetime (ns)
1.6
Picchu-X
Picchu-X + PD168393

(B)

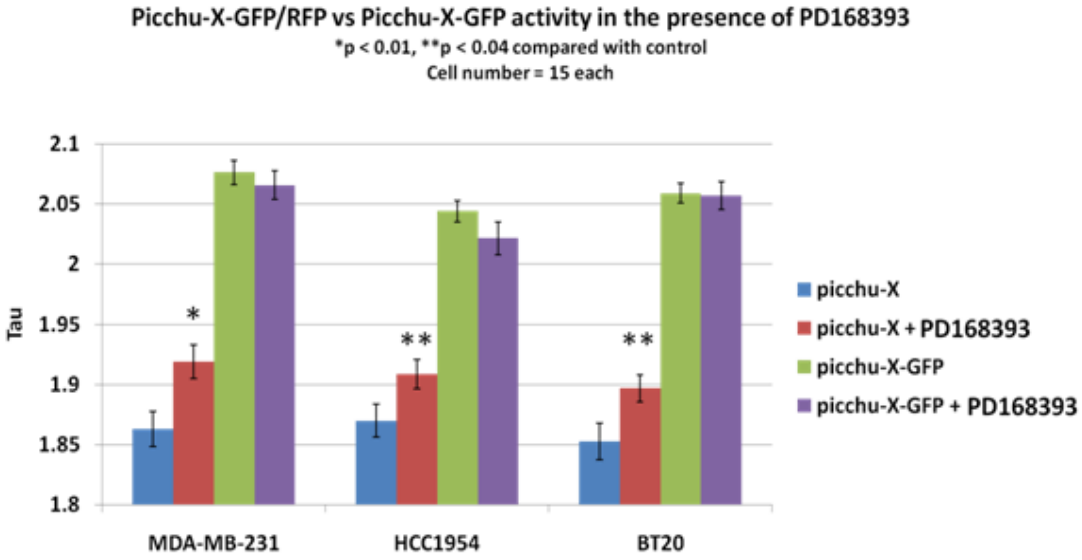

Result figure 4.1.3: Quantification of lifetime measurements of Picchu-X

(A) MDA-MB-231 and HCC1954 cells were transfected with Picchu-X plasmid DNA. After 48hr, cells were treated with PD168393 (10µM) for one hour. Images are representative of cells seen, white scale bar represents 10µm. (B) Quantification of lifetime measurements of Picchu-X or Picchu-X-GFP for MDA-MB-231, HCC1954 and BT20 cells, before and after treatments with PD168393 (10µM) for one hour. Data were expressed as means ± SEM, statistical significance was analysed using unpaired two-tailed Student's t-test.

Fluorescence lifetime measurement of Picchu-X sensor activity

FRET-FLIM imaging of Picchu-X sensor in individual cells allow us to study the spatial and temporal activation/regulation of EGFR activity on a single cell level. To examine the dynamic range of the sensor in its open (inactive) or closed (active) state, we performed fluorescence lifetime measurements in both absence and presence of the EGFR kinase inhibitor, in this case PD168393 (**Result figure 4.1.3**).

The introduction of eGFP/mRFP1 fluorophore pair have been proven to be a better suitable pair for donor FRET-FLIM assays, whereas mRFP1 has lower aggregation problems to form oligomers and has little or no green component in its fluorescence emission. This solved the problem of emission cross-talk, since eGFP can be excited at a wavelength beyond the excitation spectrum of mRFP1. In addition, eGFP is a photo-stable fluorophore that displays mono-exponential fluorescence decay, offering multiple advantages over the CFP/YFP pairs (Peter, Ameer-Beg et al. 2005).

Result figure 4.1.3A demonstrated SP-FLIM images of MDA-MB-231 and HCC1954 cells in their basal activity and in response to PD168393 treatment. Basal active Picchu-X activity was represented in the lifetime colour maps with yellow/green colours, whereas low activity was represented as blue colour and area with a low signal-to-noise ratio on which a lifetime measurement cannot be achieved was in black.

In MDA-MB-231 cells, Picchu-X exhibited an increase in lifetime (from average basal lifetime of 1.86ns to 1.92ns) in response to EGFR inhibitory treatment. In contrast, control Picchu-X-GFP sensor (without expression of acceptor mRFP1) recorded a maximum lifetime of 2.06ns and remained the same in the presence of inhibitors. Similar response was observed in other two basal-like breast cancer cell-lines, HCC1954 and BT20 **(Result figure 4.1.3B)**.

On the technical side, it was easier to characterize the FRET signal from intra-molecular biosensors as they were built with one donor and one acceptor, the stoichiometry was guaranteed to be 1:1 and thus they were less sensitive to the relative concentration than inter-molecular sensors. However, notably, these data indicated that the dynamic ranges of this type of intra-molecular FRET-based sensors were quite narrow, mostly with less than 0.1ns changes in lifetime (this issue will be further discussed in **Result figure 4.2.5**). In spite of that, the increases in Picchu-X sensor lifetime in response to inhibitor treatment were reproducible in a variety of human cancer cell types (MDA-MB-2231, HCC1954, BT20, MDA-MB-468, SW1222 and Hela cells, data was not include in here).

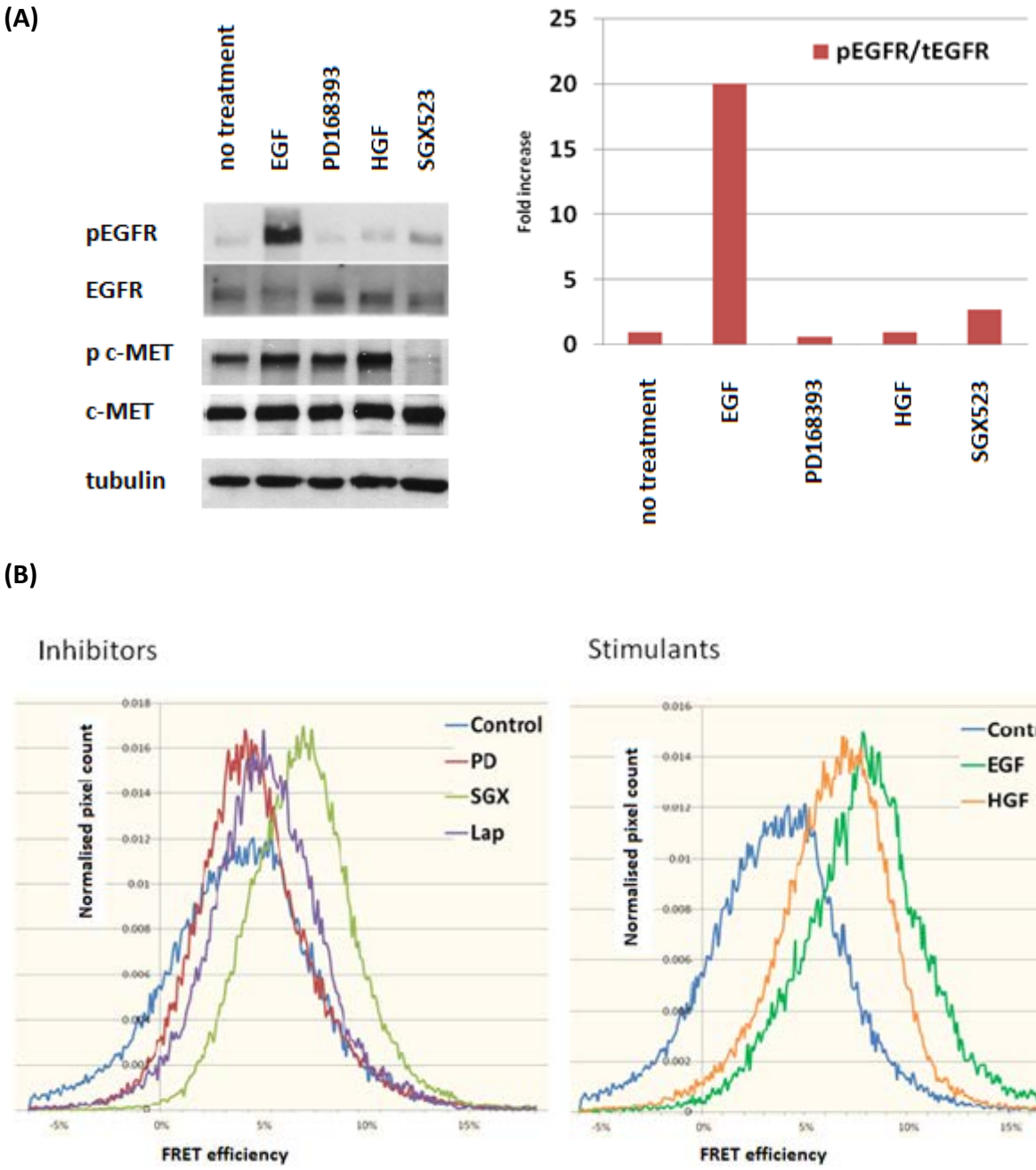

Result figure 4.1.4: Effect of ligands and inhibitors on EGFR phosphorylation and FRET efficiency

(A): HCC1954 cells were transfected with Picchu-X plasmid DNA. After 48hr, cells were treated with 10µM of inhibitor (PD168393, SGX523 or Lapatinib) for one hour, or with stimulant (EGF, 100ng/ml; HGF, 50ng/ml) for 30min, prior to lysis. Immunoblots were carried out using the antibodies indicated above. Western blot results were analysed with Quantity One software. (B) FRET efficiency measurement for the effect of inhibitor or stimulant treatment. FRET efficiency correlated to lifetime measurement = 1- τ donor-acceptor/τ donor.

Picchu-X sensor activity upon ligand stimulation and receptor inhibition

The purpose of this experiment was to examine the sensitivity and specificity of the Picchu-X sensor. As with most signalling molecules, it was known that more than one signal pathway could contribute to the activity of the CrkII protein (Kobashigawa, Sakai et al. 2007).

We applied recombinant human hepatocyte growth factor (HGF) and SGX523, a small molecule ATP-competitive kinase inhibitor that stabilised the inactive conformation of c-MET catalytic domain (Buchanan, Hendle et al. 2009), and measured the activity of EGFR and Picchu-X sensor in HCC1954 cells in order to determine the regulation between EGFR, c-MET and the CrkII-based sensor **(Result figure 4.1.4)**.

Since Picchu-X sensor was a direct target for EGFR kinase activity we assessed the FRET efficiency changes upon stimulations with EGF. As shown in **Result figure 4.1.4A**, EGF caused activation of EGFR with the increased phosphorylation of Tyr1173 **(second lane)**, which corresponded to the shift to the right of FRET efficiency histogram indicating the change from 4% to 9% **(4.1.4B)**. FRET efficiency was calculated according to the equation = 1- τ donor-acceptor/τ donor.

Apart from the c-MET inhibitor (SGX523), all the FRET efficiencies in cells treated with the other TKIs (such as the EGFR inhibitor PD168393 or EGFR-HER2 dual inhibitor Lapatinib) were similar to that observed in untreated control, in

agreement with the phosphor-EGFR immunoblots in **4.1.4A**. The effect of various inhibitors on EGF-stimulated increase in Picchu-X activity will need to take into account the intensity-dependent lifetime time quenching effect, which will be described in a subsequent section **Result figure 4.2.5**.

Impact of c-MET signalling pathway on sensor activity

As HGF is not a natural ligand for EGFR, it was clear that from the immunoblot there was no increase in phosphorylated-EGFR after HGF treatment (**fourth line, Result figure 4.1.4A**). However, there was an increase in FRET efficiency of the sensor, hinting an interaction of CrkII protein with activated c-MET. Interestingly, a TKI for c-MET also caused the phosphorylation of EGFR (and increased sensor activity) as judged by phosphorylation level in the immunoblot (**fifth line, Result figure 4.1.4A**).

My supervisor (in collaboration with Prof. Yossi Yarden (the Weizmann Institute of Science, Rehovot, Israel) previously demonstrated in breast cancer cells, the conformational effects of anti-EGFR TKIs (Erlotinib and Gefitinib), in inducing EGFR:EGFR homodimer formation (Bublil, Pines et al. 2010). Lapatinib, another TKI that dually targets EGFR and HER2, has been shown by our laboratory and others to enhance the formation of HER2:HER3 heterodimer through an allosteric/conformational mechanism (Scaltriti, Verma et al. 2009; Patel 2013); which we have shown to lead to HER3 rephosphorylation, a known drug resistance mechanism that occurs in tumour cells under long term TKI treatment pressure (Sergina, Rausch et al. 2007; Amin, Sergina et al. 2010; Garrett, Olivares et al. 2011). The underlying mechanism and significance of anti-c-MET TKI-induced EGFR phosphorylation/activation are the subjects of further investigation in my supervisor's lab but this is beyond the scope of this thesis.

Presently, the major application of Picchu-X sensor has been published as a reporter of EGFR tyrosine kinase activity, however it was known that other signalling pathways can affect the sensor activity (Kurokawa, Mochizuki et al. 2001). Cipres et al. have demonstrated that c-MET signalling could induce phosphorylation of CrkII on Tyr221, and this phosphorylation was mediated by Abl tyrosine kinase activity (Cipres et al, 2007). Furthermore, Trusolino et al. has showed an indirect association of CrkII and c-MET through the large docking protein Grb2-associated binding protein 1 (GAb1) (Trusolino, Bertotti et al. 2010). The mechanism by which c-MET associated with the EGFR remained to be determined. The activation of platelet-derived growth-factor receptor β (PDGFβR) signalling pathway might also contribute to sensor activity, which played fundamental roles in actin cytoskeleton remodelling and cell migration (Antoku and Mayer 2009).

Chapter summary

By monitoring the sensor conformation changes with FRET-FLIM, we could indirectly detect the EGFR activity related molecular events, such as the stimulation of ligand binding and the inhibition with small molecule inhibitors, and monitor the cellular signalling pathways. Furthermore, sensor might undergo conformational changes by the endocrine signals. However when the sensory domain was activated by EGF-triggered activation of EGFR, it would induce a large overall conformational change that changed the FRET signal.

The Picchu-X sensor was selected to be employed in a large scale siRNA screen against a protein network consisted of 533 genes. It would be important to design these experiments carefully based on the sensitivity and specificity of the sensor. These data can potentially served as system response profiles of the cells to provide a better understanding of the functional regulation of the EGFR sub-network in cancers.

4.2: High-content screen of 533 genes interconnected with EGFR

Chapter introduction - High-content screen of 533 genes interconnected with EGFR

The next objective was to use an in-house semi-automated protein activity sensing/imaging technique to interrogate the EGFR-centric subnetwork of proteins, in order to obtain a better understanding of what molecular factors involved in the regulation of EGFR activity upon stimulation with EGF.

A library of siRNA targeting genes interconnected with EGFR directly or indirectly (up to second degree of interaction), was chosen from the Human Protein Reference Database. Three different sequences were available for the silencing of each 533 genes. To exploit this library, we developed a high-content SP-FLIM screen using the Picchu-X sensor (described in previous chapters) in HCC1954 basal-like breast cancer cells.

In this result section, we will describe the development of the screening procedure and the statistical analysis method to interpret the complex and large amount of FRET-FLIM data generated. 22 target genes (4.1% of the siRNA library) were identified as modulators of EGFR response to natural ligand. A couple of the genes were selected for further validation to establish the biological importance of the genes identified as primary hits in the EGFR signalling network.

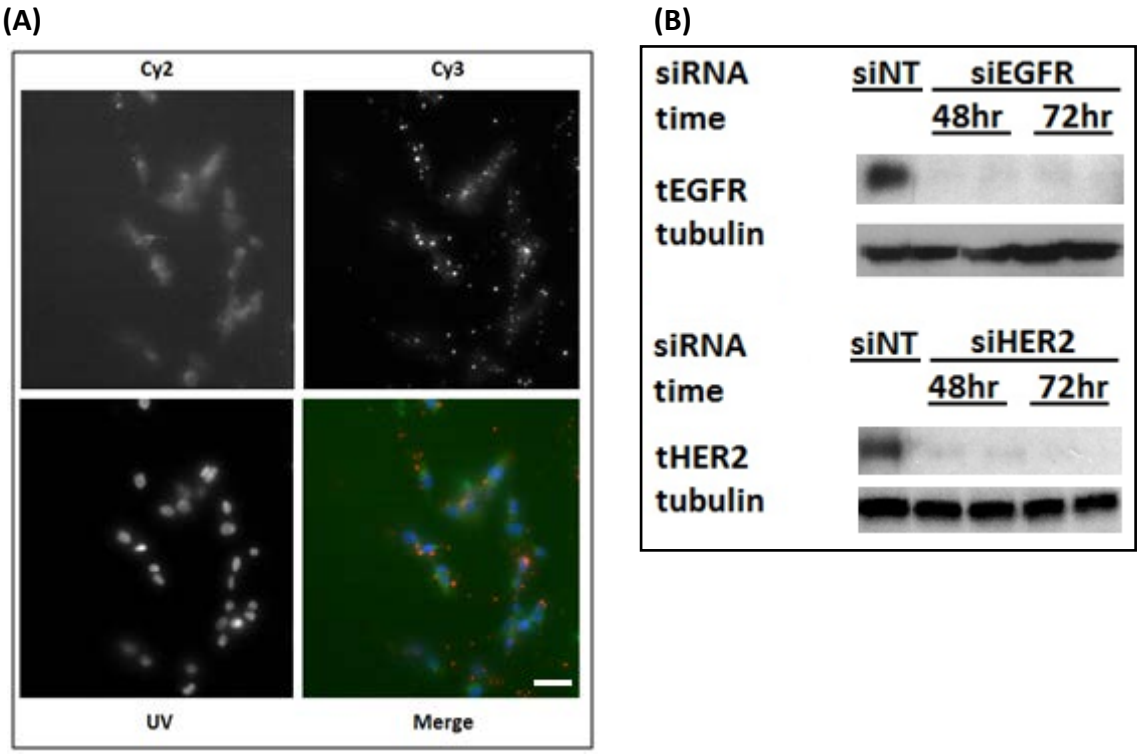

Result figure 4.2.1: Indication of successful siRNA transfection into HCC1954 cells.

(A) 10nM BLOCK-iT Alexa 555 Fluor-Red fluorescent oligo were transfected into HCC1954 cells using Lipofectamine RNAiMAX transfection reagent, scale bar represents 40µm. Images were obtained 72hr post-transfection. (B) HCC1954 cells were transfected with 10nM non-targeting siRNA (siNT) for 72hr, or siRNA against EGFR or HER2 for either 48hr or 72hr in duplicates.

Since MDA-MB-231 and BT20 cells were proven to be difficult to transfect efficiently in small format of 384-well plate and were not strongly attached to substratum leading to loss of cell during the fixation procedure, we use HCC1954 cells which grow at a fast rate and have superior transfection efficiency.

siRNA transfection efficiency

Successful gene silencing in siRNA-mediated RNA interference experiments required efficient uptake of siRNA into the cells. Two verification experiments were done to confirm successful transfection and gene knockdown.

BLOCK-iT Alexa Fluor red fluorescent oligo (10nM) was transfected into HCC1954 cells to enable the visualization of transfected dsRNA oligomers (**Result figure 4.2.1A**). This reverse transfection method using Lipofectamine RNAiMAX reagent has been proven to be a rapid and effective method for cellular lipid-mediated siRNA delivery. After proving the effectiveness of uptake, we verified the release and knockdown efficacy of the siRNA by immunoblotting, showed in **Result figure 4.2.1B**. In addition to control scrambled negative control siRNA sequence, EGFR and HER2 siRNA were transfected into cells. The expression level of the receptor protein was assessed after 48hr and 72hr of knockdown to ensure efficient gene silencing.

(A)

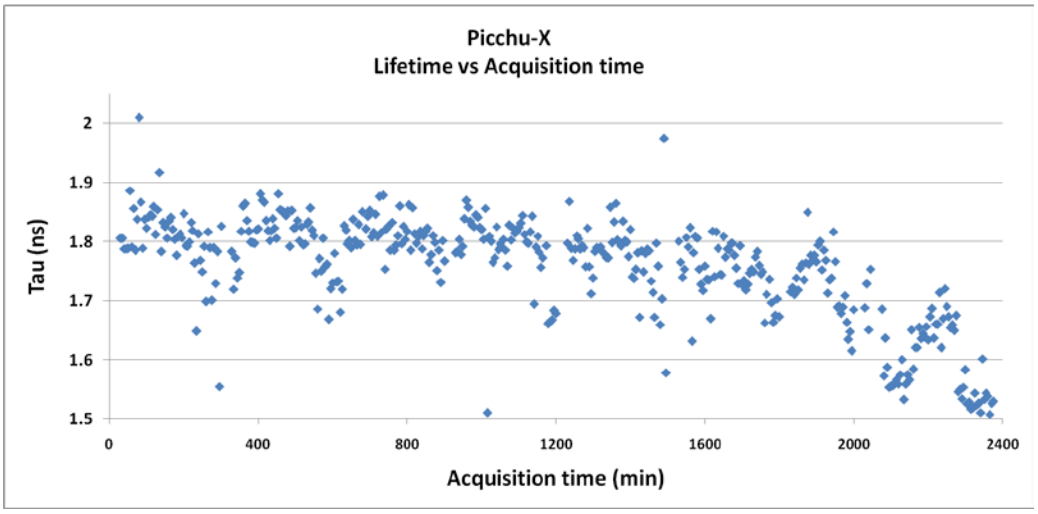

(B)

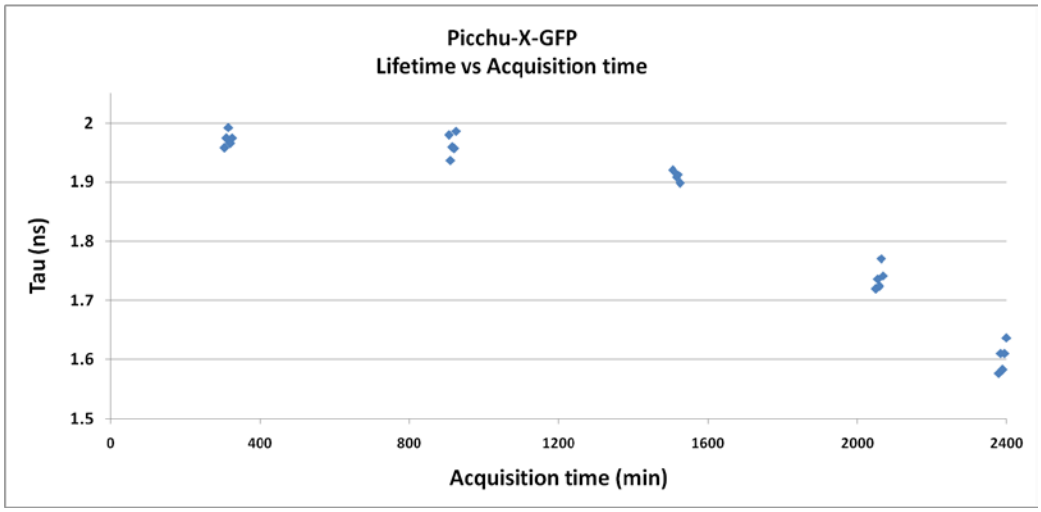

Result figure 4.2.2: Decrease in lifetime measurement after long hour of acquisition.

HCC1954 cells were seeded in 384-well-plate and transfected with library of siRNA. After 24hr, cells were transfected with (A) Picchu-X or (B) Picchu-X-GFP plasmid DNA and were fixed 48hr later. Lifetime images were acquired with SP-FLIM. Acquisition time for each image was 150sec. Data was analysed using TRI2 software.

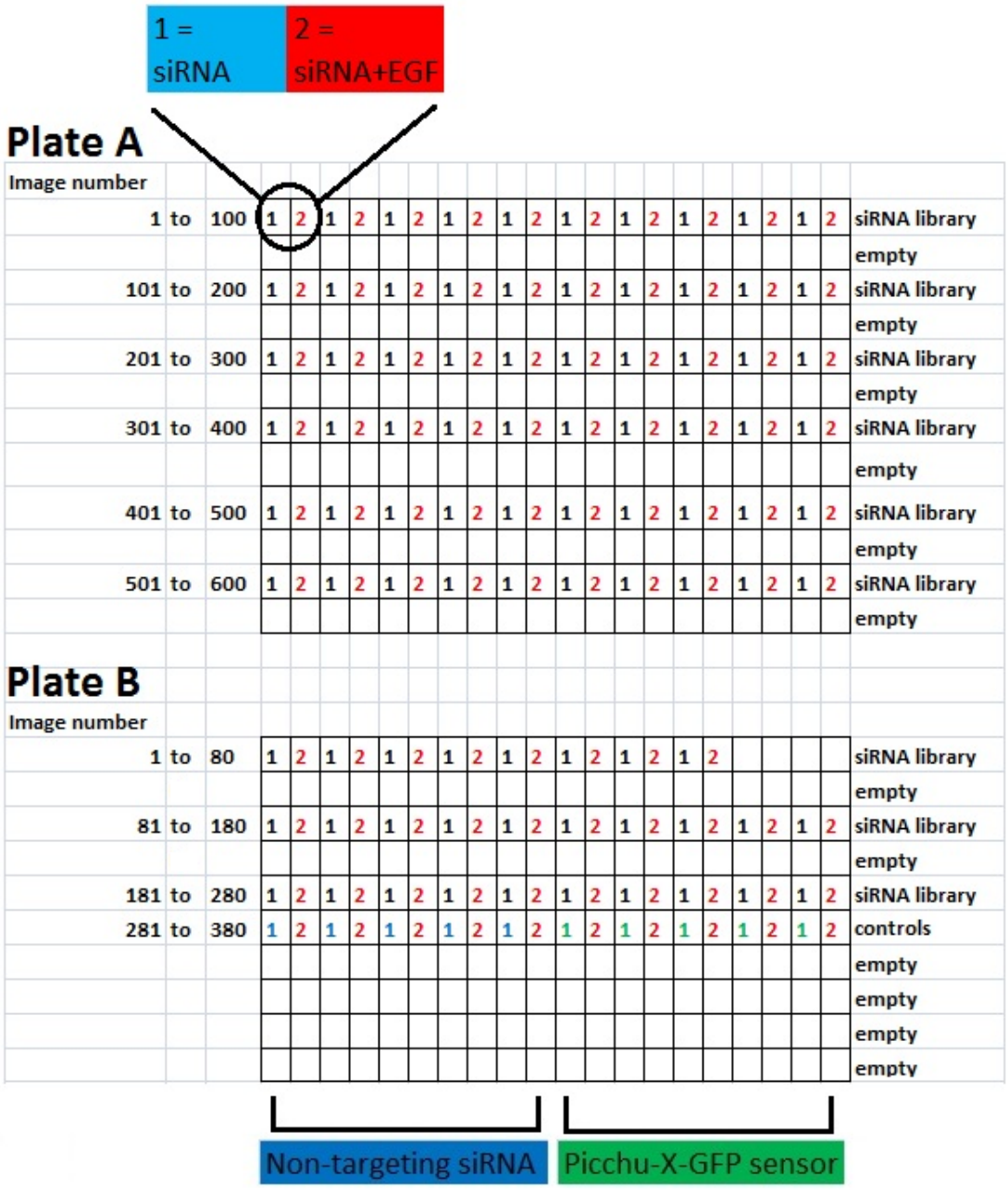

Result figure 4.2.3: Plate-well design for the siRNA screen.

The content of each siRNA-library plate was divided into two 384-well-plates for SP-FLIM imaging. Library of siRNA or non-targeting siRNA (10nM) was transfected into each set of neighbouring-wells (well number 1 and 2) containing HCC1954 cells. After 24hr, cells were transfected with Picchu-X or Picchu-X-GFP plasmid DNA and allowed further 48hr for the sensor protein to mature. Cells on well number 2 were then treated with EGF (100ng/ml) for 30min before fixation.

As anticipated, the development of this large-scale protein activity screen using FRET-based biosensor has been proven to be a major challenge. The initial review of the screen data revealed a series of flaws that fall into a few categories, which included **(1) experimental layout, (2) image acquisition and (3) data analysis.** One must standardise the screening condition carefully and design appropriate data analysis method to generate result in a meaningful way throughout the whole screening process.

(1) Experimental layout

The application of time-correlated single-photon counting (TCSPC) detection for FLIM imaging has been proven to be a powerful technique to give high resolution and sensitive readout of the donor fluorescence lifetime signals. However, long acquisition time is required to achieve reliable photon statistics. The siRNA screen was performed in 384-well plates and typically up to five minutes was required to capture each image. **Result figure 4.2.2** illustrated the problem with such long acquisition period. The scatter plot showed a gradual decrease in lifetime in the first 24 hours, followed by a much sharper decay for the rest of the samples. This drop in lifetime occurred in both samples transfected with Picchu-X **(4.2.2A)** and control donor sensor without the mRFP1 acceptor **(4.2.2B)**, suggesting presence of problem is not related to the presence or absence of the FRET acceptor. When we analysed the images carefully, we noticed a significant decrease in signal to background ratio in samples that were imaged in prolonged acquisition overnight.

For our standard cellular imaging experiments, cells were usually plated on glass coverslips and mounted on slides with mounting medium (Mowiol) mixed with DABCO (an antifading agent to prevent photobleaching). The medium was hardened as it dried overnight. For the screening experiment, medium remained in aqueous form inside 384-well-plate at room temperature due to the volume and geometry of the well, and this might be the reason affecting lifetime measurements with the increasingly unstable noise level over time. This made it very difficult, if not impossible, to compare data obtained from different regions in the optical plate.

In **Result figure 4.2.3**, we presented the reconstruction and optimisation procedures that enable us to reduce systematic errors, including plate-to-plate, temporal and spatial variability. Aliquoted siRNA solutions ready to use in experiment were store in 96-well-plates and contained 88 siRNA sequences with last column free, each well contained reagent that was directed to only one gene. This 96-well-plate was used to make two 384-well-plates to reduce the acquisition time for each 384-well-plate (see the plate layout in **Result figure 4.2.3**). The siRNA treated cells was aliquoted in duplicate; one replicate well left untreated, while the other replicate well would be treated with EGF (100ng/ml) subsequently in order to access EGF-induced biosensor conformational changes. This way, we eliminated the possible contribution of position in plate and time delay between two acquisitions, allowing us to access the effect of gene knockdown by analysing data obtained from individual set of neighbouring wells.

Multiple control wells were also present in the end of each assay plate. Control cells were treated with scrambled siRNA sequence and should not affect sensor activation after EGF treatment. Cells transfected with Picchu-X-GFP sensor (with mRFP1 acceptor cut out from the sequence) were used to calculate FRET efficiency according to the equation = 1- τ donor-acceptor/τ donor. Furthermore, only the inner 240 wells were used for imaging to reduce edge-effects and all pipetting steps were performed using the JANUS Automated Workstation to minimise pipetting errors during sample preparation, compound addition and plate washing.

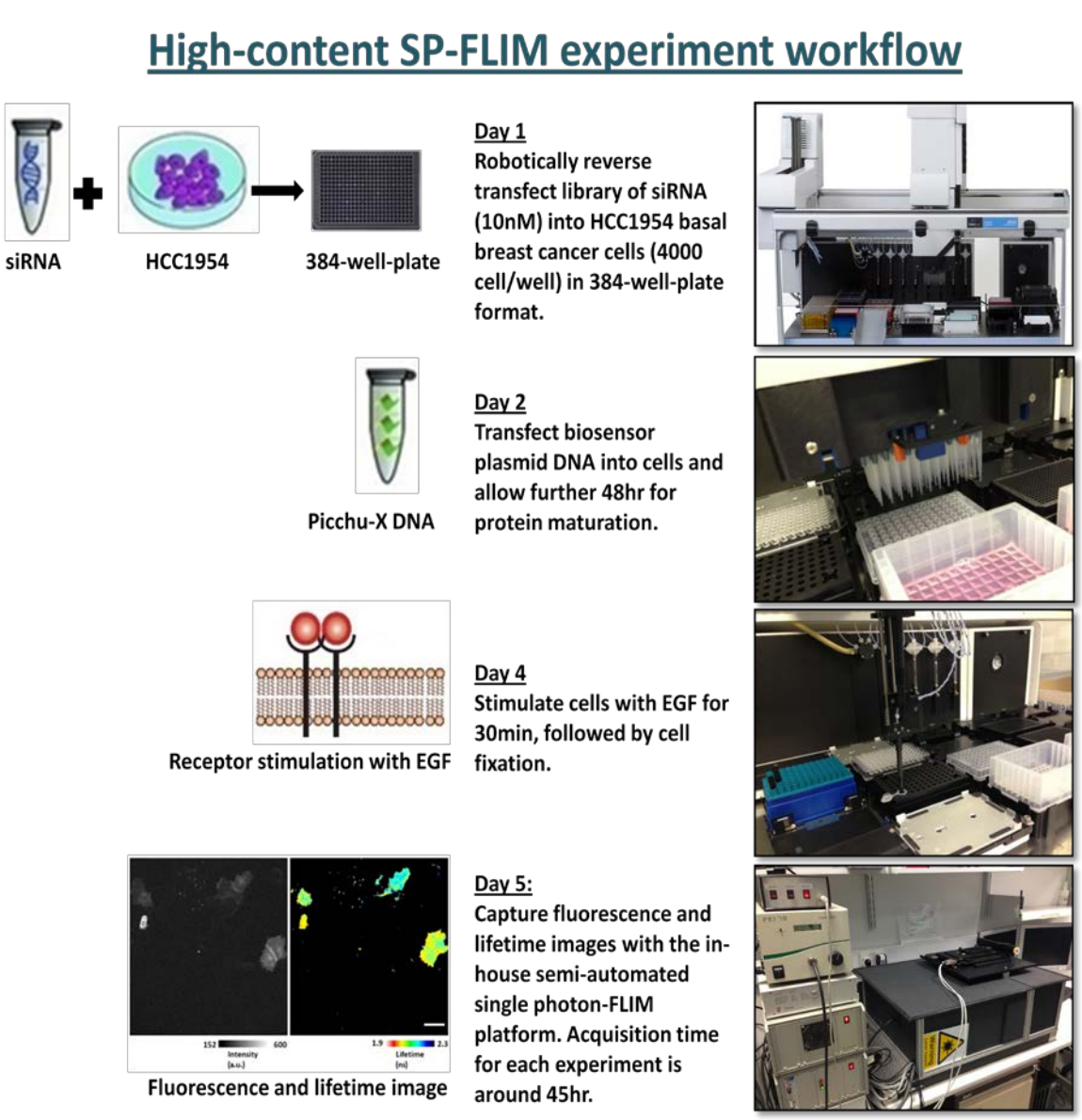

Result figure 4.2.4: The principle steps for the high-content SP-FLIM experiment with a library of siRNA consisting 533 genes interconnected with EGFR.

Result figure 4.2.4 demonstrated a simple workflow of the high content siRNA screen comprised into five different steps: reverse transfection of the library of siRNA, transfection of sensor DNA, stimulation of EGFR, fixation and image acquisition by SP-FLIM.

We conducted a primary screen applying pools of three individual non-overlapping siRNAs against the same gene in one well, by which each sequence was presented at one-third of the original concentration. 1599 siRNAs for 533 genes were pooled in seven 96-well-plates (the first six plates contained 88 genes and the seventh plate contained only 5 genes). Several siRNAs should give the same phenotypic outcome but extremely unlikely to have the same off-target effects, therefore the risk of unwanted off-target effects was lowered in the pools with the reduced concentrations of individual siRNA sequences (3.33nM), while keeping the total concentration of siRNA molecules targeting the desired gene (10nM) (Krausz 2007).

The library of pool siRNA was robotically transfected into HCC1954 cells and sensor DNA was transfected on the second day. After 72hr of gene silencing and 48hr of sensor protein maturation, one of the duplicate well was treated with EGF before fixation of the plates. Fluorescence and lifetime images were acquired using in-house semi-automated SP-FLIM.

(A)

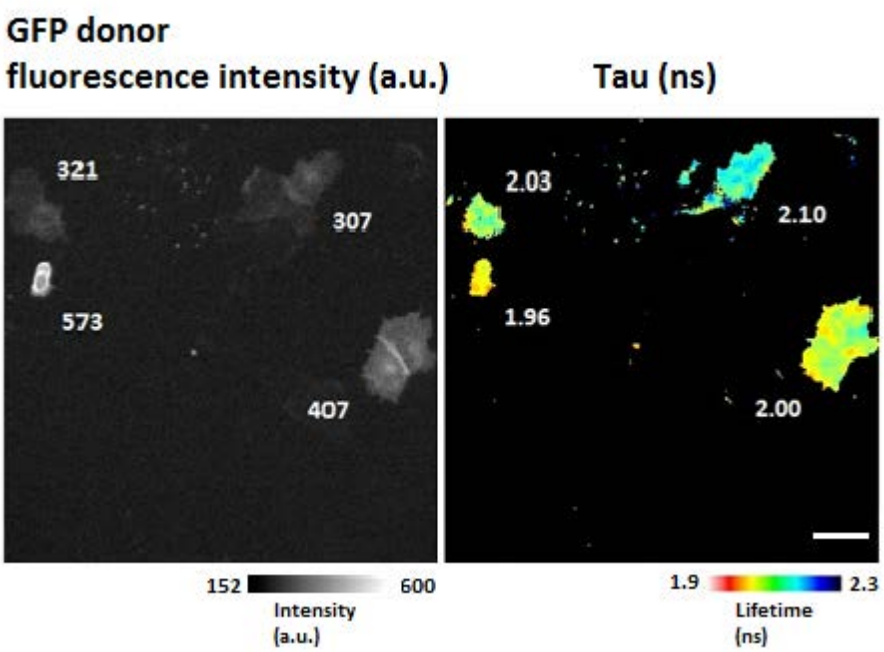
GFP donor
fluorescence intensity (a.u.)
Tau (ns)
321
307
573
407
2.03
2.10
1.96
2.00
152
600
Intensity
(a.u.)
1.9
2.3
Lifetime
(ns)

(B)

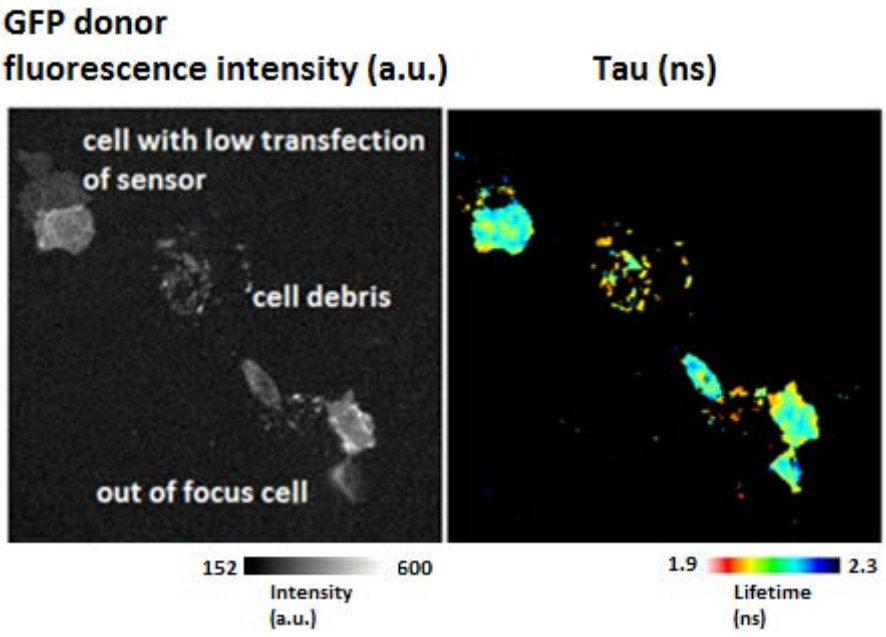
GFP donor
fluorescence intensity (a.u.)
Tau (ns)
cell with low transfection
of sensor
cell debris
out of focus cell
152
600
Intensity
(a.u.)
1.9
2.3
Lifetime
(ns)

(C)

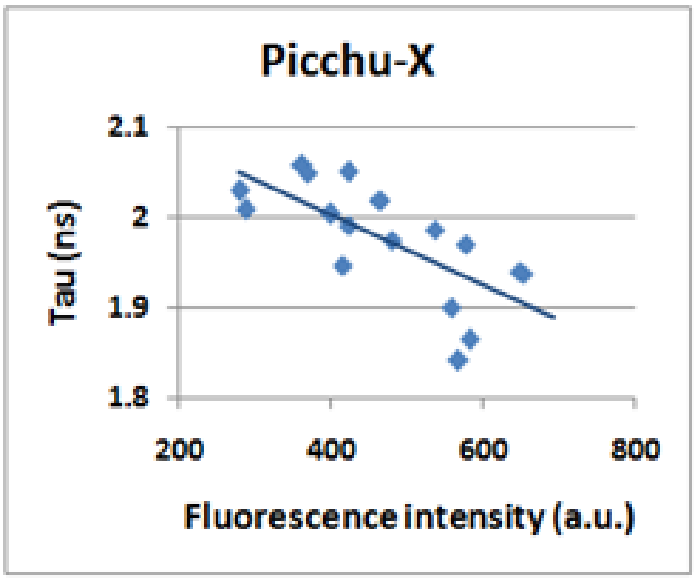

(D)

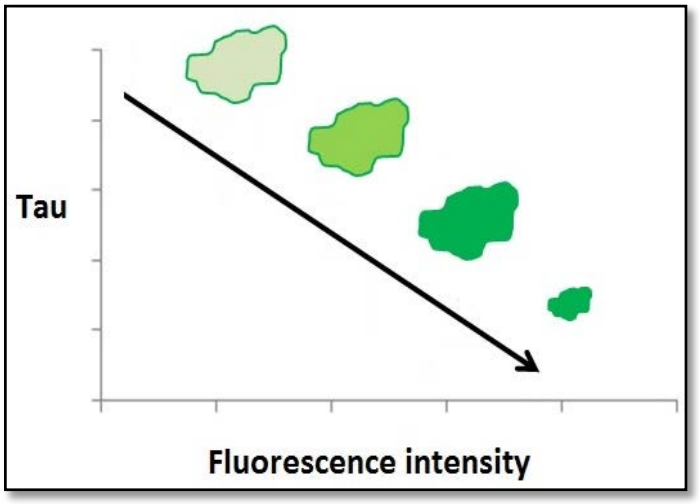

Result figure 4.2.5: Correlation between biosensor lifetime and fluorescence intensity.

Representative image of HCC1954 cells transfected with Picchu-X sensor, white scale bar represents 40µm. Images required 'cell masking' analysis (A) to extract individual values of fluorescence lifetime and intensity and (B) to remove unspecific noise, such as unfocused cell or cell debris. (C) The correlation between fluorescence lifetime and fluorescence intensity was shown in scatter plot; with each data point represented the information of one cell. (D) Diagram illustrated linear correlation between lifetime and brightness of donor fluorescence intensity.

(2) Image acquisition

The second category of error was with respect to image acquisition. It was found that the fluorescence intensity and shape of the cell could alter the lifetime of the sensor significantly, regardless of any biochemical treatment. These were taken into account during the analysis of the data.

Measured fluorescence lifetimes were plotted alongside with donor fluorescence intensities in **result figure 4.2.5A**. It was evident that these two parameters were correlated when displayed as a scatter plot **(4.2.5C)**, in which each data point represented the lifetime and fluorescence intensity measurement of an individual cell. The value was obtained by applying mask to cells using TRI2 software to get the image data only within the mask. Masking could also eliminate the noise levels which could be generated by unfocused cell, dying cell or cell debris **(4.2.5B)**. The data showed the fluorescence brightness could affect lifetime measurement, cells with higher brightness had a lower measured fluorescence lifetime comparing to less bright cells. A greater reduction in fluorescence lifetime was also observed in round cells that were entering cell division, and those cells were usually the brightest (as illustrated in **4.2.5D**). In addition, similar intensity-based fluorescence quenching effect was also found in another membrane-anchored Raichu-X probe, which was a RhoA-based sensor (Graham, Lowe et al. 2001; Yoshizaki, Ohba et al. 2003).

Since this effect on fluorescence intensity can be a constant factor affecting lifetime measurement, false positive data could be generated by measuring cell populations with different fluorescence intensity instead of measuring its true response to the growth factor stimulation. For the siRNA screen, we avoided the brightest cell population that had the most lifetime quenching due to intermolecular FRET which was unrelated to EGFR activity.

Furthermore, cell debris was avoided prior to data acquisition as we manually selected cells with phenotype that represented the normal cell population. Five view-fields per well were logged manually. The automated imaging system saved the marked x, y and z coordinates for each point. On completion of field of view marking, the system returned to each point and focussed using a high precision (auto-focus in 0.2µm lateral resolution) computer-controlled objective piezo mounting unit, then imaged consecutively for eGFP image and mRFP1 image. The system then switched automatically to laser-scanning mode to acquire the single photon data and save time-resolved images, continued in a high throughput fashion described in **Material & Method section 3.15**.

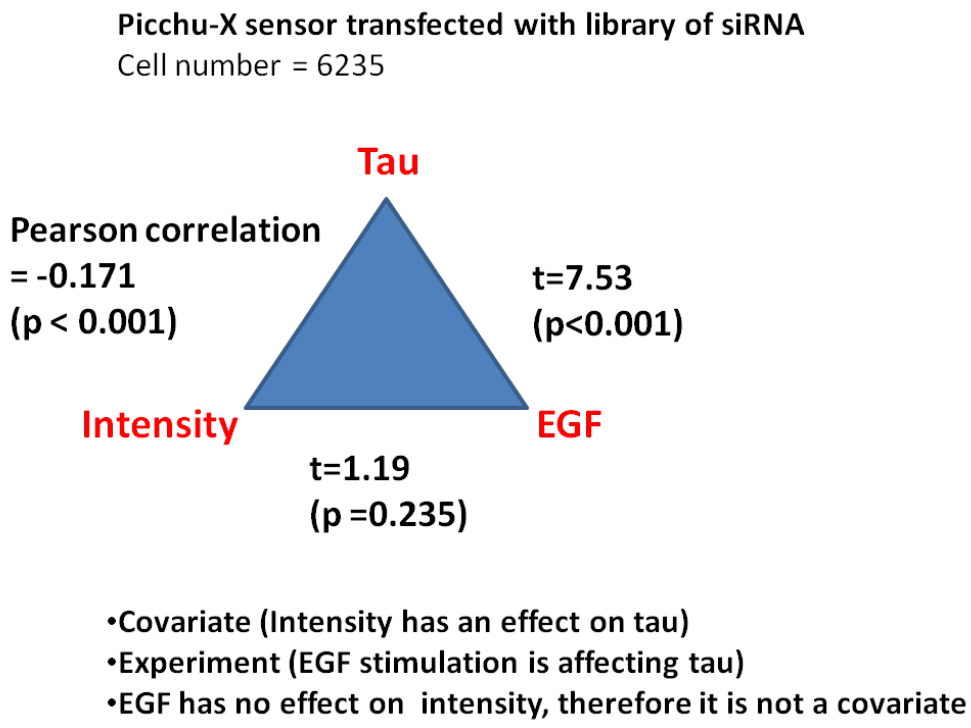

Result figure 4.2.6: Associations between biosensor lifetime, fluorescence intensity and EGF stimulation.

Fluorescence lifetime and intensity data for the HCC1954 cells transfected with the library of siRNA were imported into SPSS statistical software for correlation analysis. Pearson correlation coefficient (two-tailed) was reported for the association between intensity and Tau, statistical significant with $P < 0.05$.

(3) Data analysis

In the next couple of sections, we analysed the intensity-based variation further and developed the statistical method to analyse the FRET-FLIM data.

Once the FLIM data acquisition has been completed, the fluorescence lifetime was calculated by fitting mono-exponential fluorescence decay model. The FLIM images obtained were batch analysed using in-house exponential fitting software (TRI2) written by Dr Paul Barber (Barber, Ameer-Beg et al. 2009). These files were then analysed to produce average lifetime data. We masked the fluorescence intensity image of each cell in parallel with its lifetime image, and exported the data to SPSS software to determine the association between donor GFP fluorescence lifetime, intensity, and EGF treatment.

Large amount of cellular data was used for this analysis, cells were transfected with the siRNA library (with or without EGF treatment) (**Result figure 4.2.6**). Based on our pervious observation, we tested the hypothesis that there was a continuous variable (intensity) that was not part of the main experiment (EGF stimulation) but had an effect on the biosensor lifetime. Statistical data has confirmed this hypothesis. The Pearson correlation coefficient indicated a degree of correlation between fluorescence lifetime and intensity (= -0.171, $p < 0.001$), it showed that intensity had a constant influence on the lifetime value.

As expected, EGF also showed a significant effect on tau ($t=7.53$, $p < 0.001$), showing the response of the Picchu-X biosensor upon EGF receptor activation and underwent a change in intra-molecular folding, which promotes binding of SH2 domain to phosphorylated Tyr221 and brings eGFP in close proximity to mRFP1, thereby triggering FRET. Furthermore, there was no association between intensity and EGF treatment ($t=1.19$, $p=0.235$), showing EGF had no effect on the brightness of the cells.

(A) Scrambled non-targeting control siRNA:

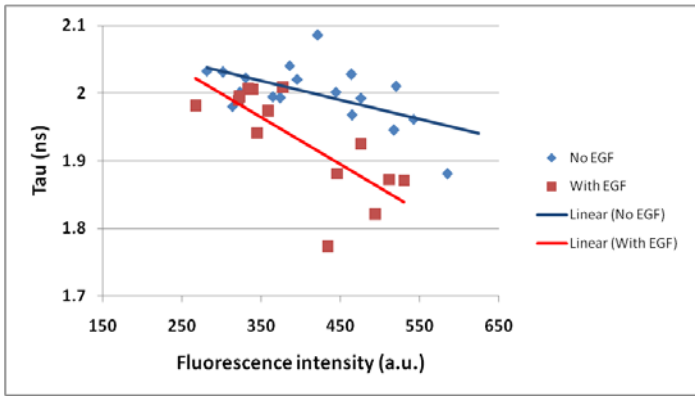

Linear regression line:

No EGF **-0.051**

With EGF **-0.141**

P value for interaction: **p=0.044**

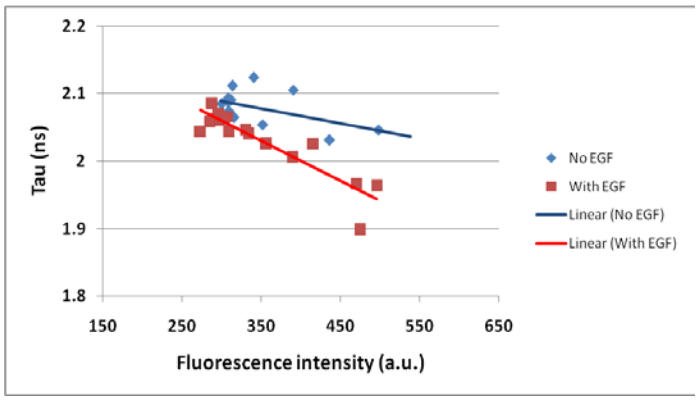

Linear regression line:

No EGF **-0.034**

With EGF **-0.102**

P value for interaction: **P=0.023**

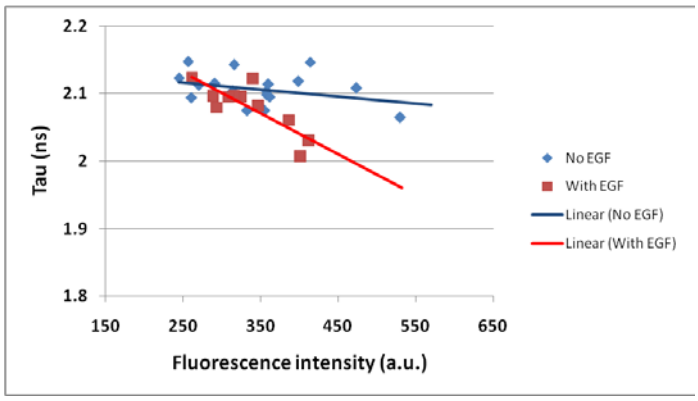

Linear regression line:

No EGF **-0.017**

With EGF **-0.089**

P value for interaction: **P=0.009**

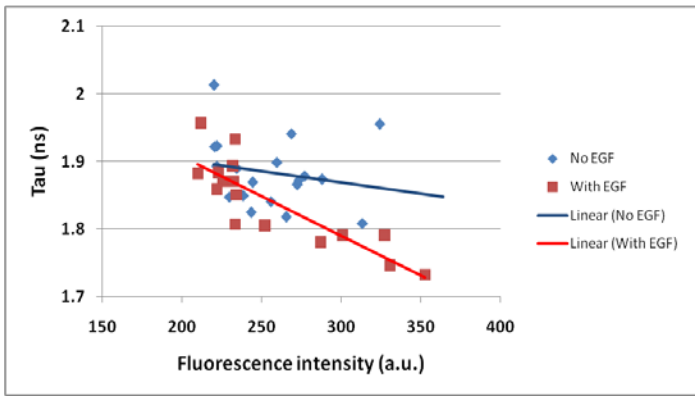

Linear regression line:

No EGF **-0.054**

With EGF **-0.177**

P value for interaction: **P=0.048**

(B) Examples from the library of siRNA classified not as hit:

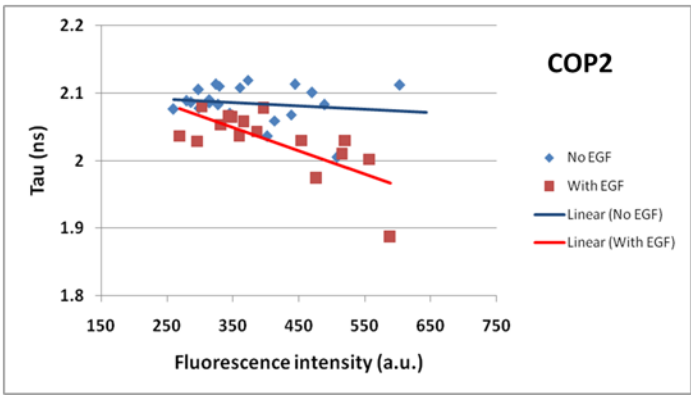

Linear regression line:

No EGF **-0.011**

With EGF **-0.069**

P value for interaction: **p=0.020**

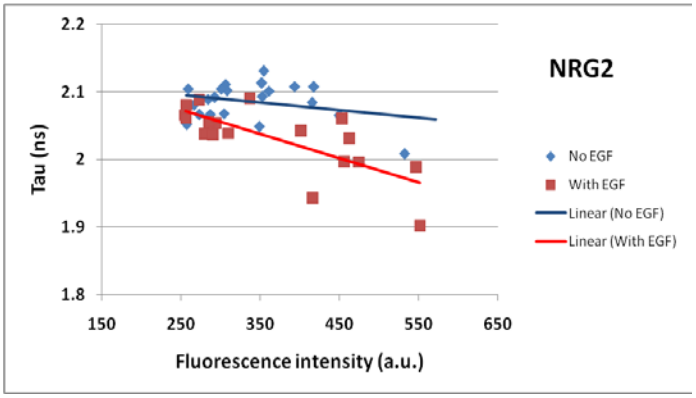

Linear regression line:

No EGF **-0.011**

With EGF **-0.066**

P value for interaction:: **P=0.024**

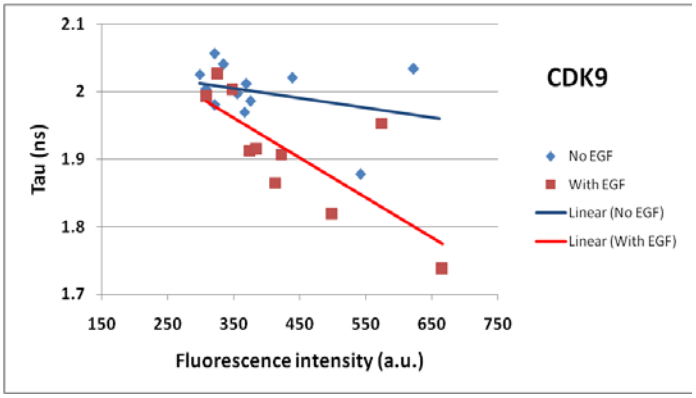

Linear regression line:

No EGF **-0.036**

With EGF **-0.150**

P value for interaction: **P=0.033**

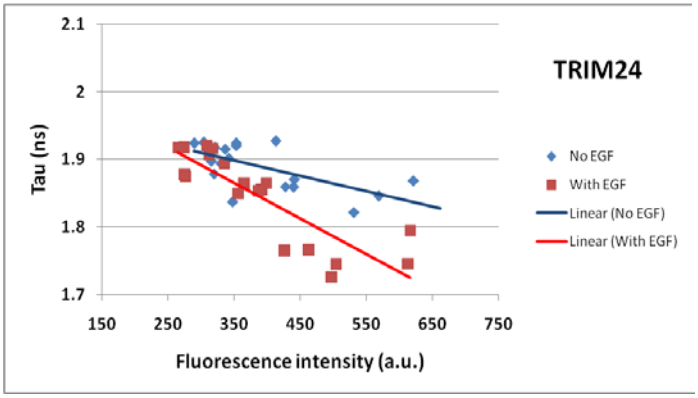

Linear regression line:

No EGF **-0.048**

With EGF **-0.119**

P value for interaction: **P=0.003**

Result figure 4.2.7: Picchu-X sensor response upon EGF stimulation for (A) non-targeting siRNA and (B) library of siRNA classified not as hit.

Tau distributions displayed as linear regression lines indicating Picchu-X sensor's response upon EGF stimulation. Blue lines represented sensor lifetime after specific gene-knockdown, while red lines represented sensor lifetime after specific gene-knockdown with EGF treatment. Linear regression models including an interaction term with EGF were performed using SPSS statistical software. The interaction term (between EGF and Tau, independently of the correlation between intensity and Tau) was statistically significant when $p < 0.05$.

Result (with control and non-hit examples)

Previously we confirmed the associations between fluorescence intensity and lifetime, and for this reason, we cannot measure the effect of EGF stimulation based on the lifetime differences alone. A linear regression model was applied to observe the effect of EGF towards this association between intensity and Tau.

To confirm the validity of our experimental approach, in **Result figure 4.2.7**, examples of the analysis for control scrambled non-targeting siRNA (**4.2.7A**) and 'non-hits' from the siRNA library (**4.2.7B**) were shown. Maximum and minimum y-axis values were set as 0.4ns apart (between 1.7 to 2.1ns or 1.8 to 2.2ns, depended on the time of acquisition/ decrease in lifetime, see Result figure 4.2.2). The parameters are described below:

-Linear regression line

Linear regression model, where Tau= slope*intensity + intercept (y= mx + c) was applied to observe the effect of EGF towards the association between intensity and Tau. An interaction term with EGF (dichotomous values, where EGF=0 or EGF=1) was included in the analysis, resulting in two linear equations of individual line. Blue lines represented sensor lifetime in cells after specific gene-knockdown; while red lines represented additional EGF stimulation.

In majority of samples, negative values were found (demonstrated as declining lines), which implied the linear relationship between fluorescence intensity and lifetime.

- P value for interaction

The Pearson correlation coefficient analysis discussed previously in **Result figure 4.2.6** identified a linear association between intensity and Tau. The primary purpose of the linear regression model was to determine the effect of EGF stimulation toward this linear association.

A T-test was reported for the association, if the p value was < 0.05 then there was a statistically significant interaction. When there was an interaction, the regression coefficient should have a low p-value of interaction, showing heterogeneity of regression lines, the gene was then classified as a 'non-hit'; whereas if no interaction was presented, the lines would be approximately parallel with a high p-value, those genes would be classified as 'hit'.

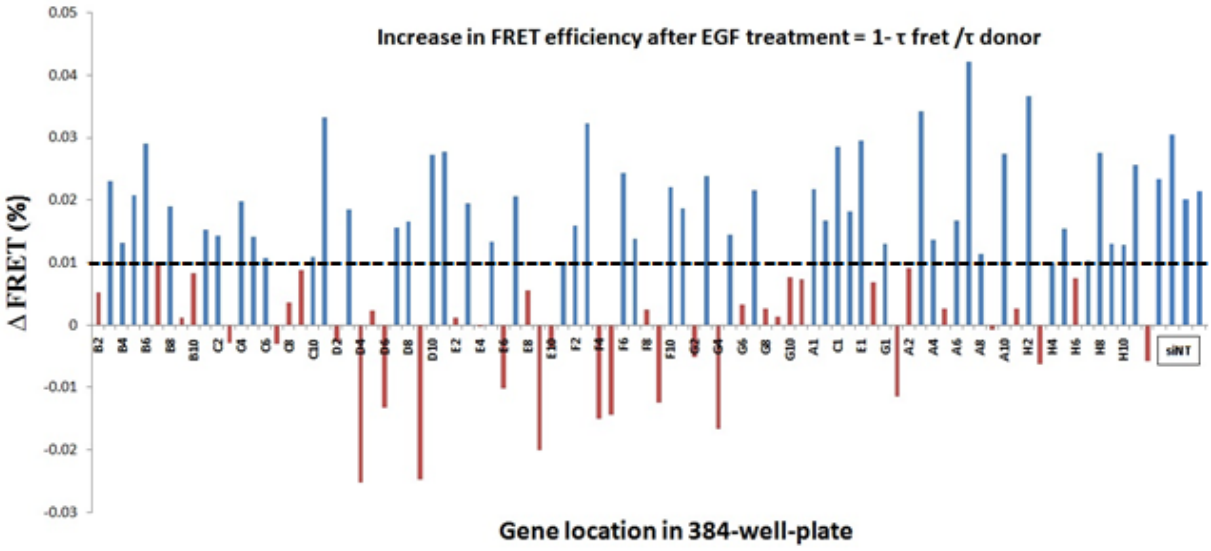

Result figure 4.2.8: Biosensor activity upon EGF treatment was calculated and possible hits were identified for further analysis.

FLIM data was analysed using TRI2 software. Average tau data was extracted to calculate biosensor response to EGF stimulation after the knockdown of each specific gene. FRET efficiency correlated to lifetime measurement = 1- τ donor-acceptor /τ donor. Genes coloured in BLUE indicated an increase in FRET efficiency after EGF treatment, hence classified as 'non-hits'; while genes highlighted in RED colour were the possible hits, which shown no increase in FRET efficiency upon EGF treatment.

In addition to the primary screen with the pooled library, we repeated the experiment using a single siRNA sequence. In total we imaged twenty four 384-well-plates in a dozen of individual experiments; each experiment acquired 980 images; whereas each image contained between three to six cells. Over 50,000 cells were imaged in total for the screen. Since we needed to use single cell data for comprehensive analysis, masking of cells was the most time-consuming, and yet important part of the analysis. Since it was impossible to individually mask and analyse each of the 50,000 cells for its fluorescence intensity and lifetime value, we designed preliminary test to eliminated non-hit samples, which responded to EGF treatment in similar manner as samples without non-targeted knockdown.

Result figure 4.2.8 showed representative results from one of the experiments containing 88 siRNAs. Each blue bar showed increase in FRET efficiency due to EGF treatment and each red bar showed samples with abolished effect of EGF due to the absence of the targeted gene. Last five bars illustrated the effect of EGF in samples transfected with scrambled siRNA as control. Genes with an increase in FRET efficiency after EGF treatment were classified as 'non-hit' and would not be selected for further analysis; genes highlighted in red colour were further processed manually to validate statistical significance of target gene on EGFR activity.

Detailed analysis was required by applying masks to cells using TRI2 software for two purposes. First reason was to eliminate the noise levels which were generated by unfocused cell, dying cell or cell debris **(as seen in Result figure 4.2.5B)**; secondly, to obtain individual fluorescence lifetime and intensity measurements in order to plot linear lines for regression coefficient analysis to identify genes that did not response to EGF-induced activation of the receptor.

(A) Possible hits that were overlapped in the first and second round of the screen.

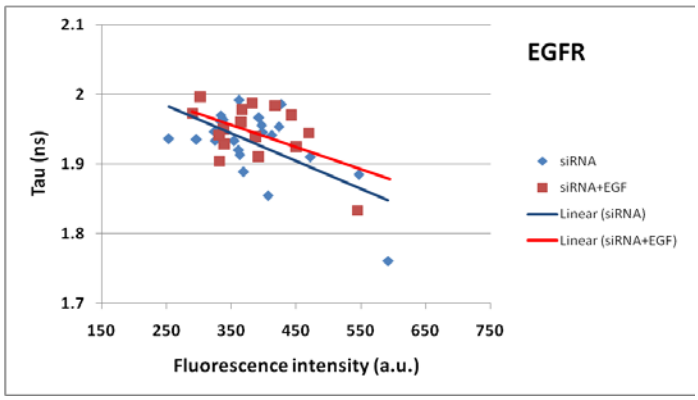

Linear regression line:

No EGF **-0.077**

With EGF **-0.062**

P value for interaction: **p=0.676**

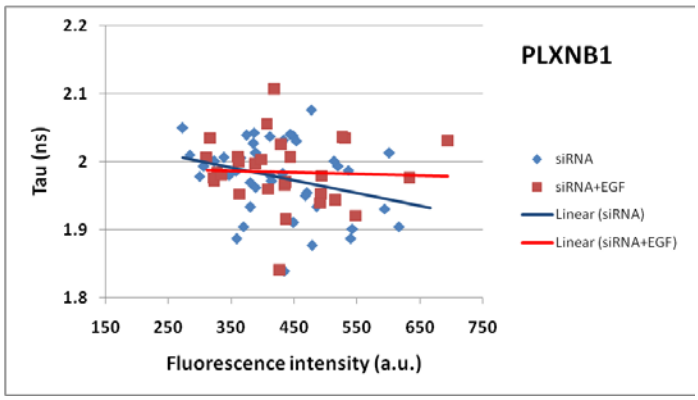

Linear regression line:

No EGF **-0.041**

With EGF **-0.009**

P value for interaction: **p=0.254**

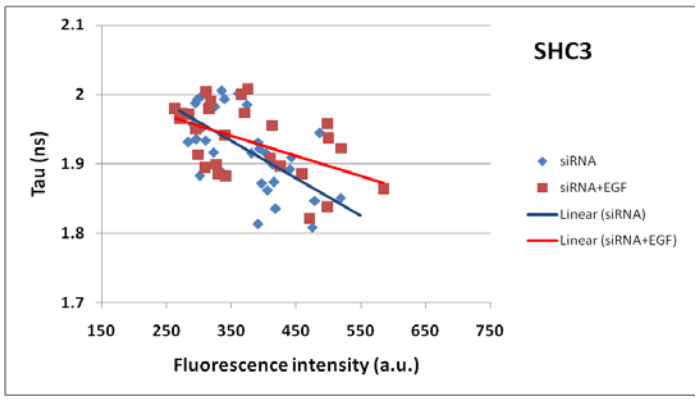

Linear regression line:

No EGF **-0.104**

With EGF **-0.059**

P value for interaction: **p=0.110**

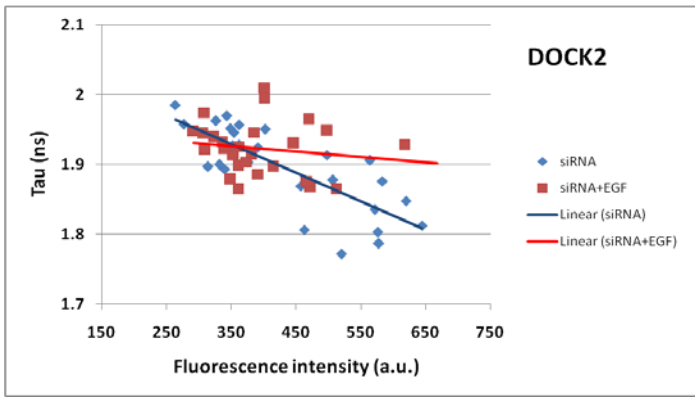

Linear regression line:

No EGF **-0.095**

With EGF **-0.019**

P value for interaction: **p=0.007**

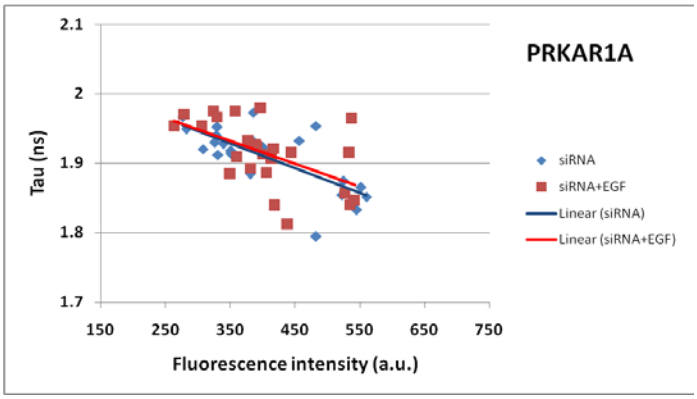

Linear regression line:

No EGF **-0.076**

With EGF **-0.071**

P value for interaction: **p=0.850**

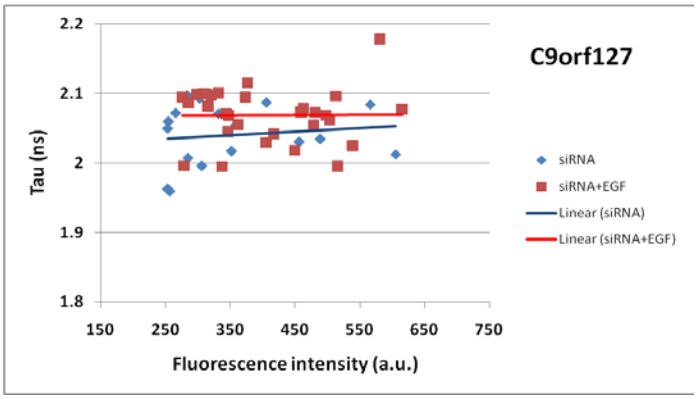

Linear regression line:

No EGF **0.120**

With EGF **-0.002**

P value for interaction: **p=0.698**

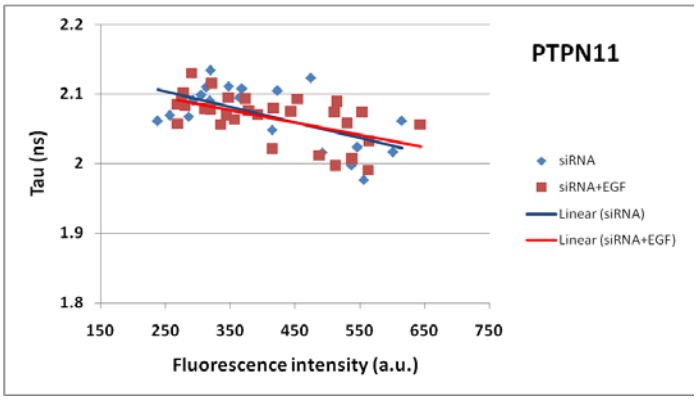

Linear regression line:

No EGF **-0.041**

With EGF **-0.035**

P value for interaction: **p=0.567**

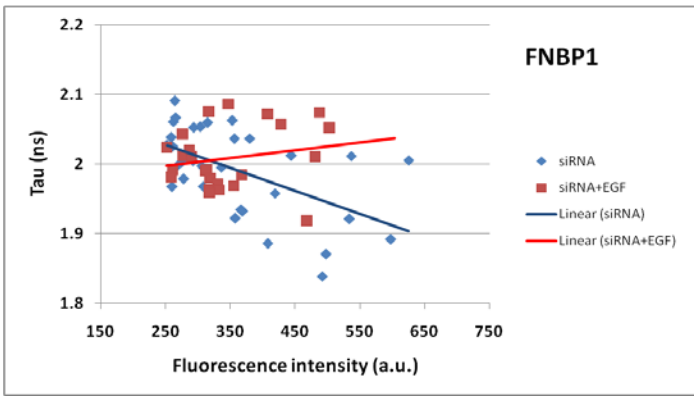

Linear regression line:

No EGF **-0.069**

With EGF **0.019**

P value for interaction: **p=0.008**

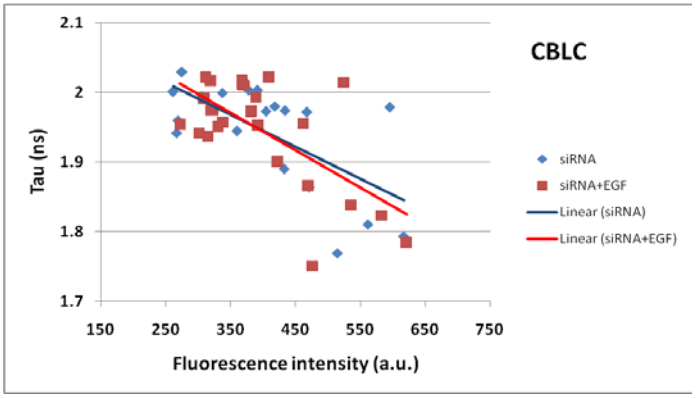

Linear regression line:

No EGF **-0.094**

With EGF **-0.114**

P value for interaction: **p=0.677**

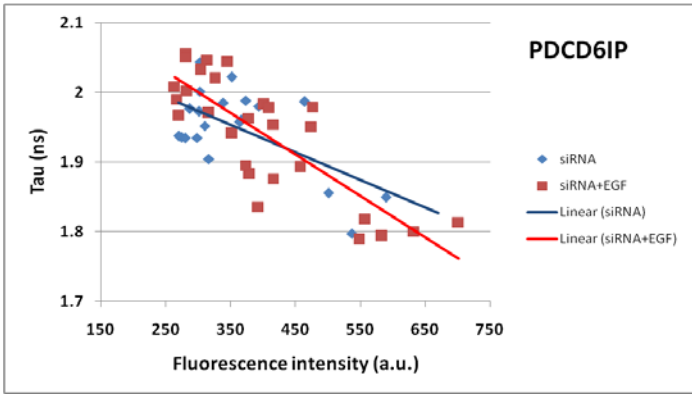

Linear regression line:

No EGF **-0.077**

With EGF **-0.132**

P value for interaction: **p=0.187**

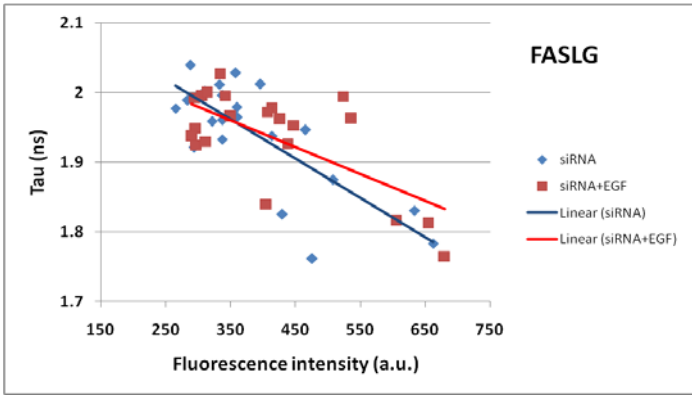

Linear regression line:

No EGF **-0.127**

With EGF **-0.084**

P value for interaction: **p=0.218**

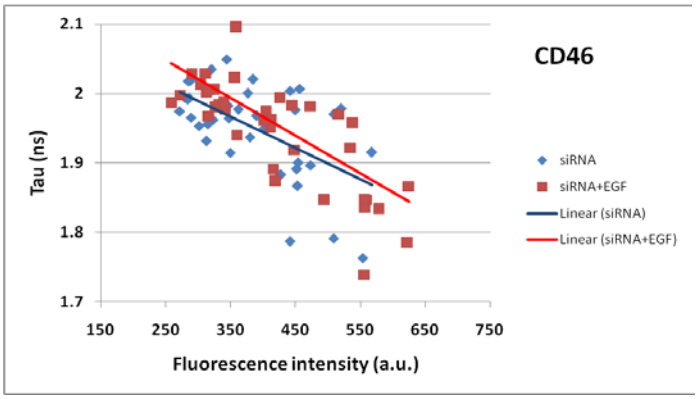

Linear regression line:

No EGF **-0.090**

With EGF **-0.115**

P value for interaction: **p=0.566**

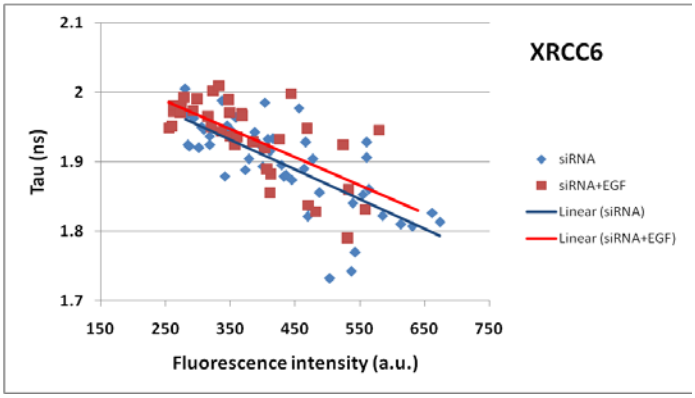

Linear regression line:

No EGF **-0.098**

With EGF **-0.081**

P value for interaction: **p=0.849**

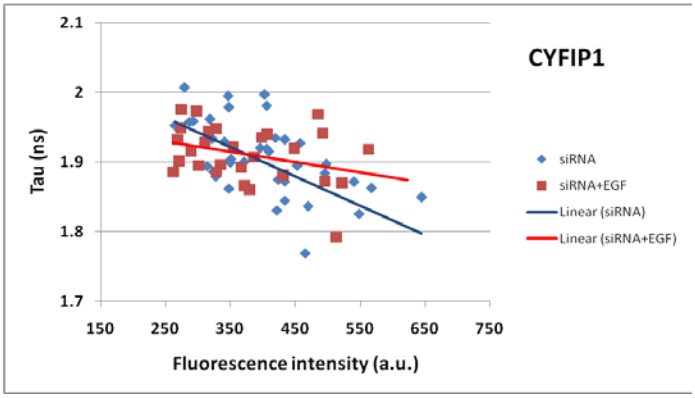

Linear regression line:

No EGF **-0.093**

With EGF **-0.030**

P value for interaction: **p=0.042**

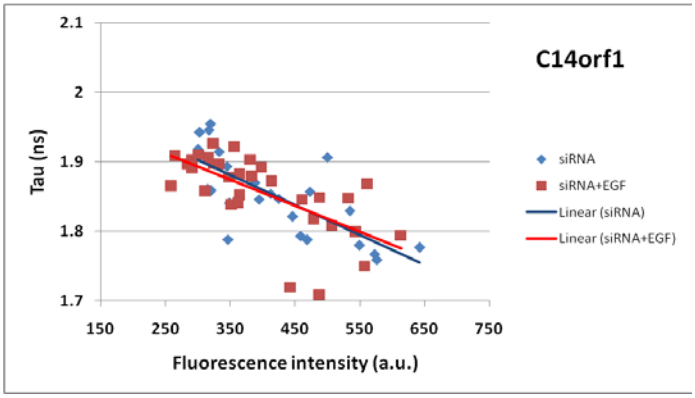

Linear regression line:

No EGF **-0.101**

With EGF **-0.083**

P value for interaction: **p=0.634**

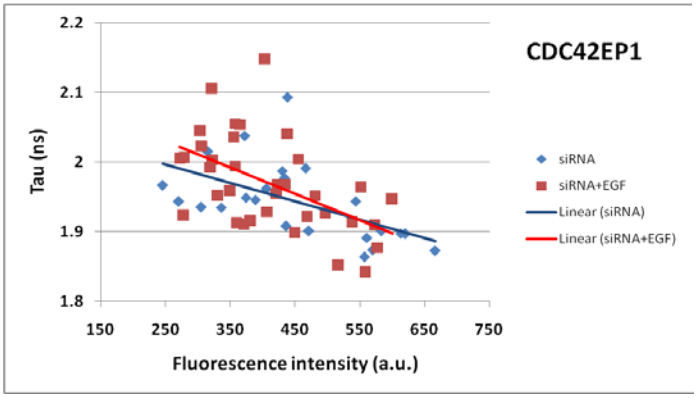

Linear regression line:

No EGF **-0.054**

With EGF **-0.078**

P value for interaction: **p=0.422**

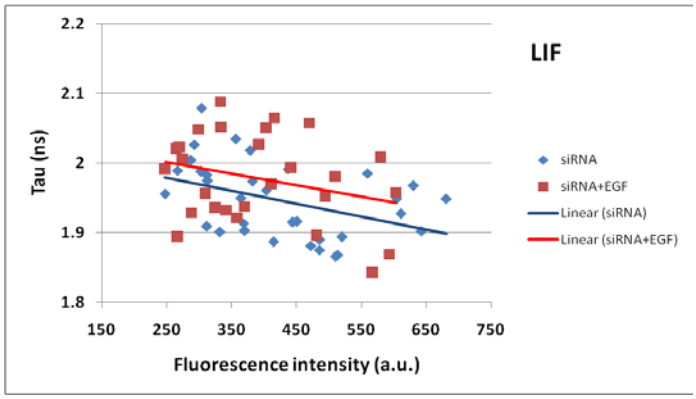

Linear regression line:

No EGF **-0.045**

With EGF **-0.030**

P value for interaction: **p=0.870**

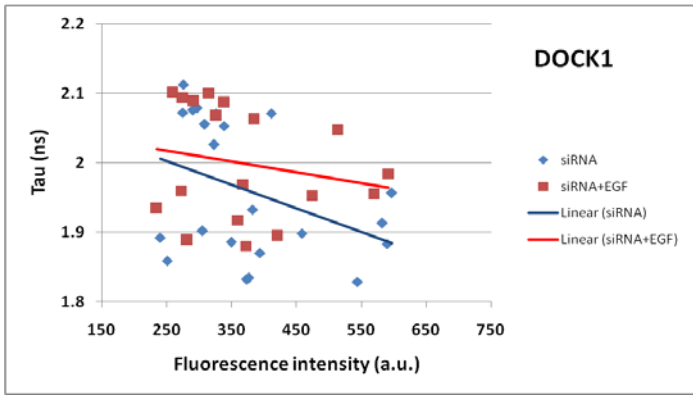

Linear regression line:

No EGF **-0.069**

With EGF **-0.030**

P value for interaction: **p=0.487**

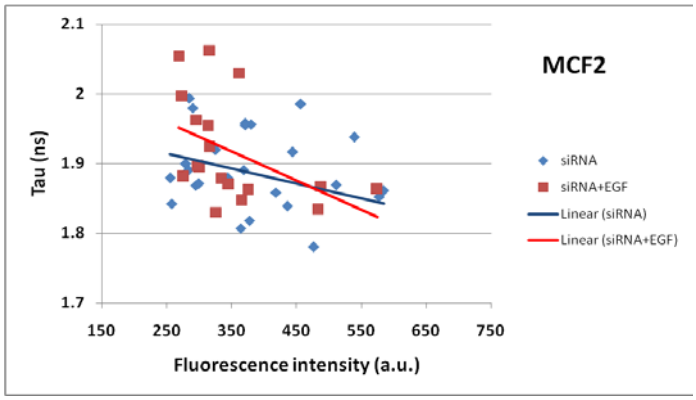

Linear regression line:

No EGF **-0.044**

With EGF **-0.090**

P value for interaction: **p=0.404**

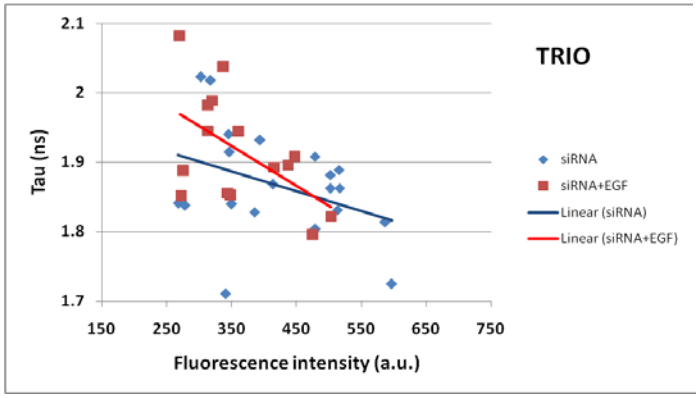

Linear regression line:

No EGF **-0.058**

With EGF **-0.107**

P value for interaction: **p=0.357**

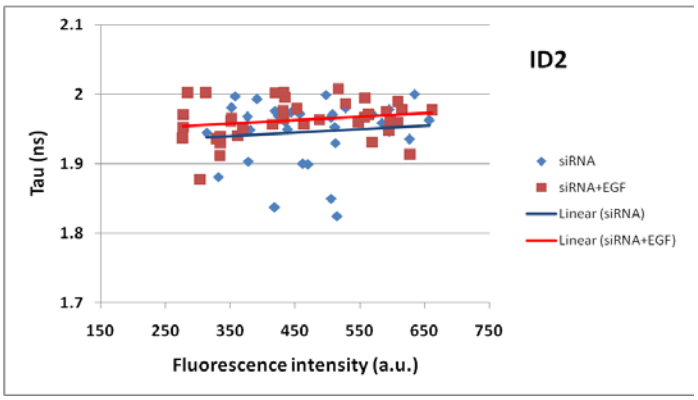

Linear regression line:

No EGF **0.010**

With EGF **0.013**

P value for interaction: **p=0.986**

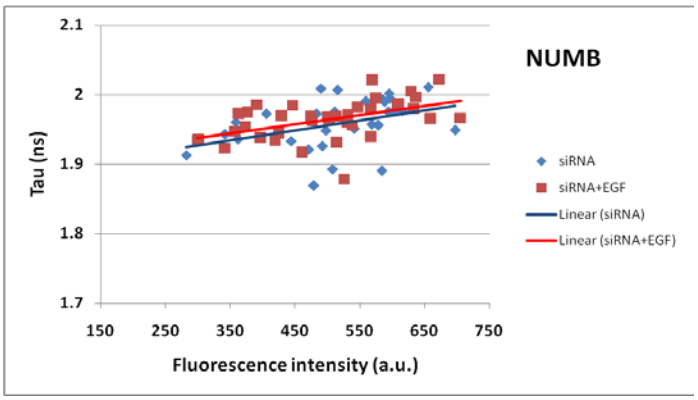

Linear regression line:

No EGF **0.034**

With EGF **0.031**

P value for interaction: **p=0.840**

Result figure 4.2.9: siRNA classified as possible hits.

Tau distributions displayed as linear regression lines indicating Picchu-X sensor's response upon EGF stimulation. Blue lines represented sensor lifetime after specific gene-knockdown, while red lines represented sensor lifetime after specific gene-knockdown with EGF treatment. Linear regression models including an interaction term with EGF were performed using SPSS statistical software. The EGF-Tau interaction term was statistically significant when $p<0.05$. When $p>0.05$ or when the +EGF slope was less steep than the –EGF slope (in case of negative values for the slopes), hits were identified.

Result figure 4.2.10: List of the 22 candidate genes that modulate EGF-induced biosensor conformational changes identified in the siRNA library screen.

Ref. Seq. Number	Gene	Brief description	Reference
NM_002673	PLXNB1	Transmembrane semaphorin receptor; coupling with c-MET	(Giordano, Corso et al. 2002)
NM_016848	SHC3	Signalling adapter; interacts with activated EGFR.	(Nakamura, Muraoka et al. 1998)
NM_004946	DOCK2	Involves in the remodelling of actin cytoskeleton; binds to SH3 domain of Crk.	(Nishihara, Maeda et al. 2002)
NM_002734	PRKAR1A	Binds to Grb2 and allows PKA interaction with the activated EGFR.	(Tortora, Damiano et al. 1997)
NM_001042589	C9orf127	Function unknown.	
NM_002834	PTPN11	Also known as SHP2; a protein tyrosine phosphatase for signal transduction.	(Tomic, Greiser et al. 1995)
NM_015033	FNBP1	Interacts with CDC42; controls actin cytoskeleton.	(Serebriiskii, Mitina et al. 2002)
NM_012116	CBLC	E3 ubiquitin protein ligase C; interacts with EGFR and CrkII.	(Keane, Ettenberg et al. 1999)
NM_013374	PDCD6IP	Programmed cell death 6 interacting protein.	(Schmidt, Dikic et al. 2005)
NM_000639	FASLG	Interaction of FAS with this ligand is critical in triggering apoptosis.	(Reinehr, Schliess et al. 2003)
NM_002389	CD46	Acts as co-stimulatory factor for T-cells.	(Schneider-Schaulies, Dunster et al. 1995)
NM_001469	XRCC6	DNA-dependent protein kinase; interacts with EGFR.	(Bandyopadhyay, Mandal et al. 1998)
NM_001033028	CYFIP1	Component of the WAVE1 complex; regulates actin filament reorganization.	(Kobayashi, Kuroda et al. 1998)
NM_007176	C14orf1	Function unknown.	(Stelzl, Worm et al. 2005)
NM_152243	CDC42EP1	Rho GTPase; regulates actin polymerization.	(Rual, Venkatesan et al. 2005)
NM_002309	LIF	Interacts with IL6ST, which is a regulator of PTPN11 (SHP2).	(Schiemann, Bartoe et al. 1997)
NM_001380	DOCK1	Downstream of Crk protein.	(Gu, Sumida et al. 2001)
NM_005369	MCF2	Modulates the Rho family of GTPases.	(Zhu, Debreceni et al. 2000)
NM_007118	TRIO	Interacts with Rac1 and Rho guanine nucleotide exchange factor.	(Medley, Serra-Pages et al. 2000)
NM_002166	ID2	Inhibitor of DNA binding.	(Jogi, Persson et al. 2002)
NM_001005743	NUMB	Interacts with Notch1; plays a role in the process of neurogenesis.	(McGill and McGlade 2003)
NM_005228	EGFR		

Result (identified hits)

To identify regulators of the EGFR signalling pathway, we performed a siRNA screen containing 533 genes. After 72hr of gene silencing using the library of siRNA, majority of the samples reacted to the EGF treatment, showing that these genes were not involved in the regulation of the receptor tyrosine kinase function of EGFR. In comparison, a minority of the genes might have knocked down an important regulatory component and abrogated the effect of growth factor (EGF) stimulation on the sensor conformation. Individual fluorescence lifetime and intensity measurements were used for regression coefficient analysis. We elevated the candidate genes by comparing homogeneity of the linear regression lines. The same parameters were previously described in **Result figure 4.2.7**.

The scatter plots for all the candidate hits were showed in **Result figure 4.2.9** along with the statistical analysis. In the initial screen using the independent siRNA pools, 84 genes were identified as candidate hits; while 74 genes were indentified in the second screen using single siRNA sequence. Including EGFR, 22 genes overlapped between the two screens, which were 4.1% of the siRNA library.

For the candidate hits, no interaction between the lines was presented. The lines were approximately parallel and had high p-values for interaction (for EGFR, p= 0.676).

The siRNA screen had the potential to knock down an important signal transduction molecule or a crucial component of the signalling complex, led to delayed or lost of communication between EGFR and its downstream signalling targets. **Result figure 4.2.10** contained some information of the genes classified as potential hits, including the reference sequence number from the library and brief description on each gene with the corresponding reference. The reported activity could be directed to the communication between EGFR and CrkII protein, or reporting on CrkII protein alone.

(A) **(B)**

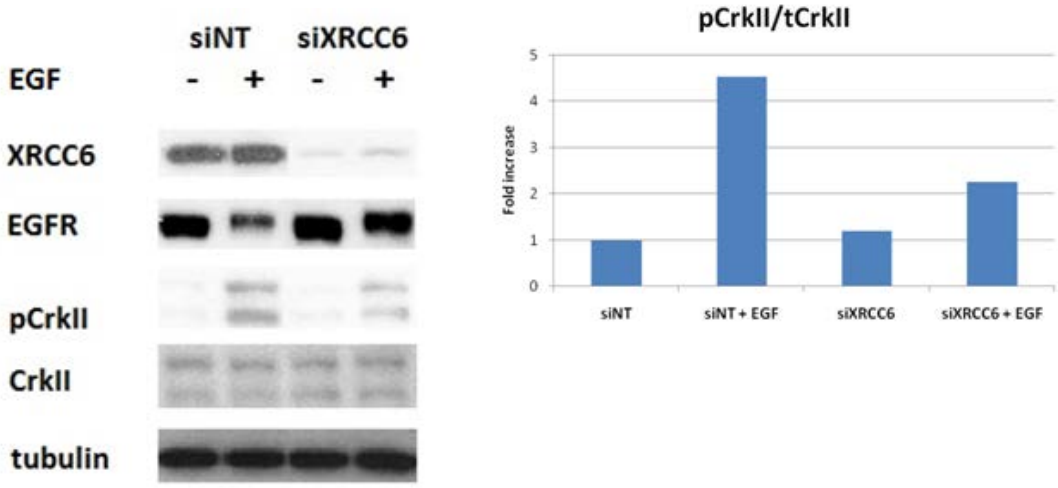

Result figure 4.2.11: Retention of EGFR and reduction of sensor activity after XRCC6 silencing.

(A): HCC1954 cells were transfected with 10nM of non-targeting siRNA (siNT) or siRNA against XRCC6 for 72hr. Cell lyses were collected with or without further treatment of EGF (10ng/ml) for 30min. Immunoblots were carried out using the antibodies indicated above. (B) Western blot results were analysed with Quantity One software. Bar chart indicated phosphorylation level of CrkII, normalised to total expression of the respective protein.

After identified the background mechanisms that were published in the literature (**see Chapter 5 discussion section**), we decided to validate the role of three putative hits, XRCC6 (p=0.849), PDCD6IP (p=0.187) and PTPN11 (p=0.567). PDCD6IP and PTPN11 are the subject of investigation by Dr Ruhe Choudhury and Miss Appitha Arulappu, respectively, as part of their PhD doctorate studies.

Effect of XRCC6 on EGFR signalling pathway and receptor degradation

Binding of EGFR ligand can stimulate EGFR nuclear transport which was linked to gene transactivation (Friedmann, Caplin et al. 2004; Brand, Iida et al. 2011). Nuclear EGFR is localised on the nuclear membrane and in the nucleoplasm (Lo, Cao et al. 2010). EGFR moves from the outer nuclear membrane to the inner nuclear membrane via interaction between importin β and the nuclear pore complex, whereas Sec61 interacts with EGFR and release the receptor from the inner nuclear membrane to the nucleus (Wang, Yamaguchi et al. 2010).

Importantly, the level of nuclear EGFR correlates with poor prognosis in a variety of cancers, including breast carcinomas (Hadzisejdic, Mustac et al. 2010; Bau, Tsai et al. 2011). Nuclear EGFR functions as a transcription cofactor that interacts with DNA-binding transcription factors (such as STAT3 or Cyclin D1) and DNA dependent-protein kinase (DNA-PK), which is required for repairing double strand DNA breakages (Friedmann, Caplin et al. 2006; Hsu, Miller et al. 2009; Liccardi, Hartley et al. 2011).

DNA-PK consists of heterodimeric regulatory complex XRCC5/XRCC6 (XRCC5 also known as ku80, while XRCC6 also known as ku70) and a large 460kDa catalytic subunit (Bandyopadhyay, Mandal et al. 1998; Collis, DeWeese et al. 2005; Martinez, Seveau et al. 2005). Although XRCC5 and XRCC6 are primarily found in nuclei, these proteins can also be found in the cytoplasm and at the plasma membrane (Prabhakar, Allaway et al. 1990; Koike 2002). Physical interaction between EGFR and XRCC5/XRCC6 was demonstrated in response to anti-EGFR monoclonal antibody treatment (Bandyopadhyay, Mandal et al. 1998) and in response to ionizing radiation, resulted in increased repair of DNA strand breaks (Liccardi, Hartley et al. 2011).

To functionally characterise the regulatory role of XRCC6 on EGFR signalling, we measured its ability to modulate CrkII-based sensor activity in response to ligand stimulation through EGFR by immunoblotting. We confirmed the expression of XRCC6 in the HCC1954 basal-like breast cancer model and verified the knockdown efficiency of the XRCC6-targeting siRNA (**Result figure 4.2.11, first row**). With the silencing of XRCC6, two-fold decrease in the ligand-induced phosphorylation of the Picchu-X sensor (**third row**) was seen, in comparison to the control with non-targeted knockdown using scrambled siRNA.

A transient signalling complex composed of adaptor proteins and effectors is assembled following the activation of EGFR. For the regulation of signal output, this process is carefully coordinated by negative regulatory mechanisms by promoting

receptor internalization (mediated by clathrin), and subsequent ubiquitination and degradation of both ligand and receptor molecules by ubiquitin ligase Casitas B-lymphoma (Cbl). The receptor can also undergo recycling to the plasma membrane (Yarden 2001; Dikic and Giordano 2003; Lemmon and Schlessinger 2010; Avraham and Yarden 2011). XRCC6 knockdown demonstrated an impaired intracellular degradation of the receptor (**second row**), suggesting that XRCC6 might interfere with normal EGFR signalling pathway and diminish receptor degradation.

Knowledge of such genes will advance our understanding the role of nuclear EGFR in basal-like breast cancer, and help clarify some of the molecular mechanisms underlying the observed association between nuclear EGFR and poor clinical outcome.

Chapter summary

In summary, we reported for the first time an integrated high-content high-throughput workflow that combined two powerful methods of cell biology and molecular imaging: siRNA screening and FLIM imaging using intra-molecular FRET-based biosensor.

These protein activity sensing/imaging techniques allowed us to interrogate an EGFR-centric subnetwork of proteins consist of 533 genes interconnected with EGFR directly or indirectly. We identified 22 candidate genes that have a potential in regulation of EGFR signalling pathway in basal-like breast cancer cells.

The screen increased our knowledge about molecular factors that may influence the therapeutic sensitivity of the EGFR network and might be translated to potential prognostic or predictive biomarkers for better understanding of tumour cell sensitivity to EGFR inhibition and may thereby suggest new combination treatments.

4.3: Liposomal transfection of Picchu-X sensor to measure intratumoural EGFR activity

Chapter introduction - Liposomal transfection of Picchu-X sensor to measure intratumoural EGFR activity

In previous chapters, we studied the dynamics of EGFR activity in a variety of cells lines and its modulation by known EGFR inhibitors using the modified FRET-based sensor (Picchu-X), providing the basis for the next phase of the project, which was to develop multifunctional EGFR-targeted liposome and to address the liposomal potential on intratumoural activity sensing in murine models of basal-like breast cancer. This part of the project was cooperated with Professor Alethea Tabor's laboratory, with the synthesis of liposome was carried out by Dr Nick Mitchell at University College London, while all cell-based and animal works were done in Professor Tony Ng's laboratory at King's College London.

We presented here a cellular and *in vivo* delivery system that was based on these nanoliposomes. These multifunctional liposomes were conjugated with EGFR-targeting peptides for the delivery of biosensor-encoding DNA. Once the transfection conditions were optimised in the cellular system, we applied the liposomes intravenously into established xenograft models of basal-like breast cancer. This approach allowed us to study the dynamics of EGFR activity in the primary tumours and demonstrated a significant degree of intratumoural heterogeneity in EGFR activity, as well as its modulation by EGFR tyrosine kinase inhibitor, Morpholino-IPQA.

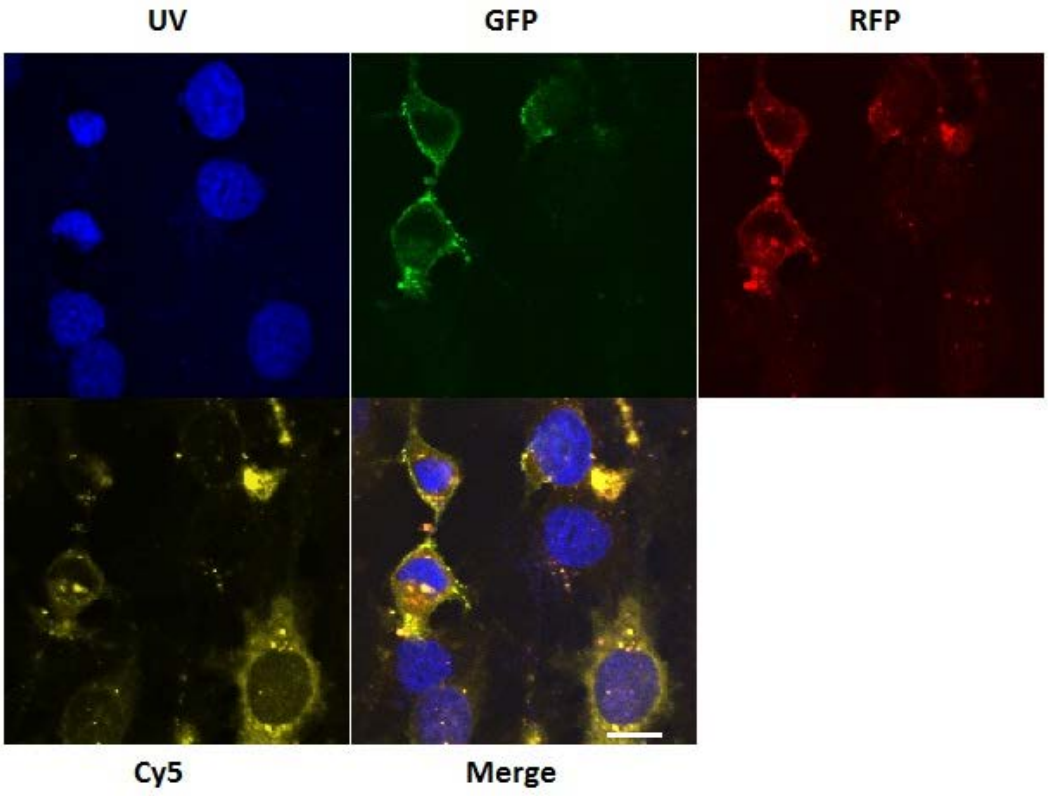

Result figure 4.3.1: Confocal fluorescence study of liposomal transfected HCC1954 cells.

Confocal fluorescence images demonstrated the expression of membrane-bound Picchu-X sensor (green and red) in liposomal transfected HCC1954 cells. Liposome contained 5% Cy5-labelled lipid (yellow) and nuclei was stained with Hochst33342 (Blue), white scale bar represents 20µm.

We aimed to develop a lipid-based nanoparticles delivery system to formulate serum-stable liposomes for effective delivery of the FRET-based sensor to study the dynamics of EGFR activity in murine model of basal-like breast cancer.

Liposomal transfection of Picchu-X sensor

Cellular experiments were performed to check liposomal transfection efficiency. We found that most transfection events took place in the first few hours of the incubation period within the culture wells. High concentration of liposome solution (> 50μM) together with longer length of incubation (longer than 4 hours) was shown to cause cytotoxicity to most cells. The optimum liposome concentration was established to be 10μM and the damage was much less severe even without washing away the unbound liposome after the initial 4-hour incubation period. Cells were left in incubator for further 48 hours to allow the expression of Picchu-X sensor protein.

Confocal fluorescence microscopy studies of the intracellular fate of liposome lipid and the transfected sensor was shown in **Result figure 4.3.1**. We observed the membrane expression of Picchu-X sensor (**green for eGFP and red for mRFP1**) in some of the HCC1954 cells and various amount of Cy5-labelled lipid intake (**yellow**) was either distributed throughout the cytoplasm or confined to endocytic vesicles distributed in almost all cells. This observation showed that Cy5-labelled lipid intake was not an indicator for DNA plasmid transfection as the sensor did not necessary expressed in all the cells that were transfected with liposome.

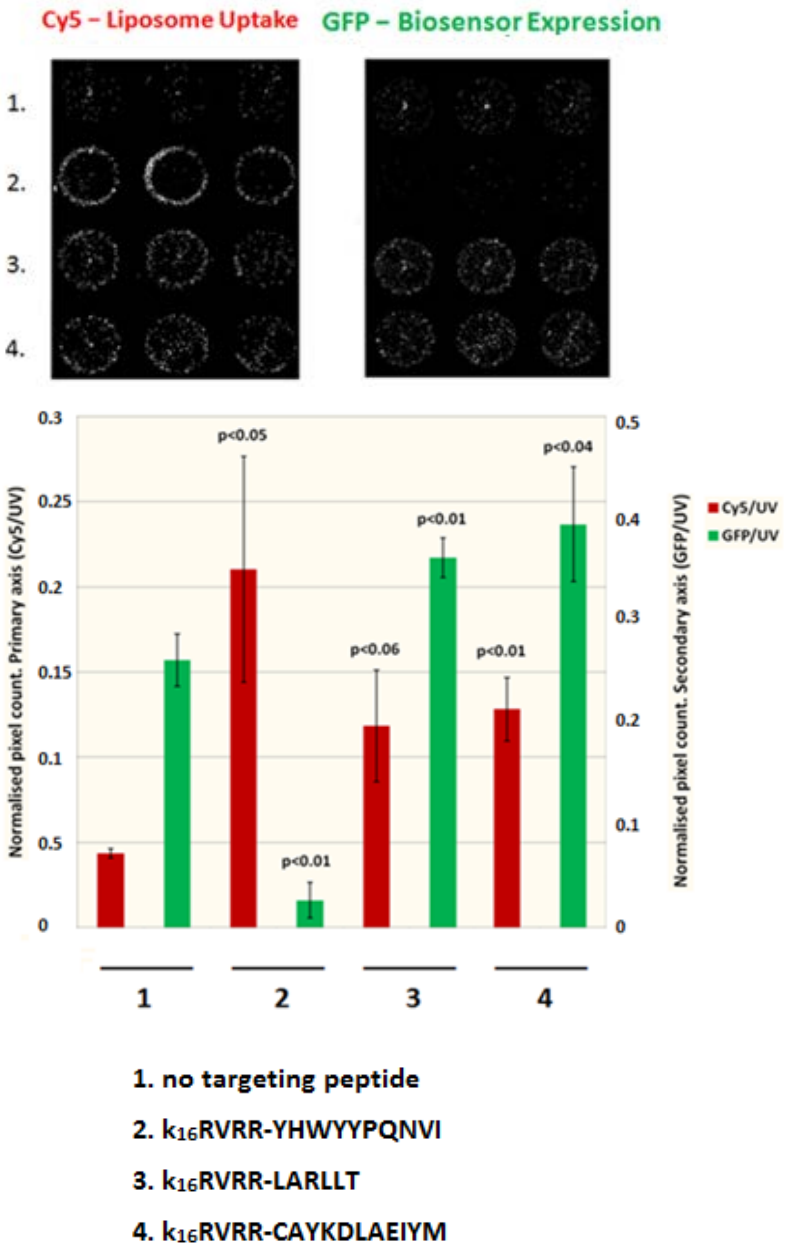

1. no targeting peptide

2. k_{16}RVRR-YHWYYPQNVI

3. k_{16}RVRR-LARLLT

4. k_{16}RVRR-CAYKDLAEIYM

Result figure 4.3.2: Selection of targeting peptides for the enhancement of liposomal uptake and DNA transfection.

Liposomes were modified with a panel of targeting peptides to enhance liposomal uptake in MDA-MB-231 cells. Epifluorescence intensity was scanned using motorized microscope system. ImageJ software was used for the analysis of normalised-pixel count (Cy5/UV for liposomal uptake and GFP/UV for DNA transfection). All complexes were prepared at 4:1 weight ratio of lipid to DNA.

Selection of targeting peptides to enhance liposomal uptake and DNA transfection

Further optimization steps were done to strengthen the efficiency and specificity of liposomal transfection. **Result figure 4.3.2** has shown that the small structural difference in the selection of peptide sequence for receptor targeting could result in pronounced differences in liposomal uptake and DNA transfection.

All liposomes contained PEG-shielding polymer in additional to DOTMA, DOPE and 30% cholesterol, which were the constituent lipids used in all formulations. We used bifunctional targeting peptide designed to both condense the DNA through the K16 (lysine-rich) region, and to facilitate EGFR specific receptor-mediated transfection. Pervious *in vitro* transfection studies revealed that ternary formulations of lipid:peptide:DNA (LPD) complexes possessed higher transfection activity compared to their respective lipid:DNA (LD) counterparts (Kudsiova, Fridrich et al. 2011). It has been recognised that the installation of targeting peptides could lead to more efficient internalization via receptor-mediated endocytosis and consequently higher transfection efficiency (Mustapa, Bell et al. 2007; Kudsiova, Fridrich et al. 2011). All complexes were prepared at 4:1 weight ratio of lipid to DNA.

MDA-MB-231 cells were incubated with Cy5-labelled liposome carrying no targeting peptide (K16 alone), or with purified EGFR-targeting peptide LARLLT, YHWYYPQNVI, or synthetic fragment of EGF CAYKDLAEIYM (Park and Yoo 2010). These peptides passed through the lipid bilayer and were exposed on the exterior surface of the

liposome complex. These peptides were connected to K16 by an enzymatically cleavable linker sequence RVRR, which was recognised by the endosomal proteases cathepsin B and furin, to allow removal of the PEG moiety and detachment of the nanocomplex from the receptor (Mustapa, Grosse et al. 2009; Grosse, Tagalakis et al. 2010).

Fluorescence emission signal was scanned using motorised microscope system described in **Material & Method section 3.15**. Signal for Picchu-X sensor was scanned in Cy2 channel (eGFP), signal for lipid intake was scanned in Cy5 channel (Cy-5 labelled lipid) and nuclei signal was scanned in UV channel (Hoechst33342). ImageJ software was used for the analysis of normalised-pixel count. Liposome uptake ratio was calculated by Cy5/UV, while sensor expression was calculated by GFP/UV.

As shown in **Result figure 4.3.2**, sensor expression were found in cells that were applied with liposome carrying no targeting peptide (K16 alone), indicating that DNA can be transfected by unspecific passive uptake through electrostatic interactions inside the cell culture system.

A 4.7-fold increase of liposomal uptake was observed with the addition of YHWYYPQNVI comparing to K16 control ($p < 0.05$), but with significantly lower expression of sensor protein (12.7-fold decrease, $p < 0.01$). This might be due to the poor endosomal release of the liposome or enzymatic degradation of the DNA in

the endosomal/lysosomal compartment (Kudsiova, Fridrich et al. 2011). In contrast, the presence of peptide sequences LARLLT and CAYKDLAEIYM showed enhancements in both liposomal uptake and transfection of sensor DNA comparing to K16 control without receptor targeting.

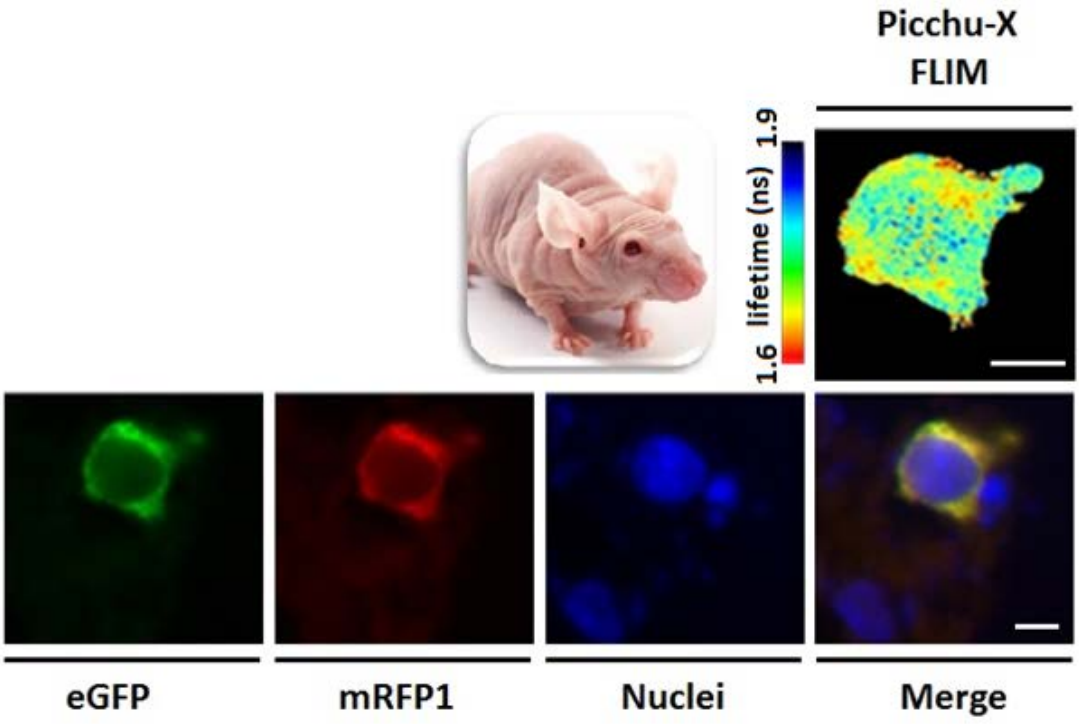

Result figure 4.3.3: Picchu-X sensor expression in xenograft model of MDA-MB-231 basal-like breast cancer.

Representative lifetime and fluorescence images of *in vivo* liposomal transfection of Picchu-X sensor-encoding DNA into primary tumour of MDA-MB-231 xenograft model of basal-like breast cancer. Nuclei were stained with Hoechst33342, white scale bar represents 10µm.

The major goal for this part of the project was the generation of multifunctional liposomes, which are loaded with lipids that carry EGFR-target peptide for cell recognition, small molecule inhibitor for inhibiting EGFR kinase activity, and DNA encoding FRET-based biosensor for measuring EGFR kinase activity.

***In vivo* liposomal delivery of Picchu-X sensor**

After the optimization of the LPD formulation in the cellular system, we tested the liposomal delivery method *in vivo* using the highly metastatic MDA-MB-231 basal-like breast cancer model. We included the CAYKDLAEIYM peptide sequence in the liposome formulation for the selective targeting of EGFR due to the enhancements in liposomal uptake (2.8-fold increase, $p < 0.01$) and transfection of sensor DNA (1.6-fold increase, $p < 0.04$) compared to K16 control without receptor targeting in the cellular system (**see Result figure 4.3.2**).

The liposome injection was performed three weeks after subcutaneously injection of cancer cells into four-week-old female Crl:CD1-Foxn1 nu/nu mice. The liposome solution was injected through tail vein into the animal and was allowed 48 hours for the Picchu-X sensor protein maturation. The liposome solution was also applied on monolayer of cultured cell to confirm the transfection efficiency of the batch used for tail vein injection. Solid primary tumours were dissected out and snap-frozen in liquid nitrogen. Frozen tumours were cut into 4µm sections with a cryostat for time-resolved multi-photon-FLIM imaging experiments.

As shown in **Result figure 4.3.3**, membrane expression of Picchu-X biosensor was observed in the primary tumour samples, with the eGFP and mRFP1 fluorescence signals associated with individual nucleus of the transfected cell. We measured an average lifetime of 1.795ns for MDA-MB-231 model; the lifetime value was comparable with the *in vitro* imaging data.

(A)

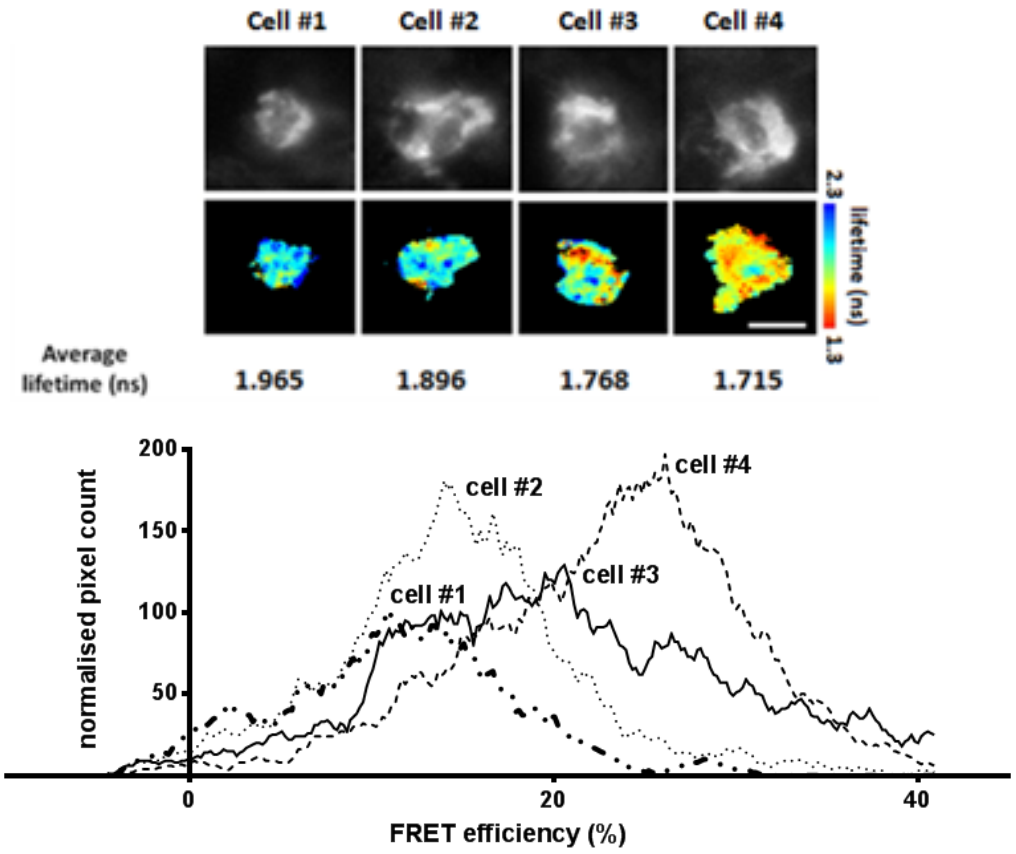
Cell #1
Cell #2
Cell #3
Cell #4
2.3
lifetime (ns)
1.3
Average lifetime (ns)
1.965
1.896
1.768
1.715
normalised pixel count
200
150
100
50
0
20
40
FRET efficiency (%)
cell #1
cell #2
cell #3
cell #4

(B)

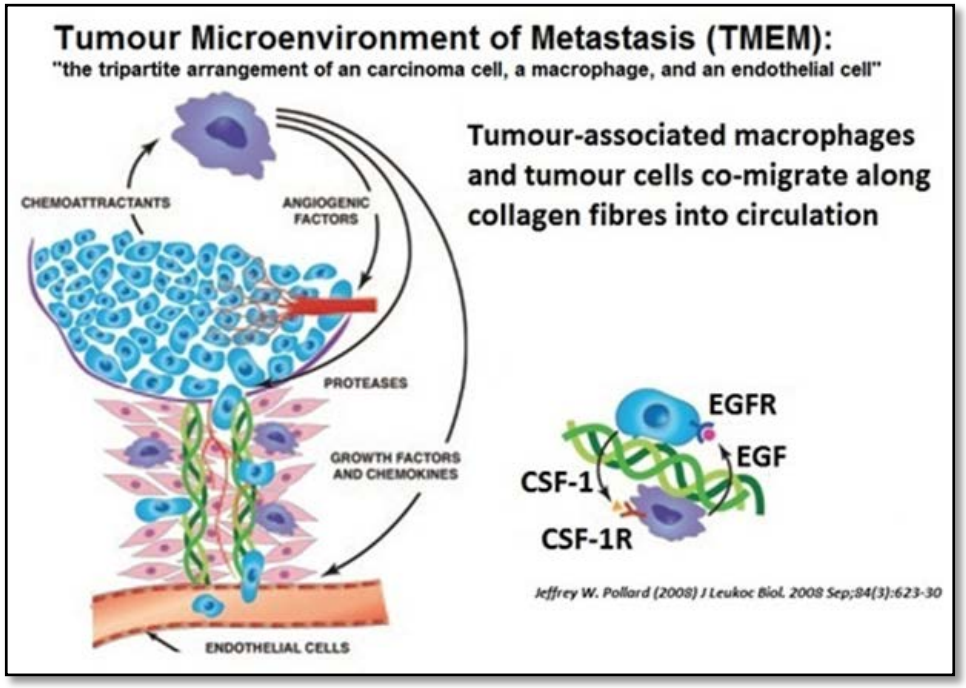
Tumour Microenvironment of Metastasis (TMEM):
"the tripartite arrangement of an carcinoma cell, a macrophage, and an endothelial cell"
Tumour-associated macrophages and tumour cells co-migrate along collagen fibres into circulation
CHEMOATTRACTANTS
ANGIOGENIC FACTORS
PROTEASES
GROWTH FACTORS AND CHEMOKINES
ENDOTHELIAL CELLS
EGFR
EGF
CSF-1
CSF-1R
Jeffrey W. Pollard (2008) J Leukoc Biol. 2008 Sep;84(3):623-30

(C)

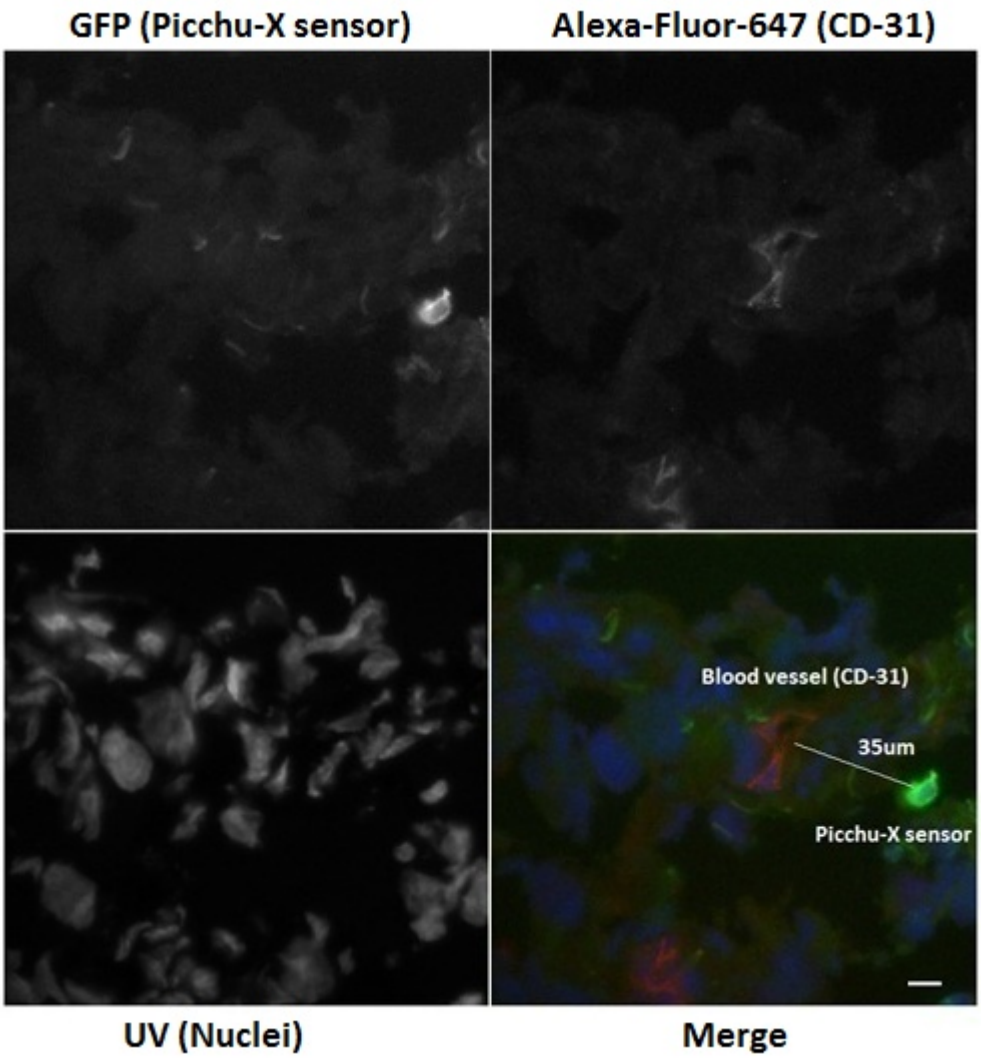
GFP (Picchu-X sensor)
Alexa-Fluor-647 (CD-31)
Blood vessel (CD-31)
35um
Picchu-X sensor
UV (Nuclei)
Merge

(D)

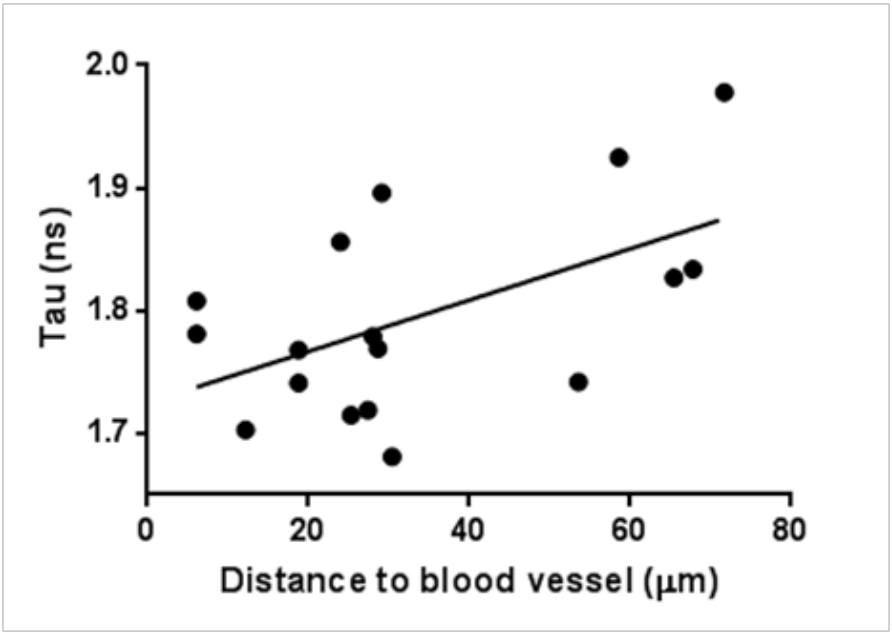

Pearson correlation coefficient = 0.545 (p = 0.024)

Result figure 4.3.4: Intratumoural heterogeneity of EGFR activity and the correlation between Picchu-X sensor activities with the distance to blood vessels within the tumour environment.

(A) Heterogeneity of Picchu-X activity in tumour environment of MDA-MB-231 model; white scale bar represents 5µm (B) Schematic model showing the co-migration of tumour cells and macrophages on collagen fibres and their intravasation into blood vessels within the tumour microenvironment of metastasis (TMEM). (C) MDA-MB-231-bearing animals were injected with LPD complex containing 68µg of Picchu-X sensor DNA. *Ex-vivo* tissue samples were stained with Alexa-Fluor-647 anti-mouse CD31 antibody to correlate Picchu-X sensor (shown in GFP) distance to blood vessels (shown in Alexa-Fluor-647). Nuclei were stained with Hochst33342 (shown in UV); white scale bar represents 10µm. (D) Correlation between Picchu-X sensor activities to distance to blood vessels. Data was imported into SPSS statistical software for correlation analysis. Statistical significant (with $P < 0.05$) was tested with Pearson correlation coefficient (two-tailed).

Heterogeneity of EGFR activity within the tumour microenvironment

Heterogeneity of EGFR activity was demonstrated by the FRET-based sensor within the tumour environment in the MDA-MB-231 basal-like breast cancer model (**Result figure 4.3.4A**); we tested the hypothesis that EGFR activity was correlated with the distance to blood vessel or to macrophage within the tumour microenvironment of metastasis (TMEM).

Robinson *et al.* have shown that density of TMEM correlates with the risk of developing systemic, haematogenous metastases in breast cancer (Robinson and Jones 2009; Robinson, Sica et al. 2009). As illustrated in **Result figure 4.3.4B**, TMEM is defined as a tripartite arrangement of a tumour cell, a macrophage and an endothelial cell. This tumour microenvironment invasion model suggests that tumour cells and macrophages participate in a paracrine loop involving macrophage-derived EGF and carcinoma cell-derived colony-stimulating factor-1 (CSF-1), results in tumour cell migration along collagen fibres and intravasation, with the assistance of perivascular macrophage (Condeelis and Pollard 2006; Pollard 2008; Qian and Pollard 2010). This cross-talk can be blocked by either EGF or CSF-1 receptor antagonists, resulting in a decrease in migration and invasion of both tumour cells and macrophages (Goswami, Sahai et al. 2005).

By liposomal delivery of the FRET-based sensor, we measured the intratumoural EGFR activity in related to the distance to blood vessels and macrophages in *ex-vivo* MDA-MB-231 tissue samples.

Tumour-bearing animals were injected with LPD complex containing 68μg of Picchu-X sensor DNA. This liposome solution was also tested in cultured cell in parallel to confirm the transfection efficient of the batch.

Primary tumours were dissected out 48hr post-injection and sectioned on imaging slides for immunostaining experiments. We stained and visualised blood vessels using Alexa-Fluor-647-conjugated CD-31 antibody (as shown in **Result figure 4.3.4C**). The result showed a correlation between the sensor activities and distance to blood vessels (Pearson correlation coefficient = 0.545, p = 0.024), whereas the EGF-receptors were more active when cells were near the blood vessels (**Result figure 4.3.4D)**.

Tumour-associated macrophages populate the tumour microenvironment and constitute a large portion of the tumour mass, particularly in breast cancers (Lewis and Pollard 2006). We stained the macrophages with F4/80 antibody and measured the sensor activity correlated to the distance to the nearest macrophage. No significant association was seen between EGFR activity and the proximity of the tumour cells to macrophages (Pearson correlation coefficient = 0.069, p = 0.830). These results (inverse correlation of EGFR activity in tumour cells with their distance from blood vessels) are being further explored mechanistically in the supervisor's laboratory; for instance in relation to redox regulation of EGFR activity (Paulsen, Truong et al. 2012; Truong and Carroll 2012).

Moreover, the expression of the sensor was poor in the model, usually only a few transfected cells were found in each tumour section. Multiple tumour sections were required to obtain data for statistical significance. Spleen and liver samples were also imaged but the expression of sensor protein was hardly observed.

(A)

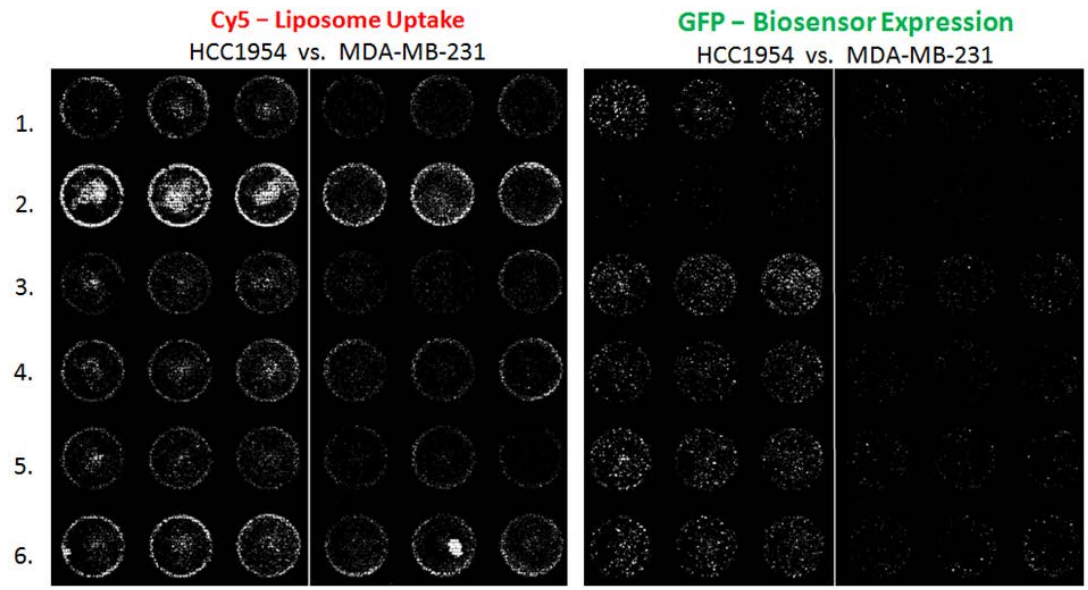

1. no targeting peptide
2. K_{16}RVRR-YHWYGYTPQNVI
3. K_{16}RVRR-LARLLT
4. YHWYGYTPQNVI-RVRRK$_{16}$
5. LARLLT-RVRRK$_{16}$
6. MYIEALDKYAC-RVRRK$_{16}$

(B)

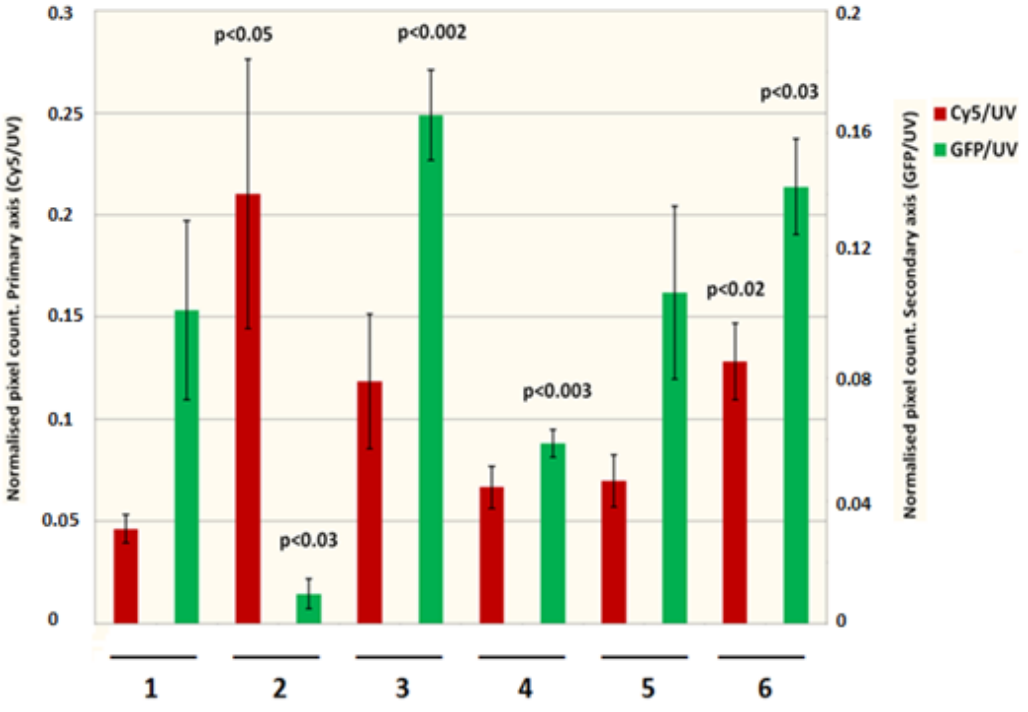

1. no targeting peptide
2. K_{16}RVRR-YHWYGYTPQNVI
3. K_{16}RVRR-LARLLT
4. YHWYGYTPQNVI-RVRRK$_{16}$
5. LARLLT-RVRRK$_{16}$
6. MYIEALDKYAC-RVRRK$_{16}$

(C)

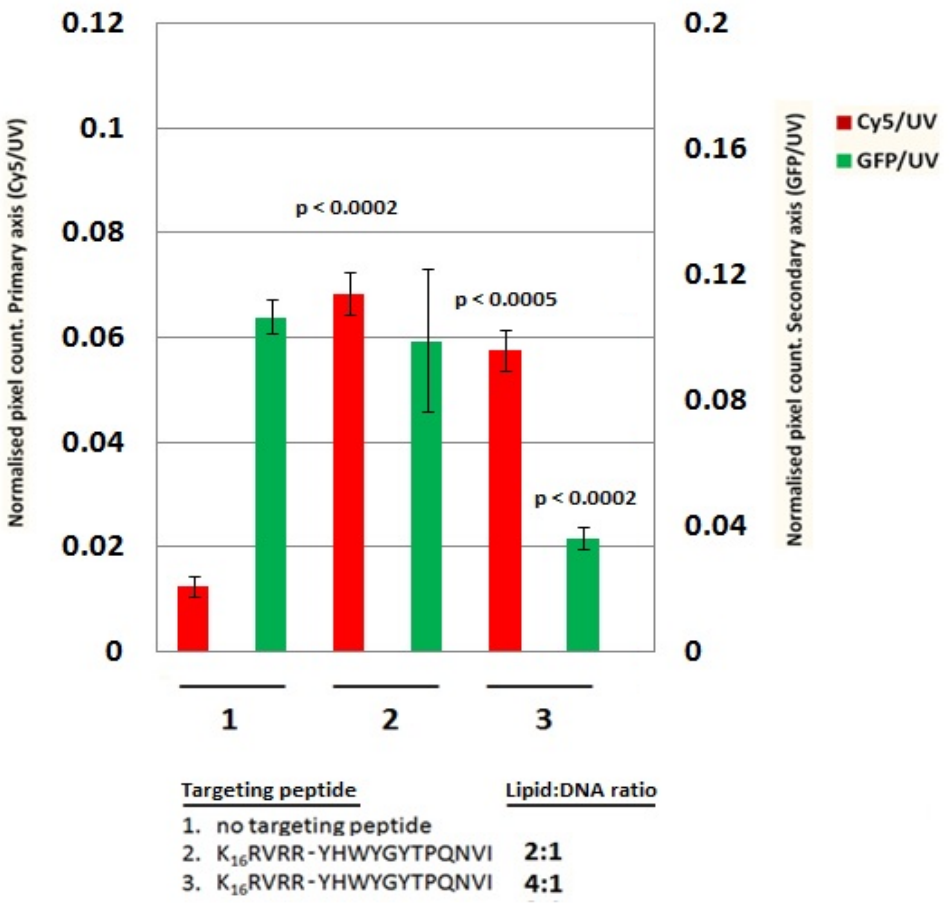

Result figure 4.3.5: Selection of cell-line and optimization of LPD formulation for the enhancement of liposomal uptake and DNA transfection.

(A) *In vitro* liposomal uptake (Cy5 scan) and biosensor expression (GFP scan) were compared between HCC1954 and MDA-MB-231 models with a panel of targeting peptides. (B) ImageJ software was used for the analysis of normalised-pixel count (Cy5/UV for liposomal uptake and GFP/UV for DNA transfection) for the HCC1954 model, while all complexes were prepared at 4:1 weight ratio of lipid to DNA. (C) Liposome complexes containing purified EGFR targeting peptide YHWYYPQNVI were prepared at 4:1 or 2:1 lipid:DNA ratio and demonstrated an enhanced level of DNA transfection with the lowered peptide ratio. Data were expressed as means ± SEM, statistical significance compared with K16 control was analysed using unpaired two-tailed Student's t-test.

Cell-line selection and *in vitro* optimisation of LPD formulation

After the initial set of *in vivo* liposomal delivery experiments for the biosensor DNA, we observed low expression of sensor expression in the MDA-MB-231 tumours. Further optimization steps were done in attempt to improve the transfection efficiency. First, it was demonstrated that HCC1954 model had a better transfection capability *in vitro,* both in liposomal uptake and expression of the sensor protein, compared to the MDA-MB-231 model (**Result figure 4.3.5A**).

We further analysed the scanned image of HC1954 cells transfected with liposomes attached with a panel of targeting peptides, which included purified EGFR-targeting peptide YHWYYPQNVI (**Result figure 4.3.5B sample 2**), LARLLT (**sample 3**), or synthetic fragment of EGF CAYKDLAEIYM (**sample 6**) (as referred to the same set of sequences used in Result figure 4.3.2 for the MDA-MB-231 model). Here, we also included two new samples of YHWYYPQNVI and LARLLT sequences that were attached to K_{16}RVRR linkers in a reverse direction (**sample 4 and 5 respectively**), to check if the orientation of peptides passing through the lipid bilayer would affect their targeting abilities.

Result showed a 2.8-fold increase in liposomal uptake ($P < 0.02$) and 1.4-fold increase in sensor expression ($p < 0.03$) with the addition of CAYKDLAEIYM peptide sequence compared to K16 control (**Result 4.3.5B, sample 6**). Data was highly comparable with previous result obtained using the MDA-MB-231 cells. It was also demonstrated a 4.7-fold increase of liposomal uptake ($p < 0.05$) with the addition of

YHWYYPQNVI sequence comparing to K16 control, but once again a significantly reduction in the expression of sensor protein (11-fold decrease, $p < 0.01$) (**sample 2**) as shown in the MDA-MB-231 cells previously. The attachment of peptides to K_{16}RVRR linkers in a reverse orientation did not enhance liposomal uptake or sensor expression (**sample 4 and 5**).

Optimisation of LPD formulation for *in vivo* targeting

For *in vitro* experiments, we would expect a degree of unspecific liposomal intake as the liposome solution was incubated directly on top of the monolayer of cell in the culture wells. However, with the consideration that once the liposome was injected into xenograft animal model, the lipid-based nanoparticle would need to circulate around the vascular system in order to locate and target the EGFR-overexpressed cancer cells; thus it would be ideal to select a liposome formulation that produce the highest targeting efficiency.

The addition of peptide sequence YHWYYPQNVI led to the highest degree of liposomal uptake among all the EGFR-targeting peptides tested. To solve the problem of its low transfection of DNA, we adjusted the weight ratio of lipid to DNA in attend to increase the release of DNA. **Result figure 4.3.5C** showed that an enhanced level of DNA release/sensor expression with the lowered 2:1 ratio comparing to the original 4:1 ratio, while the liposome intake remained highly superior.

This result suggested that the reduction in transfection efficiency was most likely a consequence of poor endosomal release of DNA due to the formation of multiple bilayers surrounding the central core. It was important to have enough lipids to form a single bilayer on the exterior of the LPD complex but not so much that multiple bilayers are formed. This LPD formulation conjugated with peptide sequence YHWYYPQNVI, with 2:1 weight ratio of lipid to DNA, was selected for the

delivery of biosensor-encoding DNA into the xenograft HCC1954 model of basal-like breast cancer. We measured an average lifetime of 1.815ns in HCC1954 model, compared to 1.795ns for MDA-MB-231 model; both of these lifetime values were comparable with the *in vitro* imaging data.

Results indicated that optimization steps can be done to strengthen the efficiency and specificity of liposomal transfection by adjusting the chemical formulations and surface properties of the liposomes. Small structural difference in the selection of targeting peptide for receptor recognition or lipid to DNA ratio could result in pronounced differences in transfection within each type of formulation.

(A)

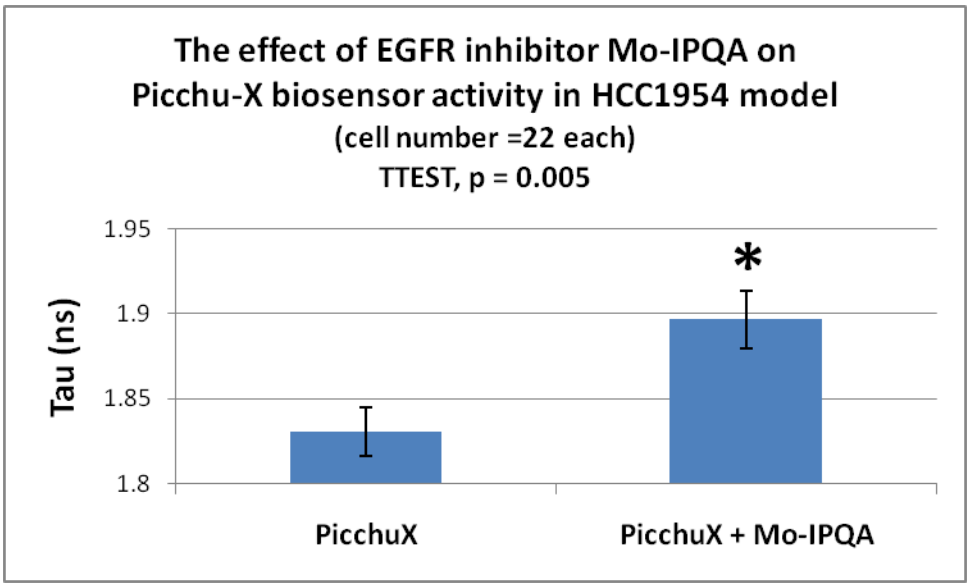

(B)

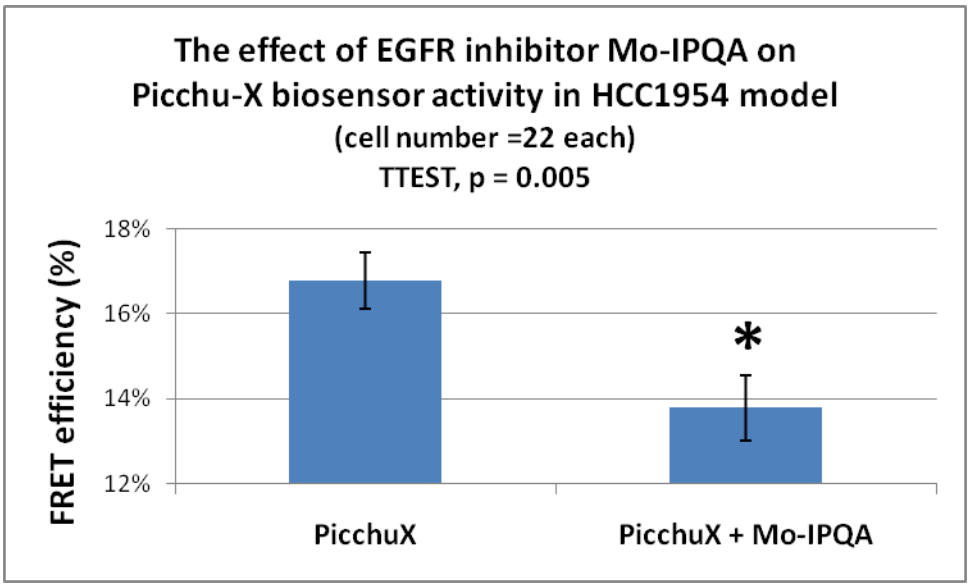

Result figure 4.3.6: Morpholino-IPQA inhibited Picchu-X sensor activity in HCC1954 xenograft model.

HCC1954-bearing animals were injected with LPD complex containing 68µg of Picchu-X sensor DNA. After 48hr, Morpholino-IPQA (MO-IPQA) was suspended in sterile and filtered water at pH 6.5 (at 10mg/ml) and 100ul was delivered intravenously to the mice (32mg/kg). Primary tumours were dissected out 4hr post-treatment of the inhibitor. Picchu-X sensor activity was measured with MP-FLIM using the *ex-vivo* tissue samples. (A) Lifetime and (B) FRET efficiency data were expressed as means ± SEM and in statistical significance was analysed using unpaired two-tailed Student's t-test.

Morpholino-IPQA inhibition of intratumoural Picchu-X sensor activity

We have previously investigated inhibitory effects of Morpholino-IPQA (Gelovani 2008) and its precursor PD168393 (Fry, Bridges et al. 1998) on EGFR activity in cultured cells (**Result figure 4.1.1**). Here we tested the inhibition of EGFR tyrosine kinase activity measured by liposomal delivery of the FRET-based sensor in the *ex-vivo* HCC1954 tissue samples.

Ten tumour-bearing animals were injected with LPD complex containing 68µg of Picchu-X sensor DNA. After 48hr, Morpholino-IPQA was suspended in sterile and filtered water at pH 6.5 (at 10mg/ml) and 100ul was delivered intravenously to the five mice (32mg/kg). Primary tumours were dissected out 4hr post-treatment of the inhibitor and sectioned on imaging slides for MP-FLIM imaging experiments.

Result figure 4.3.6A showed a change in sensor lifetime from average tau of 1.830ns, increased to 1.897ns compared with post-injection of Morpholino-IPQA (TTEST, $p < 0.005$); the data also demonstrated a 3% decrease in FRET efficiency (TTEST, $p < 0.005$). This indicated a conformational change of the CrkII-based sensor in response to the inhibition of EGFR activity in the microenvironment of those tumours.

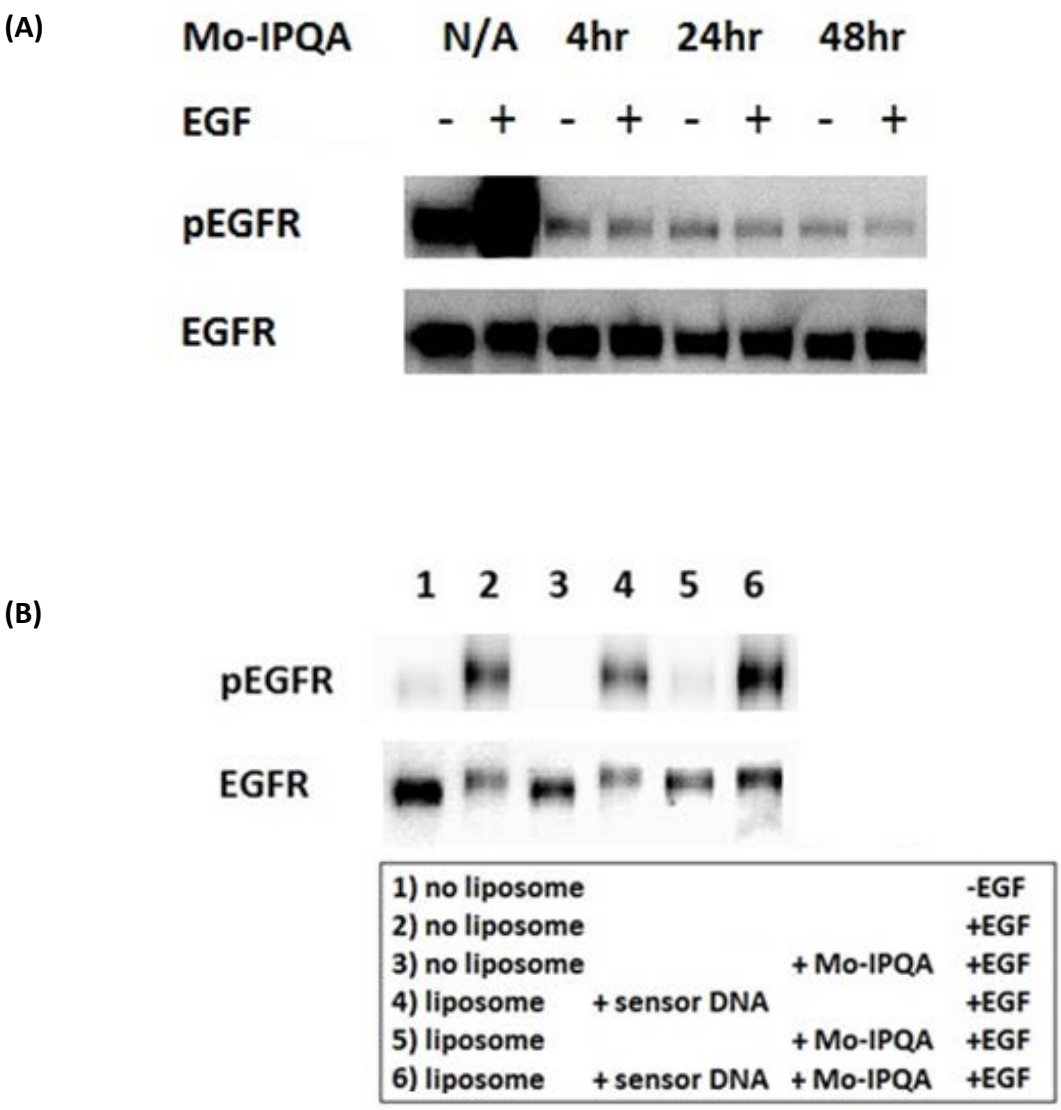

Result figure 4.3.7: EGFR-targeted nanoparticles for the delivery of Morpholino-IPQA.

(A) HCC1954 cells were treated with 10µM of Morpholino-IPQA (Mo-IPQA) for 0, 4, 24 and 48hr (without refreshing the inhibitors). One of each replicated well was treated with 100ng/ml EGF for 30min, prior to lysis. (B) HCC1954 cells were tested with (1) (2) untreated (3) Morpholino-IPQA; or tested with a panel of liposome complexes containing purified EGFR targeting peptide YHWYYPQNVI for 4hr, in addition to (4) sensor DNA (5) Morpholino-IPQA (6) sensor DNA and Morpholino-IPQA. Except the control untreated well, all samples were treated with 100ng/ml EGF for 30min, prior to lysis. Immunoblots were carried out using the antibodies indicated above.

EGFR-targeted nanoparticles for the delivery of EGFR tyrosine kinase inhibitor

Previously we have shown the result of monitoring EGFR activity in the tumour microenvironment in response to the given drug treatment. In order to create a nanoparticle delivery system that can carry both inhibitor and sensor-encoding DNA, we further tested the duration of EGFR kinase inhibition of Morpholino-IPQA to check if the effect would last for the time required for sensor protein maturation.

Result figure 4.3.7A showed the inhibitory effect of Morpholino-IPQA remained for at least 48hr in cultured cells, without the need of refreshing or additional doses of inhibitors; thus for *in vivo* experiments, only one initial injection of the LPD-drug complexes would be required. However, the production of such LPD-drug complex has been proven to be difficult and unsuccessful.

As shown in **Result figure 4.3.7B**, we tested three LP formulations that contained either **(B4)** sensor DNA **(B5)** Morpholino-IPQA or **(B6)** sensor DNA with Morpholino-IPQA; each LP complex contained EGFR targeting peptide YHWYYPQNVI. All liposome solutions were then purified in PD-10 columns in order to remove unencapsulated compounds.

The results showed that Morpholino-IPQA was successfully encapsulated in the liposome and released from the LP complexes to inhibit EGFR kinase activity in the cultured cells **(as shown in B5)**. However, no inhibition was seen with the addition of sensor DNA **(as shown in B6)**, indicating the absence of the inhibitor. This

suggested that when forming a complex with DNA, a profound structural rearrangement of the outer liposomal surface had forced all the inhibitors to be released from the LP complexes.

Chapter summary

In summary, we have demonstrated *in vivo* liposomal transfection of Picchu-X biosensor into HCC1954 and MDA-MB-231 tumour tissues. We were able to measure EGFR activity in the micro-environment in those tumours in response to the given drug treatment. Furthermore, heterogeneity of biosensor activity was demonstrated within tumour environment and we found an inverse correlation of biosensor activity with distance from the tumour cells to blood vessel (CD-31 antibody).

This work highlights the advantages of liposomal delivery of biosensor to monitor sub-cellular activity in the primary tumour, prior to and after therapeutic intervention.

CHAPTER 5: Discussion and future direction

Discussion and future direction

Combinations of new and existing techniques were used in this project to investigate and to obtain a more comprehensive picture of the EGFR signalling processes. Here we reported for the first time an integrated high-content high-throughput workflow that combined two powerful methods of cell biology and molecular imaging: siRNA screening and FLIM imaging using intramolecular FRET-based biosensor (Picchu-X). The first objective of this work was to use an in-house developed semi-automated imaging technique to conduct a high-content high-throughput FLIM screen, in combination with RNAi-based knockdown technique utilising a library of siRNA consisted of 533 genes, that were selected on the basis of the EGFR interaction subnetwork information, as explained in a previous section (Introduction chapter 1.10 Optical imaging for network screen).

The second objective of this work was to develop a liposome-based delivery system to deliver the same biosensor into murine models of basal-like breast cancer for the measurement of intratumoural EGFR activity, as well as the effect of EGFR inhibitors *in vivo*.

High-content screen using Picchu-X biosensor

We characterised the CrkII-based biosensor in the cellular systems of basal-like breast cancer in **Result chapter 4.1**. By monitoring the sensor conformation changes with FRET-FLIM imaging, we could indirectly detect the changes in EGFR

activity to biological/therapeutics perturbations *in situ*, such as stimulation upon ligand binding and inhibition with small molecule inhibitors.

The Picchu-X sensor was then selected to be employed in the large scale siRNA screen against a protein network consisted of 533 genes interconnected with EGFR directly or indirectly (up to second degree of interaction), that were chosen from the Human Protein Reference Database. As anticipated, the development of this large-scale protein activity screen require careful planning, followed by reconstructing and standardising the experimental layout, as shown in **Result chapter 4.2,** to generate result in a consistent and meaningful way throughout the whole screening process.

After careful masking analysis of the acquired images, it was found that the fluorescence intensity could alter the lifetime of the sensor significantly, regardless of any biochemical treatment. To avoid false positive data, this intensity-based fluorescence quenching effect was taken into account during the analysis of the data. One plausible explanation that this was caused by the high concentration of sensor protein on cell membrane and led to intermolecular (rather than intramolecular) FRET with the increased number of neighbouring acceptor molecules.

In addition to the overexpression that could lead to sensor multimerisation, the sensor was trapped on the cell membrane. The membrane targeting CAAX

sequence of k-RAS was cloned after the eGFP as a plasma membrane-anchoring motif to overcome the flaw that the diffusion of Picchu probe was too fast to delineate the sub-cellular localization of tyrosine kinase activity (Itoh, Kurokawa et al. 2005). The local concentration of the sensor could be very high and could be considered as a two dimensional problem, governed by the number of molecules within the area determined by the Förster radius (Lakowicz 1999). This idea supported our observation of inverse relationship between the fluorescence intensity and the fluorescence lifetime was due to the presence of multiple (intramolecular and intermolecular) acceptors for the donor molecule.

This might also explain the slightly limited dynamic range we observed with the intra-molecular FRET-based sensor. In theory, there were two populations of sensors which were active (in closed confirmation) or inactive (open confirmation); these populations under the additional condition that the membrane was crowded enough to cause intermolecular FRET. However since the lifetime of the sensor would be further reduced after EGF stimulation by intramolecular energy transfer, we expected to find a change in the gradient of the lifetime versus intensity curve.

We described the statistical analysis method to interpret the FRET-FLIM data generated, taken into account that there was an association between fluorescence intensity and lifetime. We therefore applied a linear regression model, where Tau= slope*intensity + intercept, to observe the effect of EGF towards the linear association between intensity and lifetime for 'hit' selection, with an interaction

term of EGF (dichotomous values, where EGF=0 or EGF=1) included in the analysis, resulting in two linear equations describing the ± EGF sample sets.

Overview of genes identified as candidate hits

FRET imaging microscopy has been proven to be an extremely useful tool in the detection of protein-protein interactions and protein conformational changes in single-cell level and provides temporal and spatial information on the molecular events. The siRNA screen described in **Result chapter 4.2** had the potential to knock down an important signal transduction molecule or a crucial component of the signalling complex, leading to a potentially delay or loss of signal propagation from EGFR to its downstream signalling targets. We designed the screen to specifically report on the activity of EGFR rather than other RTKs such as c-Met and PDGFRβ (that can also phosphorylate the CrkII-based sensor probe; see section 4.1 summary). This receptor specificity is introduced into the screen by defining the hits to be siRNAs that abrogate the difference between the ± EGF slopes of the linear equation (Tau= slope*intensity + intercept). Below, we discussed the 22 target genes (4.1% of the siRNA library) that were identified as modulators of EGFR activity response to its natural ligand.

Hit proteins that interact with CrkII protein

Three of the candidates have been showed to interact with CrkII protein directly. **DOCK1** is a guanine nucleotide exchange factor for Rac, it has been shown to couple with $p130^{Cas}$ and CrkII to form a complex to serve as a molecular switch, regulating

integrin-mediated cell migration through enhanced lamellipodia formation (Gu, Sumida et al. 2001); while **DOCK2** has been showed to complex with CrkII and Vav to regulate Rac activity on cell motility (Nishihara, Maeda et al. 2002). **CBLC** is a RING finger type ubiquitin-protein isopeptide (E3) ligase that interacts with EGFR and is involved in its ubiquitination and downregulation of its downstream signalling (Courbard, Fiore et al. 2002). It interacts with the SH3 domain of CrkII protein (Keane, Ettenberg et al. 1999). There were also reports on Crk involvement in the signalling of T cells and B cells by means of binding to CBLC. (Buday, Khwaja et al. 1996; Ingham, Krebs et al. 1996; Keane, Ettenberg et al. 1999).

Hit proteins that associate with EGFR

A number of the hit proteins have been reported to directly associate with EGFR. **SHC3 (N-SHC)** is an adapter molecule downstream of EGFR, and forms a complex with Grb2 following EGF stimulation (Nakamura, Sanokawa et al. 1996; Nakamura, Muraoka et al. 1998). **PRKAR1A** is a type I protein kinase A isoform, its regulatory subunit R1α is overexpressed in cancer cells and is induced by EGFR-dependent transformation (Tortora, Damiano et al. 1997). It has been shown that the downregulation of PRKAR1A inhibited EGFR dependent signalling by binding to the SH3 domain of Grb2 adaptor protein (Tortora, Damiano et al. 1997). **PTPN11** belongs to the family of protein tyrosine phosphatases (PTP) that can be categorised as receptor-like (R) or non-transmembrane (N) proteins (Tonks 2006). PTPN11 encodes for the SH2 domain-containing protein tyrosine phosphatase-2 (SHP2), which contained two SH2 domains that partner with Grb2-associated binder

1/2 (GAB1/2). The interaction is essential for the activation of the Ras-Erk cascade downstream to EGFR (Tomic, Greiser et al. 1995; Cunnick, Dorsey et al. 2000; Fragale, Tartaglia et al. 2004). In a PTPN11-dependent manner, GAB2 overexpression has been linked to breast carcinogenesis (Bentires-Alj, Gil et al. 2006; Brummer, Schramek et al. 2006). In addition, PTPN11 showed an enrichment in the activated EGFR-Shc-associated cell fraction after EGF stimulation (Blagoev, Kratchmarova et al. 2003). **XRCC6** (also known as Ku70) forms heterodimeric regulatory complex with ku80 and DNA-dependent protein kinase (DNA-PK) and plays an essential role in repairing DNA damage. A specific physical interaction between EGFR and Ku70/80 was demonstrated in response to anti-EGFR monoclonal antibody (mAb 225) treatment (Bandyopadhyay, Mandal et al. 1998). Enhanced EGFR nuclear localisation was induced by DNA damage-inducing agents and played a role in the modulation of DNA repair activity (Hsu, Miller et al. 2009; Liccardi, Hartley et al. 2011). Our result also demonstrated that XRCC6 knockdown led to a reduction of ligand-induced EGFR degradation, which was compatible with a reduced level of receptor phosphorylation (**Result figure 4.2.11**).

PDCD6IP (also known as Alix) is an Endosomal Sorting Complexes Required for Transport (ESCRT)-Associated Protein, that has been shown to bind to EGFR constitutively and negatively regulate receptor internalization by reducing the phosphorylation levels of c-Cbl, weakening the interaction between SETA/CIN85 and Cbl. These result in a reduction in Cbl-mediated degradation of EGFR (Schmidt, Hoeller et al. 2004; Schmidt, Dikic et al. 2005). **FASLG** is the natural ligand for FAS

receptor (also known as CD95). Death-inducing signalling complex (DISC) is formed upon ligand binding and initiate apoptosis. It was shown that oxidative stress can trigger the association between CD95 and EGFR (Reinehr, Schliess et al. 2003); while the interaction of FAS receptor and c-MET was shown to inhibit self-association of FAS receptors and DISC formation, and cause resistance to FAS-mediated apoptosis in endothelial cells (Smyth and Brady 2005).

Hit proteins with indirect relationship to EGFR or CrkII

Plexin B1 (PLXNB1) is a transmembrane semaphorin receptor which shares homology to the extracellular domain of hepatocyte growth factor receptor, c-MET (Giordano, Corso et al. 2002). It has been shown to the knockdown of PLXNB1 suppresses c-MET and HER2 activation through direct receptor-receptor interaction and decreases c-MET downstream effects by downregulating the activity of Shp2, which is a downstream adaptor protein for multiple receptors (Swiercz, Worzfeld et al. 2008; Soong and Scott 2013). The relationship between **Leukemia inhibitory factor (LIF)** and EGFR is unknown; however an interaction was suggested between LIF and IL6ST (Interleukin 6 receptor β) (He, Gong et al. 2005), which is a regulator of PTPN11 (Schiemann, Bartoe et al. 1997).

NUMB contains a phosphotyrosine-binding (PTB) domain and was shown to promote the ubiquitination of Notch1 receptor and controls Notch1 dependent signal transduction that has an important role in cellular differentiation, proliferation and apoptotic events during cell development (McGill and McGlade 2003). It has been reported that the inhibition of EGFR signalling pathway could induce Notch1 activity (Kolev, Mandinova et al. 2008). With the silencing of NUMB gene, we would expect an accumulation of Notch1 receptor and that might have a negative feedback effect on the EGFR signalling pathway. Furthermore, Notch1 have been suggested to interact with XRCC6 in a yeast two-hybrid screen (Stelzl, Worm et al. 2005).

Hit protein with no direct relationship with EGFR or CrkII

FNBP1, C14orf1 and **CDC42EP1** are all associated with CDC42 (Serebriiskii, Mitina et al. 2002; Stelzl, Worm et al. 2005) but have no direct connection with EGFR. **CYFIP1** was shown to function as a Rac1-associated protein to from the WAVE1 complex and regulated actin filament reorganization (Kobayashi, Kuroda et al. 1998), **MCF2** (also known as DBL) is responsible for the guanine-nucleotide exchange factors activity (Zhu, Debreceni et al. 2000), but neither have an immediate connection to EGFR. There was also no indication of **C9orf127, CD46**, **TRIO** and **ID2** associating being involved with the with EGFR or CrkII protein subnetwork.

XRCC6, PDCD6IP and PTPN11 were selected for further validation to establish the biological importance of the genes identified as primary hits in the EGFR signalling network. Although we did not have time to do further validation due to the time limit within the project, it would be ideal to extract all the candidate hits from the library and perform an addition conformational screen. This screen should contain the pooled siRNA library to test the reproducibly of initial screen, and separately three of the individual sequence targeting the same gene to discriminate between effective and ineffective siRNAs. Knowledge of such genes will advance our understanding the role of EGFR in basal-like breast cancer, and help clarify some of the molecular mechanisms underlying the association between EGFR and poor clinical outcome.

In addition, we planned to generate cell-line with knockdown of EGFR and the identified hits from the FRET-FLIM screen. Using EGFR/c-MET inhibitors in parallel with the knockdown cell-lines we will determine the role of these tyrosine kinase receptors in preclinical basal-like breast cancer models.

Liposomal delivery system

Another vital aspect of this project was to generate multifunctional serum-stable liposomes for targeted transfection of biosensor-encoding DNA and EGFR tyrosine kinase inhibitors, to address the liposomal potential on intratumoural activity sensing in murine models of basal-like breast cancer. The preparation, characterization, and optimization of the basic properties of liposomes were discussed in **Result chapter 4.3**.

We presented a cellular and *in vivo* delivery system that was based on these nanoliposomes and use them as potential DNA and drug carriers. These synthetic liposomes were made of lipid bilayer composed of natural phospholipids and they were shown to be highly biodegradable and biocompatible in our cellular and animal models. A fraction of cholesterol was included in the formulations to modulate rigidity to increase stability both *in vitro* and *in vivo* applications, and to reduce serum induced instability caused by the binding of serum protein to the liposome membrane. Low concentration of cholesterol in the lipid bilayer can also lead to an increase in transmembrane permeability (Lian and Ho 2001).

The liposomes were also modified with hydrophilic polymer polyethylene glycol (PEG) to stabilise the liposome structures, decreasing their interactions with serum proteins and reducing inter-liposomes interaction to prevent aggregation. PEGylation of the liposome surface layer can prolong *in vivo* circulating time in

systemic circulation compared to non-modified liposomes, which enhances the opportunity to target tumours. The PEGylation liposomes also have a lower tendency to be rapidly cleared and degraded by cells of the mononuclear phagocyte system results in improved biodistribution (Varga, Wickham et al. 2000; Lian and Ho 2001; Maruyama 2002; Grosse, Tagalakis et al. 2010).

Another important surface modification in the development of the liposome was the attachment of EGFR-targeting peptides for active targeted delivery. We have shown that small structural differences in the selection of peptide sequence for receptor recognition could result in pronounced differences in liposomal uptake and DNA transfection when we compared the fluorescence emission signals. It has been recognised that the installation of targeting peptides could lead to more efficient internalization via receptor-mediated endocytosis and consequently higher transfection efficiency (Mustapa, Bell et al. 2007; Kudsiova, Fridrich et al. 2011). The liposomal formulations were optimised in the cellular transfection system with the selection of cell model, EGFR-targeting peptide sequence and peptide:DNA ratio to facilitate the optimal EGFR specific receptor-mediated transfection.

We then applied the liposomes intravenously into established xenograft models of basal-like breast cancer (MDA-MB-231 and HCC1954), however, the *in vivo* transfection efficiency in both models was still suboptimal despite the efforts in cellular surface modification and optimisation experiments. However, this was

sufficient for us to sample the intratumoural heterogeneity in EGFR activity at a single cell level.

In theory, liposomal nanoparticles with a size of several hundred nanometres could leak preferably throughout the tumour vasculature as their sizes were close to the vascular opening, therefore liposomes would passively accumulate in the tumour region based on the 'enhanced permeability and retention (EPR) effect', (due to poorly-aligned defective endothelial cells with wide fenestrations in newly formed vasculature in tumours, and the lack of effective lymphatic drainage), while passage is restricted by tight cellular junctions in normal tissue (Yuan, Dellian et al. 1995; Drummond, Meyer et al. 1999; Park and Yoo 2010; Prabhakar, Maeda et al. 2013). However, significant heterogeneity of EPR and hence differences in vessel structure (in terms of leakiness), both within a single tumour type (at different sites) and between tumour types, exists and may account for differences in transfection efficiencies of these liposomal nanoparticles (Prabhakar, Maeda et al. 2013).

All LPD complexes used for the *in vivo* experiments were under 170nm in size (**see appendix for dynamic light scattering (DLS) for nanoparticle size analysis**). We hypothesised the reason for poor *in vivo* transfection was due to the poor blood supply in these solid tumour models, and therefore the liposome complex could not access freely to the tumour tissue.

In this regard, we also repeated the experiment using a highly vascularised human colorectal carcinoma SW1222 model (Zhang, Laufer et al. 2009) in order to achieve better rate of liposomal uptake; however, the number of tumour cells observed with the expression of transfected sensor did not improve. The low transfection rates could be due to a number of other reasons, such as high intestinal uptake or degradation of LPD complex with the mononuclear phagocyte system in liver and spleen; as well as DNA instability in bloodstream or poor tumour targeting and tissue accessibility of the liposome with inefficient release of DNA into the tumour cells. All of these factors also contribute to the observed low transfection of biosensor. The fate for the liposome is yet to be determined. Future *in vivo* imaging experiments using liposomes packed with radiotracer will allow us to characterise the pharmacokinetics of these LPD complexes. Further optimisation steps are required to formulate a serum-stable liposome for effective and specific delivery of the FRET-based sensor DNA.

Despite the difficulty of *in vivo* transfection, a small fraction of liposomes have distributed to the primary tumours where rapid tumour growth occurred. We managed to obtain enough biosensor-transfected cells in multiple tumour sections for the study of intratumoural EGFR activity and demonstrated a significant degree of heterogeneity of EGFR activity within the tumour microenvironment.

The result showed a correlation between the sensor activities and distance to blood vessels in the MDA-MB-231 model, whereas the EGF-receptors were more active when cells were near the blood vessels. These results might explain the intratumoural heterogeneity of EGFR activity demonstrated by the FRET-based sensor. Here we suggested that EGFR activity might not always increase when tumour cells associated with macrophages, but only with those macrophages that were close to the circulation that had an elevated level of EGF secretion to facilitate migration and intravasation of tumour cells. An alternative mechanism that is being explored to account for the observed intratumoural heterogeneity of EGFR activity, within the supervisor's laboratory, is the effect of hypoxia (one of the parameters that will depend on diffusion distances between the blood vessels and the tumour cells) (Vaupel and Harrison 2004) on the Picchu-X sensor activity. Hypoxia will in turn influence the reactive oxygen species production in cancers which through pyruvate kinase M2 (Anastasiou, Poulogiannis et al. 2011), may lead to a redox regulation of EGFR activity with the production of hydrogen peroxide (H_2O_2) (Paulsen, Truong et al. 2012; Truong and Carroll 2012).

Our FLIM measurement of the Picchu-X biosensor activity also demonstrated the inhibitory effect of EGFR tyrosine kinase inhibitor, Morpholino-IPQA, on the EGFR activity in the primary tumour of the established HCC1954 model.

Furthermore, current trends and developments of nanoparticle delivery systems are designed on drug or gene delivery alone. The original goal was to develop liposomes that can carry both inhibitor and biosensor-encoding DNA, which was referred as a theragnostics approach, meaning the combination of therapeutics and diagnostics. As it has come to the end of the project; time did not allow us to continue with the development of such LPD-drug complexes that can carry both EGFR kinase inhibitors for targeted drug therapy, and sensor-encoding DNA for monitoring EGFR kinase activity.

However, further experiments are planned in Alethea Tabor's laboratory to label the anti-EGFR inhibitor with radioiodine (I^{125}) and deliver it via the liposome for SPECT imaging. DNA will be delivered in a separate liposome solution and tumours will be harvested to correlate the radioiodine standard uptake value (SUV) with the EGFR biosensor activity, to provide the definitive evidence that the radionuclide-labelled tyrosine kinase inhibitor binding will influence the RTK activity of EGFR in these tumour cells.

Iodine-labelled Morpholino-IPQA has previously been used as a radiotracer for the PET imaging of EGFR-overexpressing A431 human tumour xenograft grown in

immunocompromised animals. Although it successfully reflected a high level of EGFR expression and activity in A431 tumour cells, it exhibited a rapid hepatobiliary clearance rate of the radiotracer (Pal, Glekas et al. 2006). With the help of liposomal encapsulation of the radio-labelled inhibitor, it should allow higher cumulative concentration and better radiotracer uptake/retention in the EGFR-expressing tumour.

Medina et al. compared the pharmacokinetics and tumour targeting of the Morpholino-IPQA with that of the same tracer embedded in liposomes (Medina, Pillarsetty et al. 2011). Liposomal Morpholino-IPQA demonstrated an improved blood circulation time and a 3 to 6-fold increase with the tumour uptake. One problem with Morpholino-IPQA is that it is an amphiphilic compound; it will eventually leak out from the liposomes. Medina et al. reported an inhibitor release rate from the liposomes of 2.5%/hour. The *in vivo* imaging experiments with ^{125}I-Morpholino-IPQA and liposomally delivered Picchu-X sensor, that are aimed to demonstrate the relationship between the ^{125}I-drug concentration at the target site (tumour) and the corresponding intratumoural EGFR activity *in situ*, are being carried out in the supervisor's laboratory. It would also be ideal to test the release rate of our liposomal drug in future experiments and avoid prolonged storage.

This work highlights the advantages of liposomal delivery of biosensor to monitor sub-cellular activity in the primary tumour. In addition, this method might also be

adapted to assess EGFR activity at the secondary sites of metastasis using these highly metastatic models of cancer.

In the past six years, in the cancer domain, there have been large numbers of drug failures at the Phase III and submission stages; particularly with molecule-targeted drugs that have novel mechanisms of action but have relatively poor response rates in unselected patient population (Arrowsmith 2011). In an attempt to improve this poor response, the United States Food & Drug Administration (FDA) published guidelines that linked approval of molecularly targeted drugs with identification and use of diagnostic tests that select patients most likely to benefit from the drug. To date, only 17 such therapeutic-'companion diagnostic' combinations have been approved, of which 14 are indicated for stratifying cancer patients for anti- Human Epidermal Growth Factor Receptor therapies. The prediction of response to HER therapy (such as Panitumumab and Cetuximab) on the basis of EGFR expression and specific mutations (KRas/BRAF/PIK3CA/PTEN), as a positive and negative predictor of therapeutic response, respectively (Bardelli and Siena 2010; De Roock, De Vriendt et al. 2011); is beginning to be translated into clinic (e.g. the DAKO EGFR PharmDx Kit and KRAS RGQ PCR Kit).
(http://www.fda.gov/MedicalDevices/ProductsandMedicalProcedures/InVitroDiagnostics/ucm301431.htm)

However, the improvement of patient survival by stratification on the basis of EGFR expression and specific mutations alone has been disappointing low (e.g. only 10-

20% of chemotherapy-refractory CRC patients whose tumours express EGFR actually respond and, from these a large percentage will develop resistance and eventually relapse (Saltz, Meropol et al. 2004). It is our hope that the work begun in this thesis may lead to the clinical use of *in vivo* transfected fluorescence lifetime based biochemical sensors. These sensors will provide a more accurate readout of the sensitivity of tumour cells to EGFR inhibition, than receptor expression alone, among the heterogeneous patient population.

CHAPTER 7: Appendix

Material and Method from Dr Nick Mitchell

Development of a Theranostic Liposomal Delivery System for targeted Drug Treatment and FRET-based Biosensing of EGFR Activity

Materials and Methods - Synthesis of lipids and preparation of liposomes. 1,2-dioleoyl-sn-glycero-3-phosphoethanolamine (DOPE) was purchased from Avanti Polar Lipids Inc. (Alabaster, AL). All other reagents were purchased from Sigma-Aldrich Co. Ltd. unless otherwise stated, and used without further purification. All reagents were of commercial quality and used as received and all solvents anhydrous. Thin Layer Chromatography (TLC) was performed on aluminium backed Sigma-Aldrich TLC plates with F_{254} fluorescent indicator. Visualisation was done by quenching of UV fluorescence or by staining the plates with potassium permanganate solution [$KMnO_4$ (1.25 g), Na_2CO_3 (6.25 g), water (250 mL)]. Normal phase flash chromatography was carried out using silica gel (43–60 μm) supplied by Merck. LC/MS was performed on a Waters Acquity uPLC SQD using HPLC grade water and acetonitrile (both with 0.1% formic acid) as the solvents. MALDI MS was performed on a Waters MALDI MicroMX machine using α-cyano-4-hydroxycinnamic acid (CHCA) or sinapinic acid (SA) as the matrix (1 mg/mL in methanol). NMR (^1H and ^{13}C as performed on either 500 or 600 MHz AMX Bruker Spectrometers (as stated). The chemical shifts (δ) were given in units of ppm relative to tetramethylsilane (TMS), where δ (TMS) = 0 ppm. Coupling constants (J) were measured in Hertz (Hz), multiplicities for ^1H coupling are shown as s (singlet), d (doublet), t (triplet), m (multiplet), or a combination of the above. Deuterated chloroform ($CDCl_3$), dimethylsulfoxide (d_6-DMSO) and methanol (CD_3OD) were used as solvents (as stated) for all NMR analysis. Dynamic light scattering and zeta potential measurements were performed using a Malvern Zetasizer Nano-ZS (Malvern, UK).

Chemical Synthesis. *N*-(2-(2-(2-(2-hydroxyethoxy)ethoxy)ethoxy)ethyl)-*N*,*N*-dimethyl-2,3-bis((Z)-octadec-9-enyloxy)propan-1-aminium (DODEG4) was synthesised as previously described[i] as was *N*,*N*,*N*-trimethyl-2,3-bis((*Z*)-octadec-9-enyloxy)propan-1-aminium (DOTMA) [ii] and N,N-dimethyl-2,3-bis((Z)-octadec-9-enyloxy)propan-1-amine.

N-(3-aminopropyl)-N,N-dimethyl-2,3-bis((Z)-octadec-9-enyloxy)propan-1-aminium bromide

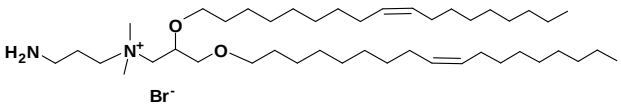

To 1.35 g (2.18 mmol) of N,N-dimethyl-2,3-bis((Z)-octadec-9-enyloxy)propan-1-amine in acetone was added 1.04 g (4.36 mmol) of *ter*t butyl 3-bromopropyl-carbamate (also in acetone - synthesised as described; *J. Med. Chem*. **2010**, 6608-6617) and the solution heated in a sealed tube at 100 °C for 48 hrs. After this time the solvent was removed under reduced pressure and the crude dissolved in 10 mL of a 1:1 solution of TFA:H_2O and stirred at room temp. for 3 hrs. The solvent was again removed and the crude material purified via silica column chromatography using a solvent system of 5 – 20 % methanol in DCM. The fractions containing the pure product were pooled and the solvent removed under reduced pressure. The salt was then washed with sat. $NaHCO_3$ (5mL) and extracted into $CHCl_3$ (10mL), dried (Na_2SO_4) and concentrated. The resulting oil was dried under high vacuum to give 1.15 g (78% yield) of the desired product. R_f 0.39 (20% MeOH in CH_2Cl_2); v_{MAX} (CHCl3)/cm^{-1} 2923, 2854, 1678; ESI-HRMS found 677.6918 *m/z* $[M+H]^+$, $C_{44}H_{89}N_2O_2$ requires 677.6924; ^1H NMR δ_H (600 MHz, $CDCl_3$): 0.86 (t, 6H, *J* = 7.1 Hz, CH_2CH_3), 1.24-1.31 (m, 44H, CH_2), 1.53 (m, 4H, CH_2CH_2O), 1.82-2.00 (m, 10H, $CH_2CHCHCH_2$ and $NCH_2CH_2CH_2NH_2$), 3.36-3.72 (m, 19H, CH_2OCH_2CH $CH_2N(CH_3)_2$ and NCH_2CH_2 CH_2NH_2), 4.01 (2x bm, 1H, $OCH_2CHCH_2N(CH_3)_2$), 5.30-

5.36 (m, 4H, CH_2*CHCH*CH_2); ^{13}C NMR (150 MHz, $CDCl_3$) δ /ppm 14.25, 20.94, 22.81, 25.13, 26.07, 26.12, 26.24, 27.35, 27.74, 29.21-30.07 (signals superimposed), 32.01, 32.76, 33.82, 36.75, 39.33, 50.99, 51.64, 53.20, 59.27, 63.19, 66.37, 68.63, 69.47, 72.13, 73.12, 115.77, 117.71, 129.91-130.48 (signals superimposed), 161.92, 162.15.

N-(3-aminopropyl)-N,N-dimethyl-2,3-bis((Z)-octadec-9-enyloxy)propan-1-aminium-Cyanine 5

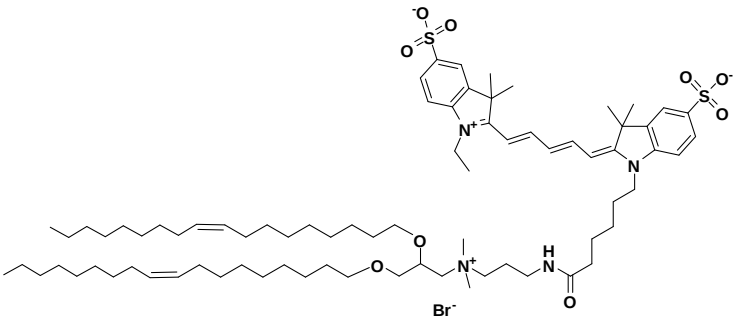

1 mg of Cy5-NHS (1.26 umol) in DCM and 2 uL (15.2 umol) of triethylamine were added to 1.2 mg (1.52 umol) of the starting lipid also in DCM and allowed to react at room temperature overnight in the dark. After this time the solvent was removed under reduced pressure and the crude product purified *via* preparative TLC using a solvent system of 20% methanol in DCM to give 1.8 mg of the desired product (90% yield, one spot on TLC). TLC analysis; Rf = 0.63 (solv. sys.; 20% methanol in DCM); MALDI MS; calculated mass - 1314 g.mol^{-1}; observed mass – 1315 g.mol^{-1} (MH^+); matrix; sinapinic acid (1 mg/mL in methanol).

(E)-ethyl 4-(3-morpholinopropylamino)-4-oxobut-2-enoate – adapted protocol

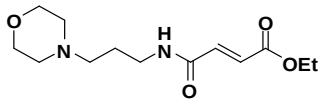

To 2.5 g (17.3 mmol) of fumeric acid monoethyl ester, 7.9 g (20.8 mmol) of HBTU and 6 mL (4.45 g, 34.4 mmol) of DIPEA in anhydrous DCM was added 2.5 g (17.3 mmol) of N-(3-aminopropyl) morpholine. The reaction was allowed to stir at room temp. and over the following 3h a further 0.15 eq of N-(3-aminopropyl) morpholine and DIPEA was added. After this time the solvent was removed under reduced pressure and the crude oil purified via flash chromatography to give 3.41 g of the desired product (73% yield). LC/MS; calculated mass 270.16 $g.mol^{-1}$ ($C_{13}H_{22}O_4N_2$); observed mass 271.5 *m/z* (MH^+).^{1}H NMR (500 MHz, $CDCl_3$) δ /ppm 1.3 (3H, t, J = 7.17, ethyl gp), 1.7 (2H, q, J = 6.31, -C**H$_2$**-), 2.5 (6H, m), 3.45 (2H, m, -C**H$_2$**-), 3.7 (4H, t, J = 4.57, -OC**H$_2$**-), 4.2 (2H, q, J = 7.10, ethyl gp.), 6.8 (2H, dd, J = 15.61, alkene), 7.5 (1H, s, -N**H**-). ^{13}C NMR (125 MHz, $CDCl_3$) δ /ppm 14.21, 24.25, 39.70, 53.57, 57.72, 60.94, 61.20, 66.81, 130.10, 136.64, 163.68, 165.65.

(E)-N'-(2-cyano-4-nitrophenyl)-N,N-dimethylformimidamide

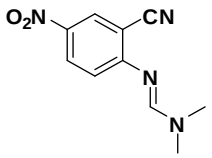

25 mL (22.4 g, 188.2 mmol) of N,N-dimethylformamide dimethyl acetal was added to 10.23 g (62.7 mmol) of 5-nitroanthranitrile. The solution was refluxed at 100 °C for 4.5h then filtered. The orange solid was washed with diethyl ether and dried in a desiccator to give 12.52 g (91.6%) of the desired product. LC/MS; calculated mass 218.08 $g.mol^{-1}$ ($C_{10}H_{10}O_2N_4$); observed mass 219.2 *m/z* (MH^+).1H NMR (500 MHz, $CDCl_3$) δ /ppm 3.15 (6H, s, N(C**H$_3$**)$_2$), 7.0 (1H, d, J = 9.06, aromatic), 7.7 (1H, s, imine),

8.2 (1H, dd, J = 2.68, aromatic), 8.4 (1H, d, J = 2.68, aromatic). ^{13}C NMR (125 MHz, $CDCl_3$) δ /ppm 35.18, 40.94, 107.29, 116.76, 118.88, 128.65, 129.58, 141.45, 154.36, 160.20.

N4-(3-iodophenyl)quinazoline-4,6-diamine

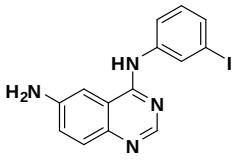

75 mL of acetic acid was added to 5 g (22.9 mmol) of (E)-N'-(2-cyano-4-nitrophenyl)-N,N-dimethylformimidamide and 6 g (3.32 mL, 27.6 mmol) of 3-iodoanaline. The reaction was refluxed at 125 °C until it reached completion. The solution was stored at 4 °C overnight and the resulting precipitate filtered and washed with diethyl ether. The yellow solid was dried in a descicator to give 10.32 g (88.2% yield) of the acetate salt product. No further purification was necessary. 2.5 g (mmol) of this product was dissolved in 50 mL ethanol, 10 mL distilled water and 5 mL acetic acid and refluxed at 100 °C for 15 min. After this time 5 g of Fe powder was washed with 1N HCl and distilled water and suspended in distilled water. The slurry was added slowly using a dropping funnel and the reaction allowed to reflux using a mechanical stirrer. After 2h the reaction was filtered through celite the filtrate was diluted up in ethyl acetate and to this solution conc. HCl was added dropwise. The HCl salt of the amine crashed out of solution and was filtered. Further c.HCl was added to the filtrate and the process repeated. The solid was dried in a desiccator, redissolved in distilled water, basified with 1M NaOH and extracted into DCM. The organic phase was dried over $MgSO_4$ and the solvent removed under reduced pressure to give 1.32 g of a dark brown solid. LC/MS; calculated mass 362.00 g.mol^{-1} ($C_{14}H_{11}N_4I$); observed mass 363.3 *m/z* (MH^+).^{1}H NMR (500 MHz d_6-DMSO) δ /ppm 5.6 (2H, bs, NH_2), 7.1 (1H, t, J = 7.95), 7.2 (1H, d, J = 7.50), 7.35 (2H, m), 7.5 (1H, d, J = 8.75), 8.34 (1H, s), 8.35 (1H, s), 9.4 (1H, bs, -NH-); ^{13}C NMR (125 MHz, d_6-DMSO) δ

/ppm 30.69, 94.13, 100.96, 116.71, 120.59, 123.77, 128.70, 129.31, 130.35, 131.04, 141.61, 142.66, 147.39, 149.58, 155.70.

N1-(4-(3-iodophenylamino)quinazolin-6-yl)-N4-(3-morpholinopropyl)fumar amide

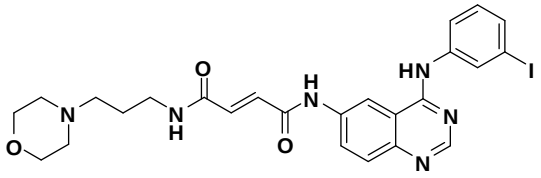

0.5 g of compound **15** was dissolved in 20 mL of distilled water and 1 mL of triethylamine added. The solution was allowed to stir at room temp. overnight. After this period the solvent was removed under reduced pressure and the oil dried on a high vacuum line overnight. To 0.729 mmol of the acid (0.250 g) in anhydrous pyridine was added 0.154 mg (0.802 mmol) of EDC also in pyridine. 0.266 g (0.729 mmol) of compound **17** in dry pyridine was then added to the reaction which was left stirring under $Ar_{(g)}$ for 2h. After this time a further 0.5 eq. of EDC (70 mg) was added and the reaction left strirring for another overnight. The solvent was then removed under reduced pressure the crude was purified by silica gel chromatography using a solvent system of 0 – 10% methanol in DCM (material dry loaded onto the column) to afford 153 mg of the desired product (36% yield). To generate the water soluble TFA salt the compound was eluted through a semi-prep HPLC column (Phenomenex C_{18}) using a gradient of 2 – 40 % acetonitrile (0.1% TFA) in HPLC grade water (0.1% TFA) over 20 min. Fractions containing the desired product were combined and the solvent removed under reduced pressure. The material was redissolved in 5 mL of distilled water and freeze-dried overnight. LC/MS; calculated mass 586.12 $g.mol^{-1}$ ($C_{25}H_{27}O_3N_6I$); observed mass 587.3 *m/z* (MH^+). ^1H NMR (500 MHz MeOD) δ /ppm 2.0 (2H, m), 3.1 (4H, m), 3.4 (2H, m), 3.5 (2H, m), 3.8 (2H, m), 4.0 (2H, m), 7.1 (2H, dd, J = 15.05), 7.25 (1H, t, J = 7.49), 7.7 (2H, dd, J = 8.0), 7.85 (1H, d, J = 8.91), 8.1 (1H, d, J= 8.91), 8.2 (1H, s), 8.7 (1H, s), 9.0 (1H, s). ^{13}C NMR (125 MHz, MeOD) δ /ppm 14.0, 24.6, 37.1, 52.8, 55.7, 64.7, 93.8, 113.5, 121.0, 124.7, 130.3, 133.5, 135.1, 136.9, 138.7, 140.1, 150.6, 166.6.

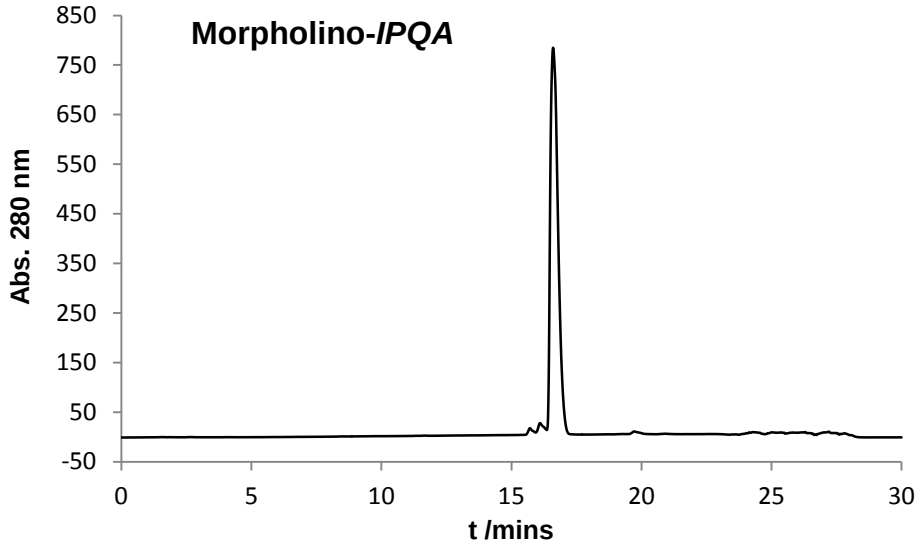

Lipid Structures

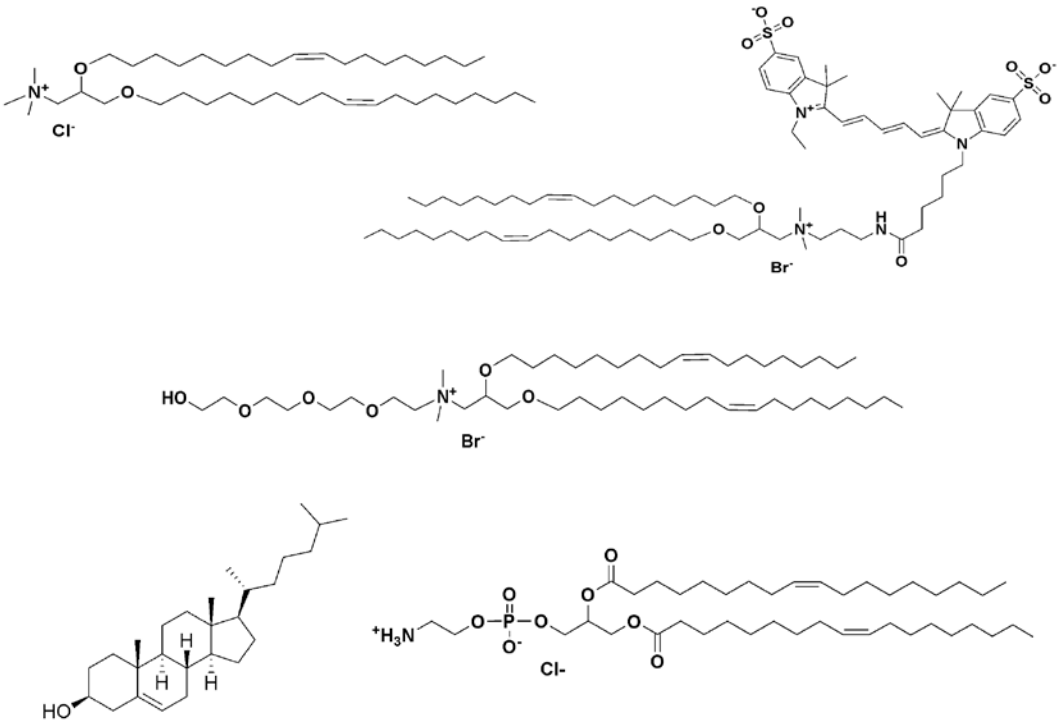

General method for solid phase peptide synthesis (SPPS). All peptides were synthesized using standard Fmoc solid-phase peptide synthesis on a Syro automated system. Pre-loaded Wang or TGT resin was used with standard HBTU/DIPEA coupling chemistry. All amino acids were purchased as N-protected Fmoc and appropriately protected R group compounds. Each coupling step was conducted for 40 mins and each Fmoc deprotection allowed to proceed for 3 min in 40 % piperdine and then 10 min in 20% piperidine. Four equivalents of amino acids and associated reagents were used. After completion of the synthesis, peptides were deprotected and cleaved from the resin by incubation in TFA/TES/EDT/H_2O (2500:150:75:150 µL) for 3 hours. The collected peptide solution was mixed with diethyl ether and allowed to precipitate at -20°C. The suspension was centrifuged at 4000 rpm for 5 min, and the pellet was re-dissolved in diethyl ether. This purification process was repeated three times after which the precipitate was dissolved in deionized H_2O or 0.1% TFA containing HPLC grade water if necessary, frozen in liquid N_2 and freeze-dried overnight. The peptides were analyzed and if necessary purified via reversed phase HPLC using a Varian ProStar system with a Model 210 solvent delivery module and a Model 320 UV detector. The preparative purification was performed using either a Varian preparative column (C_{18}, 250 x 21.2 mm, 10 µm beads, flow rate of 10 mL/min) or Phenomenex semi-prep (C_{18}, 100 x 10 mm, flow rate of 8 mL/min). The mobile phase was a linear gradient beginning with 98:2 water (0.1% TFA) / acetonitrile (0.1% TFA) to 2:98 water (0.1% TFA) / acetonitrile (0.1% TFA) over 30 min, this gradient was adapted when necessary. Fractions containing the correct peak were pooled, the solvent removed under reduced pressure to approximately 5 mL, and the solution freeze-dried overnight. ESI-MS analysis was performed on a Waters Acquity Ultra Performance LC/MS machine in positive ion mode using the same solvent system and gradient as the analytical HPLC procedure detailed above (0.6 ml/min, 0.1% formic acid used in place of TFA).

MYIEALDKYACRVRRK$_{16}$

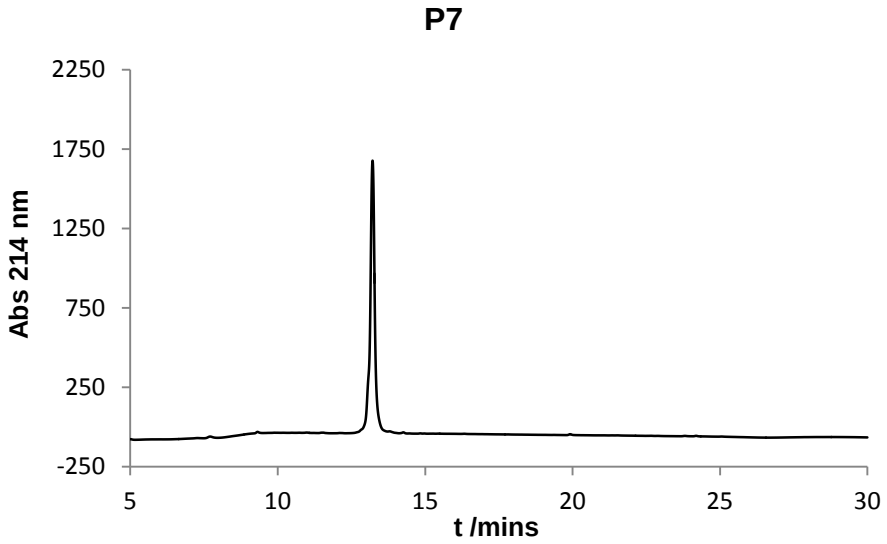

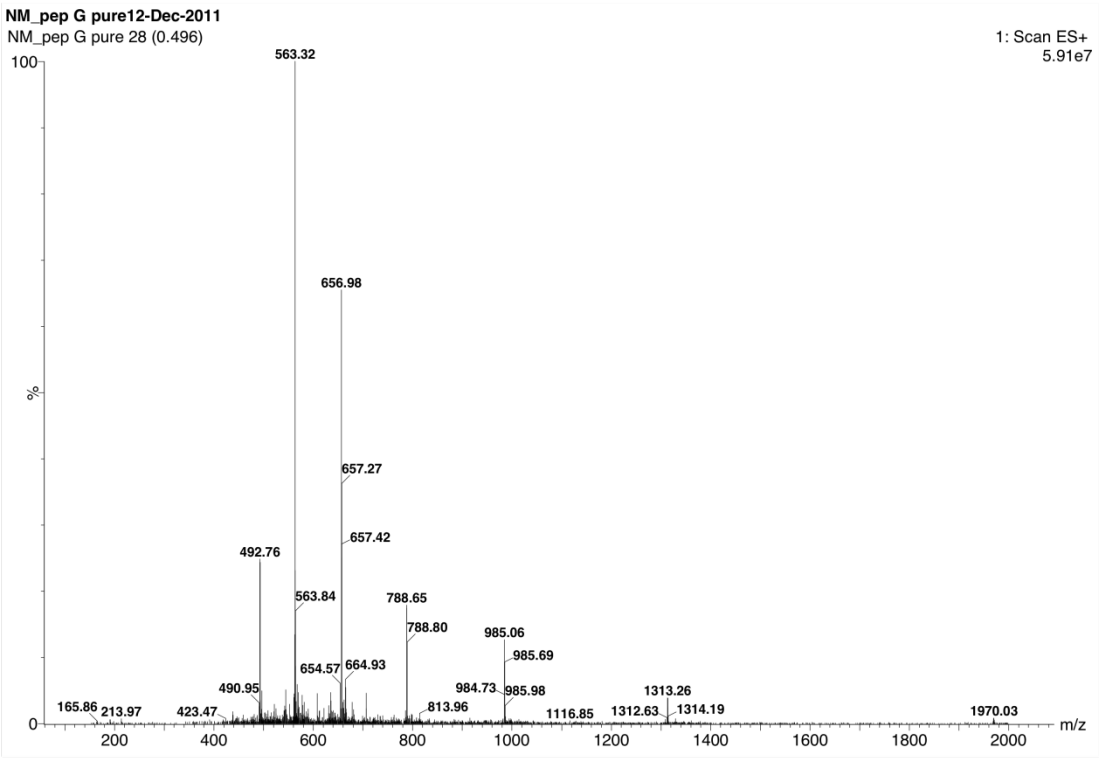

K_{16}RVRRYHWYGYTPQNVI

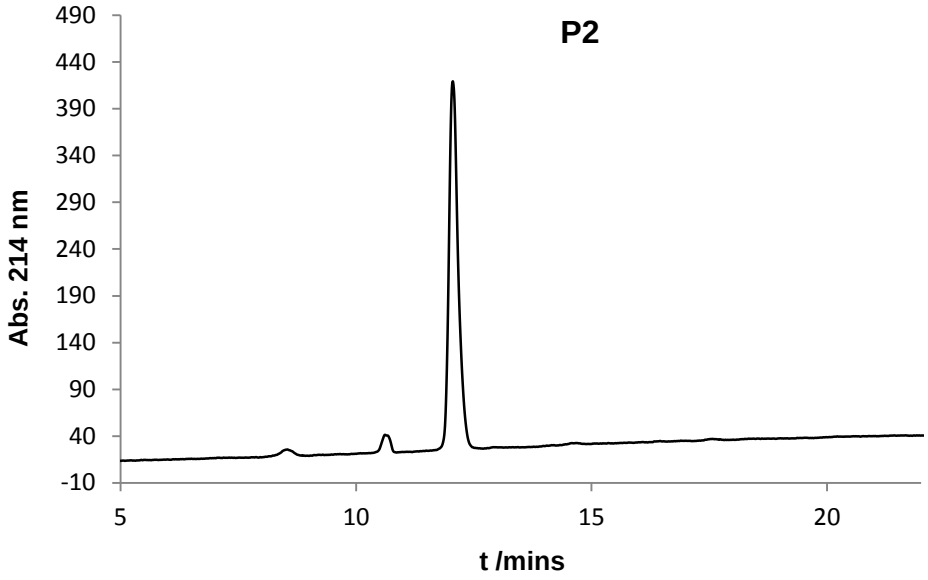

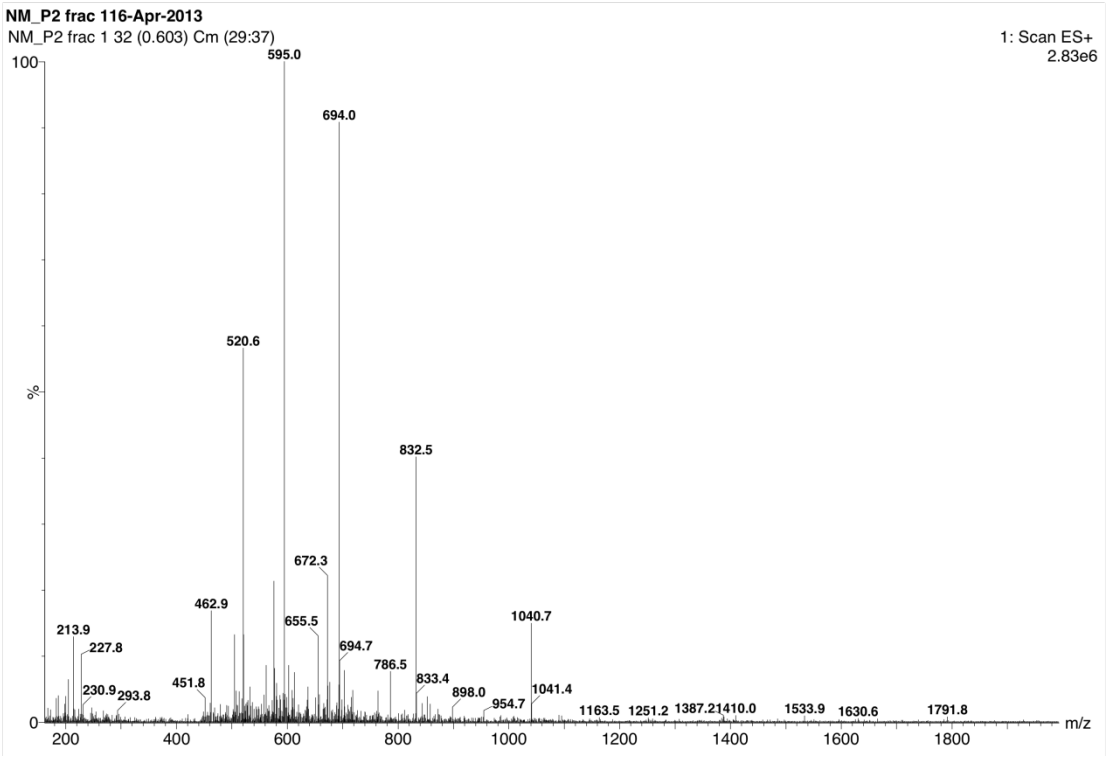

K_{16}RVRRLARLLT

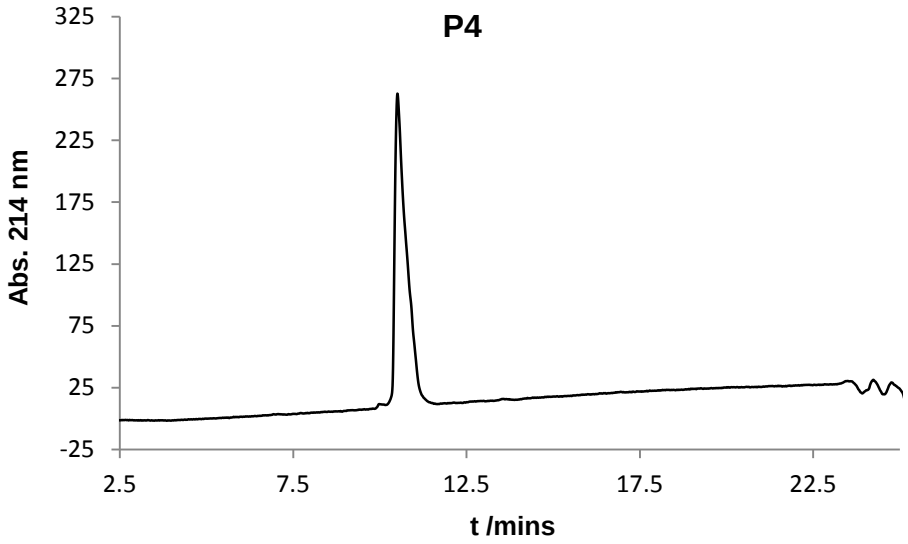

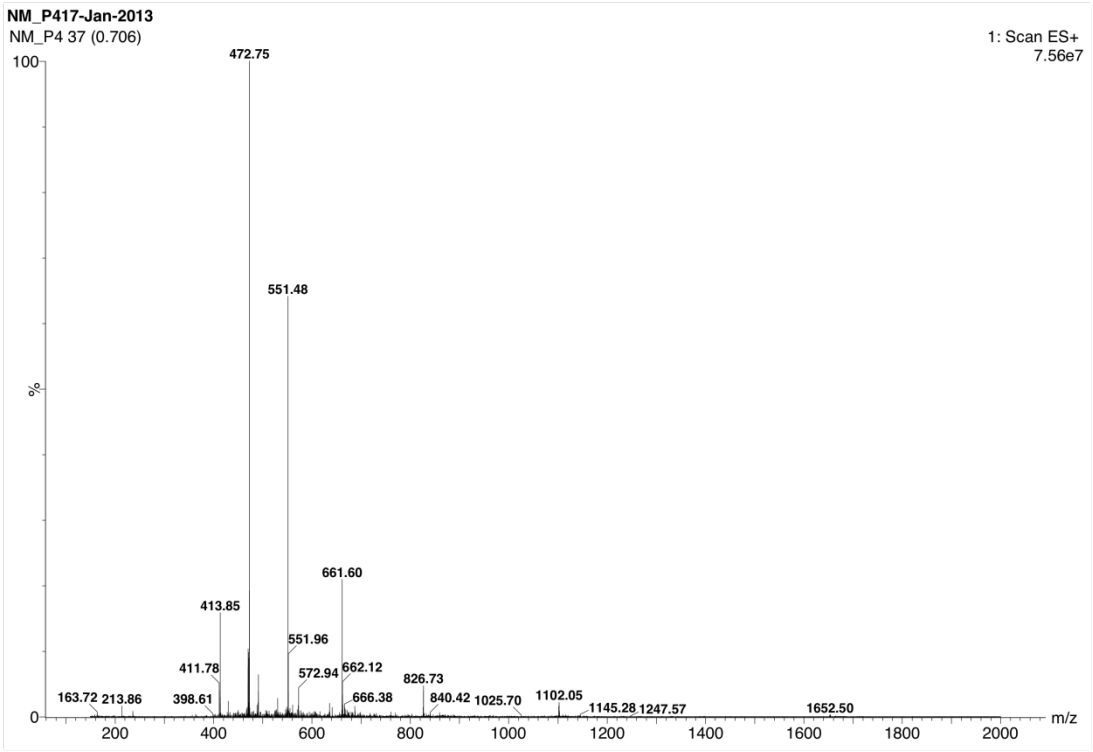

YHWYGYTPQNVIRVRRK$_{16}$

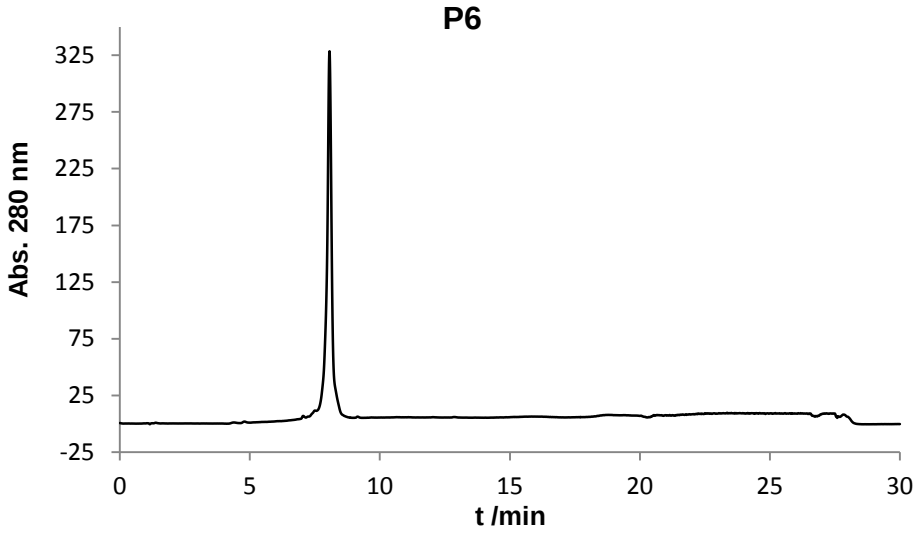

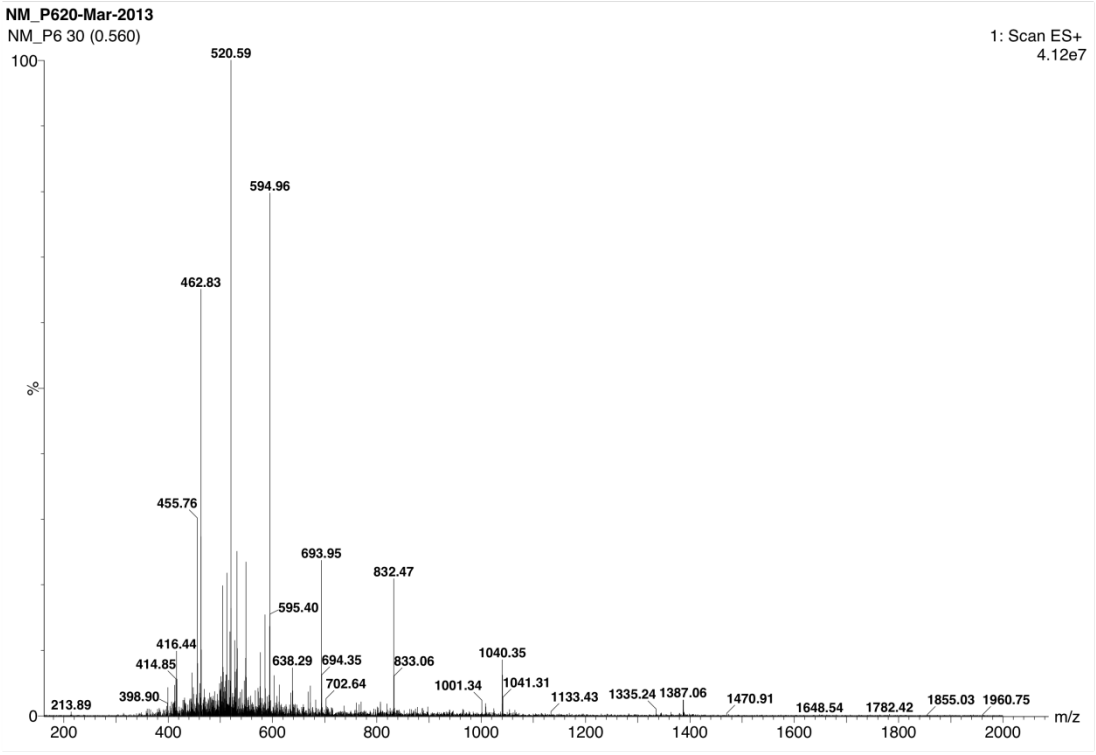

LARLLTRVRRK$_{16}$

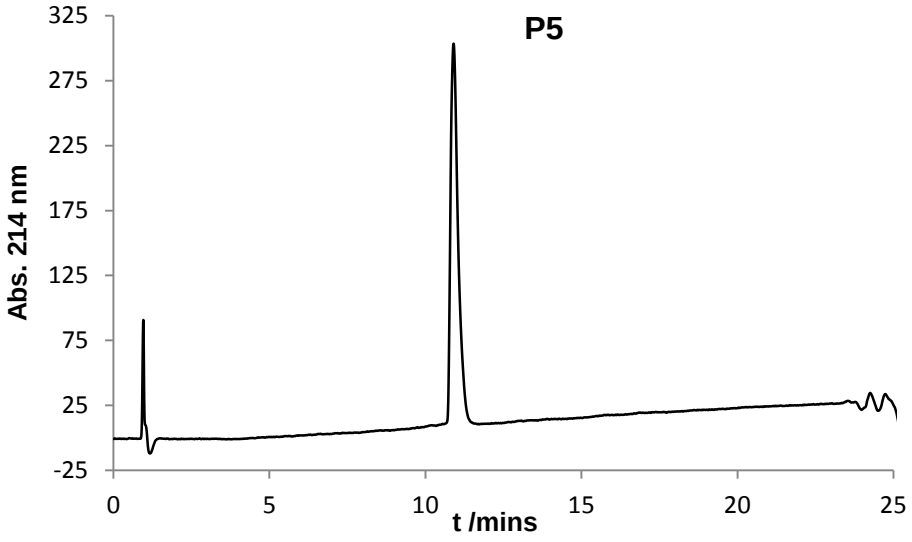

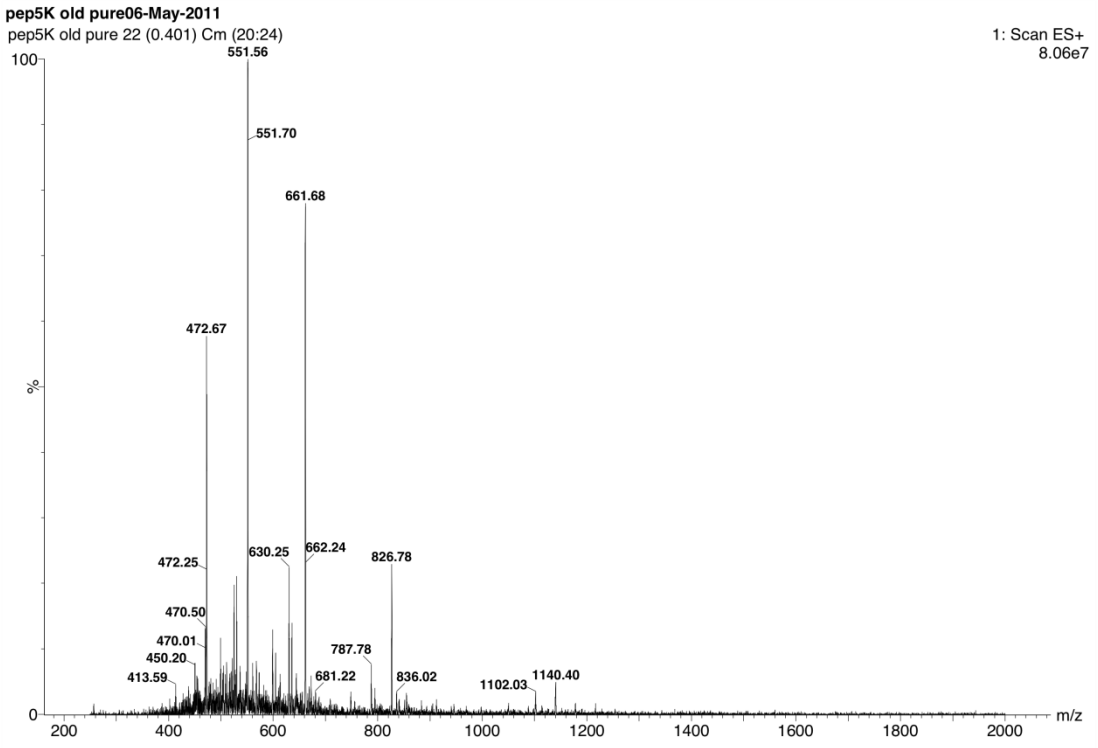

K_{16}

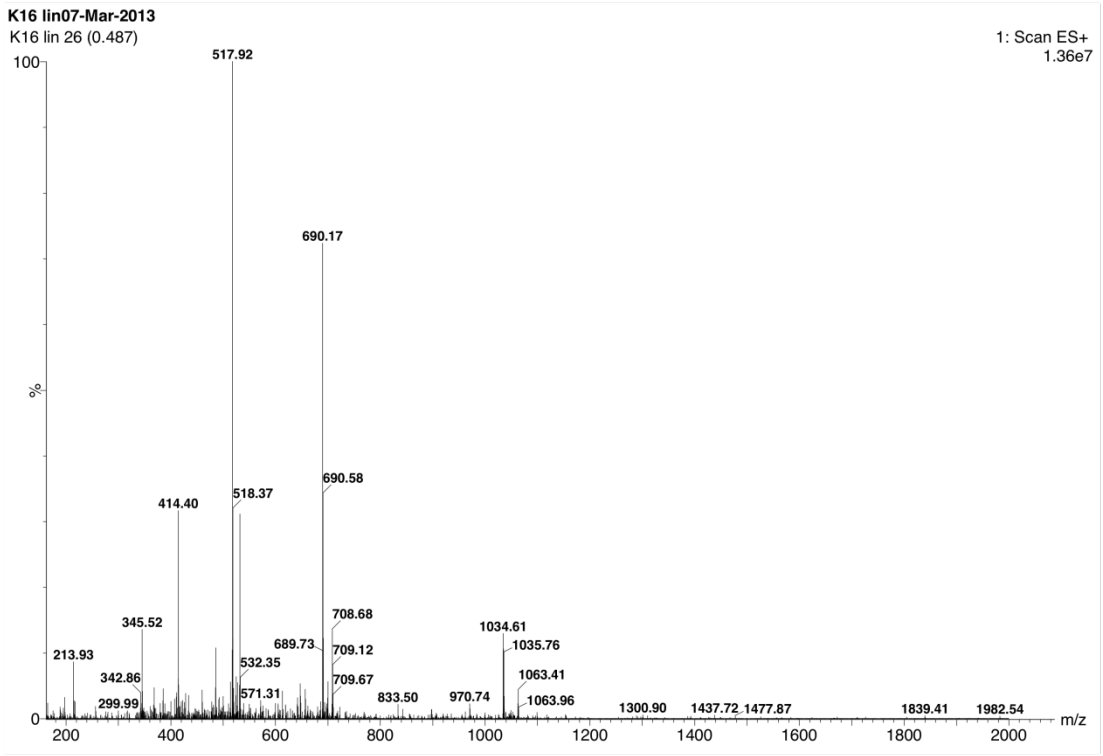

Formation of LPD complexes. All lipid components were dissolved in either $CHCl_3$ or methanol to a concentration of 1 mM. The lipids were mixed together in the appropriate molar ratios (CH300 50 mol%, DOPE 30 mol%, DOTMA 20 mol%, Cholesterol 30 mol% - if Cy5 lipid used then replaces 1 mol% of DOPE) and the solvents removed under reduced pressure to form a thin film. This film was further dried on a high vacuum line for 4 h (or overnight in a desiccator) then hydrated with sterilized water. For in vitro samples the formulations were sonicated using a bath sonicator for 10 mins. A total lipid conc. of 100 uM was favoured; 4 – 16 ug of peptide was added to the liposome solution followed by 1 – 4 ug of plasmid DNA (Picchu biosensor), the samples were then used immediately. For *in vivo* samples the formulations were prepared using a probe sonicator (Sonifier SLPe, Branson (USA)). A total lipid conc. of 1.5 mM was used with addition of 136 ug mg of K_{16} peptide (or equal molar amount if alterative sequences were used) and 68 ug of DNA per injected sample. The peptide (in sterilized water) was added to the liposome solution

and diluted to 2 mL. The appropriate volume of DNA solution (also in sterilized water) was also diluted to 2 mL and combined with the LP solution. The samples were then concentrated to an appropriate volume for injection using VivaSpin columns (MWCO 10,000). The liposomes were characterized using DLS and Zeta potential; aliquots of

25 – 50 uL were diluted to 1 mL in sterilized water and analysed in triplicate at 25 °C.

Liposome	DODEG-4	DOPE	DOTMA	Cy5-L	Cholesterol	DLS (PDI)	Zeta pot.
In vitro	50%	29%	20%	1%	30%	-	-
*In vivo (**1**)*	50%	30%	20%	0%	30%	146.3 nm (0.264)	52.4 mV
*In vivo (**2**)*	50%	30%	20%	0%	30%	147.1 nm (0.355)	40.6 mV
*In vivo (**3**)*	50%	30%	20%	0%	30%	140.2 nm (0.407)	56.7 mV
*In vivo (**4**)*	50%	30%	20%	0%	30%	85.7 nm (0.274)	44.8 mV
*In vivo (**5**)*	50%	30%	20%	0%	30%	168.5 nm (0.3)	33.1 mV

Table 1; (**1**) Liposome sample; (**2**) LPD Picchu-X plasmid + P2; (**3**) LPD GFP plasmid + P2; (**4**) Liposome sample; (**5**) LPD Picchu-X plasmid + P2.

CHAPTER 8: References

Amin, D. N., N. Sergina, et al. (2010). "Resiliency and vulnerability in the HER2-HER3 tumorigenic driver." Sci Transl Med **2**(16): 16ra17.

Anastasiou, D., G. Poulogiannis, et al. (2011). "Inhibition of pyruvate kinase M2 by reactive oxygen species contributes to cellular antioxidant responses." Science **334**(6060): 1278-1283.

Andl, C. D., T. Mizushima, et al. (2004). "EGFR-induced cell migration is mediated predominantly by the JAK-STAT pathway in primary esophageal keratinocytes." Am J Physiol Gastrointest Liver Physiol **287**(6): G1227-1237.

Anido, J., P. Matar, et al. (2003). "ZD1839, a specific epidermal growth factor receptor (EGFR) tyrosine kinase inhibitor, induces the formation of inactive EGFR/HER2 and EGFR/HER3 heterodimers and prevents heregulin signaling in HER2-overexpressing breast cancer cells." Clin Cancer Res **9**(4): 1274-1283.

Antoku, S. and B. J. Mayer (2009). "Distinct roles for Crk adaptor isoforms in actin reorganization induced by extracellular signals." Journal of Cell Science **122**(22): 4228-4238.

Aoki, K., E. Kiyokawa, et al. (2008). "Visualization of growth signal transduction cascades in living cells with genetically encoded probes based on Forster resonance energy transfer." Philos Trans R Soc Lond B Biol Sci **363**(1500): 2143-2151.

Aoki, K., T. Nakamura, et al. (2005). "Local phosphatidylinositol 3,4,5-trisphosphate accumulation recruits Vav2 and Vav3 to activate Rac1/Cdc42 and initiate neurite outgrowth in nerve growth factor-stimulated PC12 cells." Mol Biol Cell **16**(5): 2207-2217.

Arrowsmith, J. (2011). "Trial watch: phase III and submission failures: 2007-2010." Nat Rev Drug Discov **10**(2): 87.

Athauda, G., A. Giubellino, et al. (2006). "c-Met ectodomain shedding rate correlates with malignant potential." Clin Cancer Res **12**(14 Pt 1): 4154-4162.

Avraham, R. and Y. Yarden (2011). "Feedback regulation of EGFR signalling: decision making by early and delayed loops." Nat Rev Mol Cell Biol **12**(2): 104-117.

Bandyopadhyay, D., M. Mandal, et al. (1998). "Physical interaction between epidermal growth factor receptor and DNA-dependent protein kinase in mammalian cells." J Biol Chem **273**(3): 1568-1573.

Barber, P. R., S. M. Ameer-Beg, et al. (2009). "Multiphoton time-domain fluorescence lifetime imaging microscopy: practical application to protein-protein interactions using global analysis." Journal of the Royal Society Interface **6**: S93-S105.

Barber, P. R., S. M. Ameer-Beg, et al. (2005). "Global and pixel kinetic data analysis for FRET detection by multi-photon time-domain FLIM." Multiphoton Microscopy in the Biomedical Sciences V **5700**: 171-181.

Bardelli, A. and S. Siena (2010). "Molecular mechanisms of resistance to cetuximab and panitumumab in colorectal cancer." J Clin Oncol **28**(7): 1254-1261.

Baselga, J. (2002). "Targeting the epidermal growth factor receptor with tyrosine kinase inhibitors: small molecules, big hopes." J Clin Oncol **20**(9): 2217-2219.

Baselga, J. and L. A. Hammond (2002). "HER-targeted tyrosine-kinase inhibitors." Oncology **63 Suppl 1**: 6-16.

Baselga, J., J. M. Trigo, et al. (2005). "Phase II multicenter study of the antiepidermal growth factor receptor monoclonal antibody cetuximab in combination with platinum-based chemotherapy in patients with platinum-refractory metastatic and/or recurrent squamous cell carcinoma of the head and neck." J Clin Oncol **23**(24): 5568-5577.

Bastiaens, P. I. and A. Squire (1999). "Fluorescence lifetime imaging microscopy: spatial resolution of biochemical processes in the cell." Trends Cell Biol **9**(2): 48-52.

Bau, D. T., C. W. Tsai, et al. (2011). "Role of the XRCC5/XRCC6 dimer in carcinogenesis and pharmacogenomics." Pharmacogenomics **12**(4): 515-534.

Bentires-Alj, M., S. G. Gil, et al. (2006). "A role for the scaffolding adapter GAB2 in breast cancer." Nat Med **12**(1): 114-121.

Bertucci, F., P. Finetti, et al. (2012). "Basal breast cancer: a complex and deadly molecular subtype." Curr Mol Med **12**(1): 96-110.

Beutler, M., K. Makrogianneli, et al. (2008). "satFRET: estimation of Forster resonance energy transfer by acceptor saturation." European Biophysics Journal with Biophysics Letters **38**(1): 69-82.

Beutler, M., K. Makrogianneli, et al. (2008). "satFRET: estimation of Forster resonance energy transfer by acceptor saturation." Eur Biophys J **38**(1): 69-82.

Beuttler, J., M. Rothdiener, et al. (2009). "Targeting of epidermal growth factor receptor (EGFR)-expressing tumor cells with sterically stabilized affibody liposomes (SAL)." Bioconjug Chem **20**(6): 1201-1208.

Bhargava, R., W. L. Gerald, et al. (2005). "EGFR gene amplification in breast cancer: correlation with epidermal growth factor receptor mRNA and protein expression and HER-2 status and absence of EGFR-activating mutations." Mod Pathol **18**(8): 1027-1033.

Blagoev, B., I. Kratchmarova, et al. (2003). "A proteomics strategy to elucidate functional protein-protein interactions applied to EGF signaling." Nat Biotechnol **21**(3): 315-318.

Brand, T. M., M. Iida, et al. (2011). "The nuclear epidermal growth factor receptor signaling network and its role in cancer." Discov Med **12**(66): 419-432.

Britten, C. D., R. S. Finn, et al. (2009). "A phase I/II trial of trastuzumab plus erlotinib in metastatic HER2-positive breast cancer: a dual ErbB targeted approach." Clin Breast Cancer **9**(1): 16-22.

Brummer, T., D. Schramek, et al. (2006). "Increased proliferation and altered growth factor dependence of human mammary epithelial cells overexpressing the Gab2 docking protein." J Biol Chem **281**(1): 626-637.

Bublil, E. M., G. Pines, et al. (2010). "Kinase-mediated quasi-dimers of EGFR." FASEB J **24**(12): 4744-4755.

Buchanan, S. G., J. Hendle, et al. (2009). "SGX523 is an exquisitely selective, ATP-competitive inhibitor of the MET receptor tyrosine kinase with antitumor activity in vivo." Mol Cancer Ther **8**(12): 3181-3190.

Buday, L., A. Khwaja, et al. (1996). "Interactions of Cbl with two adapter proteins, Grb2 and Crk, upon T cell activation." J Biol Chem **271**(11): 6159-6163.

Cappuzzo, F., V. Gregorc, et al. (2003). "Gefitinib in pretreated non-small-cell lung cancer (NSCLC): analysis of efficacy and correlation with HER2 and

epidermal growth factor receptor expression in locally advanced or metastatic NSCLC." J Clin Oncol **21**(14): 2658-2663.
Carey, L. A., H. S. Rugo, et al. (2012). "TBCRC 001: randomized phase II study of cetuximab in combination with carboplatin in stage IV triple-negative breast cancer." J Clin Oncol **30**(21): 2615-2623.
Carlin, L. M., R. Evans, et al. (2011). "A targeted siRNA screen identifies regulators of Cdc42 activity at the natural killer cell immunological synapse." Sci Signal **4**(201): ra81.
Casamassimi, A., A. De Luca, et al. (2000). "EGF-related antisense oligonucleotides inhibit the proliferation of human ovarian carcinoma cells." Ann Oncol **11**(3): 319-325.
Cheang, M. C., S. K. Chia, et al. (2009). "Ki67 index, HER2 status, and prognosis of patients with luminal B breast cancer." J Natl Cancer Inst **101**(10): 736-750.
Chen, H., J. Kovar, et al. (2005). "A cell-based immunocytochemical assay for monitoring kinase signaling pathways and drug efficacy." Anal Biochem **338**(1): 136-142.
Citri, A. and Y. Yarden (2006). "EGF-ERBB signalling: towards the systems level." Nat Rev Mol Cell Biol **7**(7): 505-516.
Cline, M. S., M. Smoot, et al. (2007). "Integration of biological networks and gene expression data using Cytoscape." Nat Protoc **2**(10): 2366-2382.
Cohen, E. E., F. Rosen, et al. (2003). "Phase II trial of ZD1839 in recurrent or metastatic squamous cell carcinoma of the head and neck." J Clin Oncol **21**(10): 1980-1987.
Collis, S. J., T. L. DeWeese, et al. (2005). "The life and death of DNA-PK." Oncogene **24**(6): 949-961.
Condeelis, J. and J. W. Pollard (2006). "Macrophages: obligate partners for tumor cell migration, invasion, and metastasis." Cell **124**(2): 263-266.
Cooper, K. L., Y. Meng, et al. (2011). "Positron emission tomography (PET) and magnetic resonance imaging (MRI) for the assessment of axillary lymph node metastases in early breast cancer: systematic review and economic evaluation." Health Technol Assess **15**(4): iii-iv, 1-134.
Corkery, B., J. Crown, et al. (2009). "Epidermal growth factor receptor as a potential therapeutic target in triple-negative breast cancer." Ann Oncol **20**(5): 862-867.
Courbard, J. R., F. Fiore, et al. (2002). "Interaction between two ubiquitin-protein isopeptide ligases of different classes, CBLC and AIP4/ITCH." J Biol Chem **277**(47): 45267-45275.
Cullis, P. R., A. Chonn, et al. (1998). "Interactions of liposomes and lipid-based carrier systems with blood proteins: Relation to clearance behaviour in vivo." Adv Drug Deliv Rev **32**(1-2): 3-17.
Cunnick, J. M., J. F. Dorsey, et al. (2000). "Requirement of SHP2 binding to Grb2-associated binder-1 for mitogen-activated protein kinase activation in response to lysophosphatidic acid and epidermal growth factor." J Biol Chem **275**(18): 13842-13848.
Cunningham, D., Y. Humblet, et al. (2004). "Cetuximab monotherapy and cetuximab plus irinotecan in irinotecan-refractory metastatic colorectal cancer." N Engl J Med **351**(4): 337-345.

Curtis, C., S. P. Shah, et al. (2012). "The genomic and transcriptomic architecture of 2,000 breast tumours reveals novel subgroups." Nature **486**(7403): 346-352.
Cusick, M. E., H. Yu, et al. (2009). "Literature-curated protein interaction datasets." Nat Methods **6**(1): 39-46.
Dacic, S., M. Flanagan, et al. (2006). "Significance of EGFR protein expression and gene amplification in non-small cell lung carcinoma." Am J Clin Pathol **125**(6): 860-865.
Dancey, J. and E. A. Sausville (2003). "Issues and progress with protein kinase inhibitors for cancer treatment." Nat Rev Drug Discov **2**(4): 296-313.
de la Rica, R., D. Aili, et al. (2012). "Enzyme-responsive nanoparticles for drug release and diagnostics." Adv Drug Deliv Rev **64**(11): 967-978.
De Roock, W., V. De Vriendt, et al. (2011). "KRAS, BRAF, PIK3CA, and PTEN mutations: implications for targeted therapies in metastatic colorectal cancer." Lancet Oncol **12**(6): 594-603.
Dennison, S. K., S. A. Jacobs, et al. (2007). "A phase II clinical trial of ZD1839 (Iressa) in combination with docetaxel as first-line treatment in patients with advanced breast cancer." Invest New Drugs **25**(6): 545-551.
Dickler, M. N., H. S. Rugo, et al. (2008). "A phase II trial of erlotinib in combination with bevacizumab in patients with metastatic breast cancer." Clin Cancer Res **14**(23): 7878-7883.
Dikic, I. and S. Giordano (2003). "Negative receptor signalling." Curr Opin Cell Biol **15**(2): 128-135.
Dorsett, Y. and T. Tuschl (2004). "siRNAs: applications in functional genomics and potential as therapeutics." Nat Rev Drug Discov **3**(4): 318-329.
Drummond, D. C., O. Meyer, et al. (1999). "Optimizing liposomes for delivery of chemotherapeutic agents to solid tumors." Pharmacol Rev **51**(4): 691-743.
Duffy, M. J., N. O'Donovan, et al. (2011). "Use of molecular markers for predicting therapy response in cancer patients." Cancer Treat Rev **37**(2): 151-159.
Dulak, A. M., C. T. Gubish, et al. (2011). "HGF-independent potentiation of EGFR action by c-Met." Oncogene.
Elbashir, S. M., J. Harborth, et al. (2001). "Duplexes of 21-nucleotide RNAs mediate RNA interference in cultured mammalian cells." Nature **411**(6836): 494-498.
Esposito, A., C. P. Dohm, et al. (2007). "Unsupervised fluorescence lifetime imaging microscopy for high content and high throughput screening." Mol Cell Proteomics **6**(8): 1446-1454.
Ferguson, K. M. (2008). "Structure-based view of epidermal growth factor receptor regulation." Annu Rev Biophys **37**: 353-373.
Ferlay, J., H. R. Shin, et al. (2010). "Estimates of worldwide burden of cancer in 2008: GLOBOCAN 2008." Int J Cancer **127**(12): 2893-2917.
Festy, F., S. M. Ameer-Beg, et al. (2007). "Imaging proteins in vivo using fluorescence lifetime microscopy." Mol Biosyst **3**(6): 381-391.
Fidler, I. J. (2003). "The pathogenesis of cancer metastasis: the 'seed and soil' hypothesis revisited." Nat Rev Cancer **3**(6): 453-458.
Fischer, J. R., F. Griesinger, et al. (2012). "Docetaxel-carboplatin chemotherapy combined with cetuximab in patients with locally advanced or metastatic non small-cell lung cancer (NSCLC)--results of the nonrandomised phase II study TaxErb." Lung Cancer **75**(3): 348-352.

Fragale, A., M. Tartaglia, et al. (2004). "Noonan syndrome-associated SHP2/PTPN11 mutants cause EGF-dependent prolonged GAB1 binding and sustained ERK2/MAPK1 activation." Hum Mutat **23**(3): 267-277.
Friedmann, B., M. Caplin, et al. (2004). "Modulation of DNA repair in vitro after treatment with chemotherapeutic agents by the epidermal growth factor receptor inhibitor gefitinib (ZD1839)." Clin Cancer Res **10**(19): 6476-6486.
Friedmann, B. J., M. Caplin, et al. (2006). "Interaction of the epidermal growth factor receptor and the DNA-dependent protein kinase pathway following gefitinib treatment." Mol Cancer Ther **5**(2): 209-218.
Fruhwirth, G. O., L. P. Fernandes, et al. (2011). "How Forster resonance energy transfer imaging improves the understanding of protein interaction networks in cancer biology." Chemphyschem **12**(3): 442-461.
Fry, D. W., A. J. Bridges, et al. (1998). "Specific, irreversible inactivation of the epidermal growth factor receptor and erbB2, by a new class of tyrosine kinase inhibitor." Proc Natl Acad Sci U S A **95**(20): 12022-12027.
Fukuoka, M., S. Yano, et al. (2003). "Multi-institutional randomized phase II trial of gefitinib for previously treated patients with advanced non-small-cell lung cancer (The IDEAL 1 Trial) [corrected]." J Clin Oncol **21**(12): 2237-2246.
Fury, M. G., A. Lipton, et al. (2008). "A phase-I trial of the epidermal growth factor receptor directed bispecific antibody MDX-447 without and with recombinant human granulocyte-colony stimulating factor in patients with advanced solid tumors." Cancer Immunol Immunother **57**(2): 155-163.
Garrett, J. T., M. G. Olivares, et al. (2011). "Transcriptional and posttranslational up-regulation of HER3 (ErbB3) compensates for inhibition of the HER2 tyrosine kinase." Proc Natl Acad Sci U S A **108**(12): 5021-5026.
Gasparri, F. (2009). "An overview of cell phenotypes in HCS: limitations and advantages." Expert Opin Drug Discov **4**(6): 643-657.
Gelovani, J. G. (2008). "Molecular imaging of epidermal growth factor receptor expression-activity at the kinase level in tumors with positron emission tomography." Cancer Metastasis Rev **27**(4): 645-653.
Gherardi, E., W. Birchmeier, et al. (2012). "Targeting MET in cancer: rationale and progress." Nat Rev Cancer **12**(2): 89-103.
Giordano, S., S. Corso, et al. (2002). "The semaphorin 4D receptor controls invasive growth by coupling with Met." Nat Cell Biol **4**(9): 720-724.
Giuliano, K. A., Y. T. Chen, et al. (2004). "High-content screening with siRNA optimizes a cell biological approach to drug discovery: defining the role of P53 activation in the cellular response to anticancer drugs." J Biomol Screen **9**(7): 557-568.
Gonzalez, J. E. and P. A. Negulescu (1998). "Intracellular detection assays for high-throughput screening." Curr Opin Biotechnol **9**(6): 624-631.
Gordon, A. N., J. T. Fleagle, et al. (2001). "Recurrent epithelial ovarian carcinoma: a randomized phase III study of pegylated liposomal doxorubicin versus topotecan." J Clin Oncol **19**(14): 3312-3322.
Goswami, S., E. Sahai, et al. (2005). "Macrophages promote the invasion of breast carcinoma cells via a colony-stimulating factor-1/epidermal growth factor paracrine loop." Cancer Res **65**(12): 5278-5283.

Gourlaouen, M., J. C. Welti, et al. (2013). "Essential role for endocytosis in the growth factor-stimulated activation of ERK1/2 in endothelial cells." J Biol Chem **288**(11): 7467-7480.
Graham, D. L., P. N. Lowe, et al. (2001). "A method to measure the interaction of Rac/Cdc42 with their binding partners using fluorescence resonance energy transfer between mutants of green fluorescent protein." Anal Biochem **296**(2): 208-217.
Grecco, H. E., P. Roda-Navarro, et al. (2010). "In situ analysis of tyrosine phosphorylation networks by FLIM on cell arrays." Nat Methods **7**(6): 467-472.
Gross, L. A., G. S. Baird, et al. (2000). "The structure of the chromophore within DsRed, a red fluorescent protein from coral." Proc Natl Acad Sci U S A **97**(22): 11990-11995.
Grosse, S. M., A. D. Tagalakis, et al. (2010). "Tumor-specific gene transfer with receptor-mediated nanocomplexes modified by polyethylene glycol shielding and endosomally cleavable lipid and peptide linkers." FASEB J **24**(7): 2301-2313.
Gu, J., Y. Sumida, et al. (2001). "Laminin-10/11 and fibronectin differentially regulate integrin-dependent Rho and Rac activation via p130(Cas)-CrkII-DOCK180 pathway." J Biol Chem **276**(29): 27090-27097.
Guo, A., J. Villen, et al. (2008). "Signaling networks assembled by oncogenic EGFR and c-Met." Proc Natl Acad Sci U S A **105**(2): 692-697.
Hadzisejdic, I., E. Mustac, et al. (2010). "Nuclear EGFR in ductal invasive breast cancer: correlation with cyclin-D1 and prognosis." Mod Pathol **23**(3): 392-403.
Haj, F. G., P. J. Verveer, et al. (2002). "Imaging sites of receptor dephosphorylation by PTP1B on the surface of the endoplasmic reticulum." Science **295**(5560): 1708-1711.
Hannon, G. J. (2002). "RNA interference." Nature **418**(6894): 244-251.
Hannon, G. J. and J. J. Rossi (2004). "Unlocking the potential of the human genome with RNA interference." Nature **431**(7006): 371-378.
Hayat, M. J., N. Howlader, et al. (2007). "Cancer statistics, trends, and multiple primary cancer analyses from the Surveillance, Epidemiology, and End Results (SEER) Program." Oncologist **12**(1): 20-37.
He, W., K. Gong, et al. (2005). "The N-terminal cytokine binding domain of LIFR is required for CNTF binding and signaling." FEBS Lett **579**(20): 4317-4323.
Heasman, S. J., L. M. Carlin, et al. (2010). "Coordinated RhoA signaling at the leading edge and uropod is required for T cell transendothelial migration." J Cell Biol **190**(4): 553-563.
Henriksen, L., M. V. Grandal, et al. (2013). "Internalization mechanisms of the epidermal growth factor receptor after activation with different ligands." PLoS One **8**(3): e58148.
Hsu, S. C., S. A. Miller, et al. (2009). "Nuclear EGFR is required for cisplatin resistance and DNA repair." Am J Transl Res **1**(3): 249-258.
Hudis, C. A. and L. Gianni (2011). "Triple-negative breast cancer: an unmet medical need." Oncologist **16 Suppl 1**: 1-11.
Hunter, K. W., N. P. Crawford, et al. (2008). "Mechanisms of metastasis." Breast Cancer Res **10 Suppl 1**: S2.

Hutchins, J. R., Y. Toyoda, et al. (2010). "Systematic analysis of human protein complexes identifies chromosome segregation proteins." Science **328**(5978): 593-599.
Inamura, K., H. Ninomiya, et al. (2010). "Is the epidermal growth factor receptor status in lung cancers reflected in clinicopathologic features?" Arch Pathol Lab Med **134**(1): 66-72.
Ingham, R. J., D. L. Krebs, et al. (1996). "B cell antigen receptor signaling induces the formation of complexes containing the Crk adapter proteins." J Biol Chem **271**(50): 32306-32314.
Inoue, A., K. Kobayashi, et al. (2009). "First-line gefitinib for patients with advanced non-small-cell lung cancer harboring epidermal growth factor receptor mutations without indication for chemotherapy." J Clin Oncol **27**(9): 1394-1400.
Irshad, S., P. Ellis, et al. (2011). "Molecular heterogeneity of triple-negative breast cancer and its clinical implications." Curr Opin Oncol **23**(6): 566-577.
Ishikawa, Y., J. Horiguchi, et al. (2011). "Triple-negative breast cancer: histological subtypes and immunohistochemical and clinicopathological features." Cancer Sci **102**(3): 656-662.
Itoh, R. E., K. Kurokawa, et al. (2005). "A FRET-based probe for epidermal growth factor receptor bound non-covalently to a pair of synthetic amphipathic helixes." Exp Cell Res **307**(1): 142-152.
Jogi, A., P. Persson, et al. (2002). "Modulation of basic helix-loop-helix transcription complex formation by Id proteins during neuronal differentiation." J Biol Chem **277**(11): 9118-9126.
Jorissen, R. N., F. Walker, et al. (2003). "Epidermal growth factor receptor: mechanisms of activation and signalling." Exp Cell Res **284**(1): 31-53.
Kang, Y., P. M. Siegel, et al. (2003). "A multigenic program mediating breast cancer metastasis to bone." Cancer Cell **3**(6): 537-549.
Kao, J., K. Salari, et al. (2009). "Molecular profiling of breast cancer cell lines defines relevant tumor models and provides a resource for cancer gene discovery." PLoS One **4**(7): e6146.
Karamouzis, M. V., P. A. Konstantinopoulos, et al. (2009). "Targeting MET as a strategy to overcome crosstalk-related resistance to EGFR inhibitors." Lancet Oncol **10**(7): 709-717.
Keane, M. M., S. A. Ettenberg, et al. (1999). "cbl-3: a new mammalian cbl family protein." Oncogene **18**(22): 3365-3375.
Kelleher, M. T., G. Fruhwirth, et al. (2009). "The potential of optical proteomic technologies to individualize prognosis and guide rational treatment for cancer patients." Target Oncol **4**(3): 235-252.
Keshava Prasad, T. S., R. Goel, et al. (2009). "Human Protein Reference Database--2009 update." Nucleic Acids Res **37**(Database issue): D767-772.
Kim, D. H. and J. J. Rossi (2007). "Strategies for silencing human disease using RNA interference." Nat Rev Genet **8**(3): 173-184.
Knowles, L. M., L. P. Stabile, et al. (2009). "HGF and c-Met participate in paracrine tumorigenic pathways in head and neck squamous cell cancer." Clin Cancer Res **15**(11): 3740-3750.

Kobashigawa, Y., M. Sakai, et al. (2007). "Structural basis for the transforming activity of human cancer-related signaling adaptor protein CRK." Nat Struct Mol Biol **14**(6): 503-510.
Kobayashi, K., S. Kuroda, et al. (1998). "p140Sra-1 (specifically Rac1-associated protein) is a novel specific target for Rac1 small GTPase." J Biol Chem **273**(1): 291-295.
Koike, M. (2002). "Dimerization, translocation and localization of Ku70 and Ku80 proteins." J Radiat Res **43**(3): 223-236.
Kolev, V., A. Mandinova, et al. (2008). "EGFR signalling as a negative regulator of Notch1 gene transcription and function in proliferating keratinocytes and cancer." Nat Cell Biol **10**(8): 902-911.
Krausz, E. (2007). "High-content siRNA screening." Mol Biosyst **3**(4): 232-240.
Krausz, E. and K. Korn (2008). "High-content siRNA screening for target identification and validation." Expert Opin Drug Discov **3**(5): 551-564.
Kudsiova, L., B. Fridrich, et al. (2011). "Lipopolyplex ternary delivery systems incorporating C14 glycerol-based lipids." Mol Pharm **8**(5): 1831-1847.
Kudsiova, L., J. Ho, et al. (2011). "Lipid chain geometry of C14 glycerol-based lipids: effect on lipoplex structure and transfection." Mol Biosyst **7**(2): 422-436.
Kumar, A., E. T. Petri, et al. (2008). "Structure and clinical relevance of the epidermal growth factor receptor in human cancer." J Clin Oncol **26**(10): 1742-1751.
Kunida, K., M. Matsuda, et al. (2012). "FRET imaging and statistical signal processing reveal positive and negative feedback loops regulating the morphology of randomly migrating HT-1080 cells." J Cell Sci **125**(Pt 10): 2381-2392.
Kurokawa, K., N. Mochizuki, et al. (2001). "A pair of fluorescent resonance energy transfer-based probes for tyrosine phosphorylation of the CrkII adaptor protein in vivo." J Biol Chem **276**(33): 31305-31310.
Lakowicz, J. R., Ed. (1999). Principles of fluorescence spectroscopy 2nd Edition Pages 429-432.
Lammers, T., F. Kiessling, et al. (2010). "Nanotheranostics and image-guided drug delivery: current concepts and future directions." Mol Pharm **7**(6): 1899-1912.
Landen, C. N., Jr., A. Chavez-Reyes, et al. (2005). "Therapeutic EphA2 gene targeting in vivo using neutral liposomal small interfering RNA delivery." Cancer Res **65**(15): 6910-6918.
Lawrie, T. A., A. Bryant, et al. (2013). "Pegylated liposomal doxorubicin for relapsed epithelial ovarian cancer." Cochrane Database Syst Rev **7**: CD006910.
Lemmon, M. A. and J. Schlessinger (2010). "Cell signaling by receptor tyrosine kinases." Cell **141**(7): 1117-1134.
Lenferink, A. E., R. Pinkas-Kramarski, et al. (1998). "Differential endocytic routing of homo- and hetero-dimeric ErbB tyrosine kinases confers signaling superiority to receptor heterodimers." EMBO J **17**(12): 3385-3397.
Lewis, C. E. and J. W. Pollard (2006). "Distinct role of macrophages in different tumor microenvironments." Cancer Res **66**(2): 605-612.
Lian, T. and R. J. Ho (2001). "Trends and developments in liposome drug delivery systems." J Pharm Sci **90**(6): 667-680.

Liang, J. C., A. L. Chang, et al. (2012). "A high-throughput, quantitative cell-based screen for efficient tailoring of RNA device activity." Nucleic Acids Res **40**(20): e154.
Liccardi, G., J. A. Hartley, et al. (2011). "EGFR nuclear translocation modulates DNA repair following cisplatin and ionizing radiation treatment." Cancer Res **71**(3): 1103-1114.
Liska, D., C. T. Chen, et al. (2011). "HGF rescues colorectal cancer cells from EGFR inhibition via MET activation." Clin Cancer Res **17**(3): 472-482.
Liu, L., H. Shi, et al. (2011). "Synergistic effects of foretinib with HER-targeted agents in MET and HER1- or HER2-coactivated tumor cells." Mol Cancer Ther **10**(3): 518-530.
Lo, H. W., X. Cao, et al. (2010). "Cyclooxygenase-2 is a novel transcriptional target of the nuclear EGFR-STAT3 and EGFRvIII-STAT3 signaling axes." Mol Cancer Res **8**(2): 232-245.
Lynch, T. J., D. W. Bell, et al. (2004). "Activating mutations in the epidermal growth factor receptor underlying responsiveness of non-small-cell lung cancer to gefitinib." N Engl J Med **350**(21): 2129-2139.
Makrogianneli, K., L. M. Carlin, et al. (2009). "Integrating receptor signal inputs that influence small Rho GTPase activation dynamics at the immunological synapse." Mol Cell Biol **29**(11): 2997-3006.
Malvezzi, M., A. Arfe, et al. (2011). "European cancer mortality predictions for the year 2011." Ann Oncol **22**(4): 947-956.
Marmor, M. D. and Y. Yarden (2004). "Role of protein ubiquitylation in regulating endocytosis of receptor tyrosine kinases." Oncogene **23**(11): 2057-2070.
Marquez, A., R. Wu, et al. (2004). "Evaluation of epidermal growth factor receptor (EGFR) by chromogenic in situ hybridization (CISH) and immunohistochemistry (IHC) in archival gliomas using bright-field microscopy." Diagn Mol Pathol **13**(1): 1-8.
Martinez, J. J., S. Seveau, et al. (2005). "Ku70, a component of DNA-dependent protein kinase, is a mammalian receptor for Rickettsia conorii." Cell **123**(6): 1013-1023.
Maruyama, K. (2002). "PEG-immunoliposome." Biosci Rep **22**(2): 251-266.
Matthews, D. R., G. O. Fruhwirth, et al. (2012). "A multi-functional imaging approach to high-content protein interaction screening." PLoS One **7**(4): e33231.
Mattila, E., T. Pellinen, et al. (2005). "Negative regulation of EGFR signalling through integrin-alpha1beta1-mediated activation of protein tyrosine phosphatase TCPTP." Nat Cell Biol **7**(1): 78-85.
McGill, M. A. and C. J. McGlade (2003). "Mammalian numb proteins promote Notch1 receptor ubiquitination and degradation of the Notch1 intracellular domain." J Biol Chem **278**(25): 23196-23203.
Medina, O. P., N. Pillarsetty, et al. (2011). "Optimizing tumor targeting of the lipophilic EGFR-binding radiotracer SKI 243 using a liposomal nanoparticle delivery system." J Control Release **149**(3): 292-298.
Medley, Q. G., C. Serra-Pages, et al. (2000). "The trio guanine nucleotide exchange factor is a RhoA target. Binding of RhoA to the trio immunoglobulin-like domain." J Biol Chem **275**(46): 36116-36123.

Minn, A. J., G. P. Gupta, et al. (2005). "Genes that mediate breast cancer metastasis to lung." Nature **436**(7050): 518-524.
Minn, A. J., Y. Kang, et al. (2005). "Distinct organ-specific metastatic potential of individual breast cancer cells and primary tumors." J Clin Invest **115**(1): 44-55.
Modi, S., G. D'Andrea, et al. (2006). "A phase I study of cetuximab/paclitaxel in patients with advanced-stage breast cancer." Clin Breast Cancer **7**(3): 270-277.
Mok, T. S., Y. L. Wu, et al. (2009). "Gefitinib or carboplatin-paclitaxel in pulmonary adenocarcinoma." N Engl J Med **361**(10): 947-957.
Morris, K. V. (2005). "siRNA-mediated transcriptional gene silencing: the potential mechanism and a possible role in the histone code." Cell Mol Life Sci **62**(24): 3057-3066.
Mueller, K. L., L. A. Hunter, et al. (2008). "Met and c-Src cooperate to compensate for loss of epidermal growth factor receptor kinase activity in breast cancer cells." Cancer Res **68**(9): 3314-3322.
Mueller, K. L., Z. Q. Yang, et al. (2010). "EGFR/Met association regulates EGFR TKI resistance in breast cancer." J Mol Signal **5**: 8.
Mustapa, M. F., P. C. Bell, et al. (2007). "Biophysical characterization of an integrin-targeted lipopolyplex gene delivery vector." Biochemistry **46**(45): 12930-12944.
Mustapa, M. F., S. M. Grosse, et al. (2009). "Stabilized integrin-targeting ternary LPD (lipopolyplex) vectors for gene delivery designed to disassemble within the target cell." Bioconjug Chem **20**(3): 518-532.
Nakajima, M., H. Sawada, et al. (1999). "The prognostic significance of amplification and overexpression of c-met and c-erb B-2 in human gastric carcinomas." Cancer **85**(9): 1894-1902.
Nakamura, T., S. Muraoka, et al. (1998). "N-Shc and Sck, two neuronally expressed Shc adapter homologs. Their differential regional expression in the brain and roles in neurotrophin and Src signaling." J Biol Chem **273**(12): 6960-6967.
Nakamura, T., R. Sanokawa, et al. (1996). "N-Shc: a neural-specific adapter molecule that mediates signaling from neurotrophin/Trk to Ras/MAPK pathway." Oncogene **13**(6): 1111-1121.
Neumann, B., T. Walter, et al. (2010). "Phenotypic profiling of the human genome by time-lapse microscopy reveals cell division genes." Nature **464**(7289): 721-727.
Nielsen, T. O., F. D. Hsu, et al. (2004). "Immunohistochemical and clinical characterization of the basal-like subtype of invasive breast carcinoma." Clin Cancer Res **10**(16): 5367-5374.
Nishihara, H., M. Maeda, et al. (2002). "DOCK2 associates with CrkL and regulates Rac1 in human leukemia cell lines." Blood **100**(12): 3968-3974.
Nishioka, T., M. A. Frohman, et al. (2010). "Heterogeneity of phosphatidic acid levels and distribution at the plasma membrane in living cells as visualized by a Foster resonance energy transfer (FRET) biosensor." J Biol Chem **285**(46): 35979-35987.
Noble, C. O., D. B. Kirpotin, et al. (2004). "Development of ligand-targeted liposomes for cancer therapy." Expert Opin Ther Targets **8**(4): 335-353.

Normanno, N., A. De Luca, et al. (2006). "Epidermal growth factor receptor (EGFR) signaling in cancer." Gene **366**(1): 2-16.
Olayioye, M. A., R. M. Neve, et al. (2000). "The ErbB signaling network: receptor heterodimerization in development and cancer." EMBO J **19**(13): 3159-3167.
Paez, J. G., P. A. Janne, et al. (2004). "EGFR mutations in lung cancer: correlation with clinical response to gefitinib therapy." Science **304**(5676): 1497-1500.
Pal, A., A. Glekas, et al. (2006). "Molecular imaging of EGFR kinase activity in tumors with 124I-labeled small molecular tracer and positron emission tomography." Mol Imaging Biol **8**(5): 262-277.
Pao, W., V. Miller, et al. (2004). "EGF receptor gene mutations are common in lung cancers from "never smokers" and are associated with sensitivity of tumors to gefitinib and erlotinib." Proc Natl Acad Sci U S A **101**(36): 13306-13311.
Pao, W. and V. A. Miller (2005). "Epidermal growth factor receptor mutations, small-molecule kinase inhibitors, and non-small-cell lung cancer: current knowledge and future directions." J Clin Oncol **23**(11): 2556-2568.
Park, S. and H. S. Yoo (2010). "In vivo and in vitro anti-cancer activities and enhanced cellular uptakes of EGF fragment decorated doxorubicin nano-aggregates." Int J Pharm **383**(1-2): 178-185.
Patel, G. S., F. Autore, A. Cameron, J. Claus, G. Weitsman, P. R. Barber, B. Vojnovic, T. Kiuchi, G. Fruhwirth, E. Ortiz-Zapater, Y. Yarden, P. A. Ellis, P. J. Parker, T. Ng and F. Fraternali (2013). Lapatinib requires a functional HER3 nucleotide binding pocket to promote a HER2:HER3 symmetric dimer linked to treatment resistance. Proc Natl Acad Sci U S A submitted.
Paulsen, C. E., T. H. Truong, et al. (2012). "Peroxide-dependent sulfenylation of the EGFR catalytic site enhances kinase activity." Nat Chem Biol **8**(1): 57-64.
Pedersen, M. W., M. Meltorn, et al. (2001). "The type III epidermal growth factor receptor mutation. Biological significance and potential target for anti-cancer therapy." Ann Oncol **12**(6): 745-760.
Peeters, M., J. Y. Douillard, et al. (2013). "Mutant KRAS codon 12 and 13 alleles in patients with metastatic colorectal cancer: assessment as prognostic and predictive biomarkers of response to panitumumab." J Clin Oncol **31**(6): 759-765.
Peeters, M., T. J. Price, et al. (2010). "Randomized phase III study of panitumumab with fluorouracil, leucovorin, and irinotecan (FOLFIRI) compared with FOLFIRI alone as second-line treatment in patients with metastatic colorectal cancer." J Clin Oncol **28**(31): 4706-4713.
Perez-Soler, R., A. Chachoua, et al. (2004). "Determinants of tumor response and survival with erlotinib in patients with non--small-cell lung cancer." J Clin Oncol **22**(16): 3238-3247.
Perou, C. M., T. Sorlie, et al. (2000). "Molecular portraits of human breast tumours." Nature **406**(6797): 747-752.
Peter, M. and S. M. Ameer-Beg (2004). "Imaging molecular interactions by multiphoton FLIM." Biol Cell **96**(3): 231-236.
Peter, M., S. M. Ameer-Beg, et al. (2005). "Multiphoton-FLIM quantification of the EGFP-mRFP1 FRET pair for localization of membrane receptor-kinase interactions." Biophys J **88**(2): 1224-1237.
Piston, D. W. and G. J. Kremers (2007). "Fluorescent protein FRET: the good, the bad and the ugly." Trends Biochem Sci **32**(9): 407-414.

Pollard, J. W. (2008). "Macrophages define the invasive microenvironment in breast cancer." J Leukoc Biol **84**(3): 623-630.
Prabhakar, B. S., G. P. Allaway, et al. (1990). "Cell surface expression of the 70-kD component of Ku, a DNA-binding nuclear autoantigen." J Clin Invest **86**(4): 1301-1305.
Prabhakar, U., H. Maeda, et al. (2013). "Challenges and key considerations of the enhanced permeability and retention effect for nanomedicine drug delivery in oncology." Cancer Res **73**(8): 2412-2417.
Qian, B. Z. and J. W. Pollard (2010). "Macrophage diversity enhances tumor progression and metastasis." Cell **141**(1): 39-51.
Reinehr, R., F. Schliess, et al. (2003). "Hyperosmolarity and CD95L trigger CD95/EGF receptor association and tyrosine phosphorylation of CD95 as prerequisites for CD95 membrane trafficking and DISC formation." FASEB J **17**(6): 731-733.
Reis-Filho, J. S., F. Milanezi, et al. (2006). "Metaplastic breast carcinomas are basal-like tumours." Histopathology **49**(1): 10-21.
Reynolds, A. R., C. Tischer, et al. (2003). "EGFR activation coupled to inhibition of tyrosine phosphatases causes lateral signal propagation." Nat Cell Biol **5**(5): 447-453.
Robinson, B. D. and J. G. Jones (2009). "Tumor microenvironment of metastasis (TMEM): a novel tissue-based assay for metastatic risk in breast cancer." Future Oncol **5**(7): 919-921.
Robinson, B. D., G. L. Sica, et al. (2009). "Tumor microenvironment of metastasis in human breast carcinoma: a potential prognostic marker linked to hematogenous dissemination." Clin Cancer Res **15**(7): 2433-2441.
Roskoski, R., Jr. (2004). "The ErbB/HER receptor protein-tyrosine kinases and cancer." Biochem Biophys Res Commun **319**(1): 1-11.
Rual, J. F., K. Venkatesan, et al. (2005). "Towards a proteome-scale map of the human protein-protein interaction network." Nature **437**(7062): 1173-1178.
Saltz, L. B., N. J. Meropol, et al. (2004). "Phase II trial of cetuximab in patients with refractory colorectal cancer that expresses the epidermal growth factor receptor." J Clin Oncol **22**(7): 1201-1208.
Scaltriti, M., C. Verma, et al. (2009). "Lapatinib, a HER2 tyrosine kinase inhibitor, induces stabilization and accumulation of HER2 and potentiates trastuzumab-dependent cell cytotoxicity." Oncogene **28**(6): 803-814.
Schiemann, W. P., J. L. Bartoe, et al. (1997). "Box 3-independent signaling mechanisms are involved in leukemia inhibitory factor receptor alpha- and gp130-mediated stimulation of mitogen-activated protein kinase. Evidence for participation of multiple signaling pathways which converge at Ras." J Biol Chem **272**(26): 16631-16636.
Schmidt, M. H., I. Dikic, et al. (2005). "Src phosphorylation of Alix/AIP1 modulates its interaction with binding partners and antagonizes its activities." J Biol Chem **280**(5): 3414-3425.
Schmidt, M. H., D. Hoeller, et al. (2004). "Alix/AIP1 antagonizes epidermal growth factor receptor downregulation by the Cbl-SETA/CIN85 complex." Mol Cell Biol **24**(20): 8981-8993.
Schneider-Schaulies, J., L. M. Dunster, et al. (1995). "Physical association of moesin and CD46 as a receptor complex for measles virus." J Virol **69**(4): 2248-2256.

Serebriiskii, I. G., O. Mitina, et al. (2002). "Detection of peptides, proteins, and drugs that selectively interact with protein targets." Genome Res **12**(11): 1785-1791.
Sergina, N. V., M. Rausch, et al. (2007). "Escape from HER-family tyrosine kinase inhibitor therapy by the kinase-inactive HER3." Nature **445**(7126): 437-441.
Shannon, P., A. Markiel, et al. (2003). "Cytoscape: a software environment for integrated models of biomolecular interaction networks." Genome Res **13**(11): 2498-2504.
Sharpe, R., A. Pearson, et al. (2011). "FGFR signaling promotes the growth of triple-negative and basal-like breast cancer cell lines both in vitro and in vivo." Clin Cancer Res **17**(16): 5275-5286.
Shattuck, D. L., J. K. Miller, et al. (2008). "Met receptor contributes to trastuzumab resistance of Her2-overexpressing breast cancer cells." Cancer Res **68**(5): 1471-1477.
Shepherd, F. A., J. Rodrigues Pereira, et al. (2005). "Erlotinib in previously treated non-small-cell lung cancer." N Engl J Med **353**(2): 123-132.
Shia, J., D. S. Klimstra, et al. (2005). "Epidermal growth factor receptor expression and gene amplification in colorectal carcinoma: an immunohistochemical and chromogenic in situ hybridization study." Mod Pathol **18**(10): 1350-1356.
Smyth, L. A. and H. J. Brady (2005). "cMet and Fas receptor interaction inhibits death-inducing signaling complex formation in endothelial cells." Hypertension **46**(1): 100-106.
Sofou, S. and G. Sgouros (2008). "Antibody-targeted liposomes in cancer therapy and imaging." Expert Opin Drug Deliv **5**(2): 189-204.
Somia, N. and I. M. Verma (2000). "Gene therapy: trials and tribulations." Nat Rev Genet **1**(2): 91-99.
Somlo, G., C. L. Martel, et al. (2012). "A phase I/II prospective, single arm trial of gefitinib, trastuzumab, and docetaxel in patients with stage IV HER-2 positive metastatic breast cancer." Breast Cancer Res Treat **131**(3): 899-906.
Soong, J. and G. Scott (2013). "Plexin B1 inhibits MET through direct association and regulates Shp2 expression in melanocytes." J Cell Sci **126**(Pt 2): 688-695.
Sorkin, A. and L. K. Goh (2009). "Endocytosis and intracellular trafficking of ErbBs." Exp Cell Res **315**(4): 683-696.
Statistics. (2011). "Mortality Statistics: Deaths Registered in 2010 (Series DR) Table 5. *Office for National Statistics*."
Statistics. (2013). "Geographic Patterns of Cancer Survival in England: Patients followed up to 2011. *Office for National Statistics*."
Stelzl, U., U. Worm, et al. (2005). "A human protein-protein interaction network: a resource for annotating the proteome." Cell **122**(6): 957-968.
Sugio, K., H. Uramoto, et al. (2009). "Prospective phase II study of gefitinib in non-small cell lung cancer with epidermal growth factor receptor gene mutations." Lung Cancer **64**(3): 314-318.
Swiercz, J. M., T. Worzfeld, et al. (2008). "ErbB-2 and met reciprocally regulate cellular signaling via plexin-B1." J Biol Chem **283**(4): 1893-1901.
Takino, T., M. Tamura, et al. (2003). "Tyrosine phosphorylation of the CrkII adaptor protein modulates cell migration." J Cell Sci **116**(Pt 15): 3145-3155.
Toft, D. J. and V. L. Cryns (2011). "Minireview: Basal-like breast cancer: from molecular profiles to targeted therapies." Mol Endocrinol **25**(2): 199-211.

Tomic, S., U. Greiser, et al. (1995). "Association of SH2 domain protein tyrosine phosphatases with the epidermal growth factor receptor in human tumor cells. Phosphatidic acid activates receptor dephosphorylation by PTP1C." J Biol Chem **270**(36): 21277-21284.

Tonks, N. K. (2006). "Protein tyrosine phosphatases: from genes, to function, to disease." Nat Rev Mol Cell Biol **7**(11): 833-846.

Torchilin, V. P. (2005). "Recent advances with liposomes as pharmaceutical carriers." Nat Rev Drug Discov **4**(2): 145-160.

Tortora, G., V. Damiano, et al. (1997). "The RIalpha subunit of protein kinase A (PKA) binds to Grb2 and allows PKA interaction with the activated EGF-receptor." Oncogene **14**(8): 923-928.

Truong, T. H. and K. S. Carroll (2012). "Redox regulation of epidermal growth factor receptor signaling through cysteine oxidation." Biochemistry **51**(50): 9954-9965.

Trusolino, L., A. Bertotti, et al. (2010). "MET signalling: principles and functions in development, organ regeneration and cancer." Nat Rev Mol Cell Biol **11**(12): 834-848.

Van Cutsem, E., C. H. Kohne, et al. (2009). "Cetuximab and chemotherapy as initial treatment for metastatic colorectal cancer." N Engl J Med **360**(14): 1408-1417.

van de Vijver, M. J., Y. D. He, et al. (2002). "A gene-expression signature as a predictor of survival in breast cancer." N Engl J Med **347**(25): 1999-2009.

Varga, C. M., T. J. Wickham, et al. (2000). "Receptor-mediated targeting of gene delivery vectors: insights from molecular mechanisms for improved vehicle design." Biotechnol Bioeng **70**(6): 593-605.

Vaupel, P. and L. Harrison (2004). "Tumor hypoxia: causative factors, compensatory mechanisms, and cellular response." Oncologist **9 Suppl 5**: 4-9.

Vuoriluoto, K., H. Haugen, et al. (2011). "Vimentin regulates EMT induction by Slug and oncogenic H-Ras and migration by governing Axl expression in breast cancer." Oncogene **30**(12): 1436-1448.

Wagner, R. W. (1994). "Gene inhibition using antisense oligodeoxynucleotides." Nature **372**(6504): 333-335.

Wallrabe, H. and A. Periasamy (2005). "Imaging protein molecules using FRET and FLIM microscopy." Curr Opin Biotechnol **16**(1): 19-27.

Wang, Y. N., H. Yamaguchi, et al. (2010). "The translocon Sec61beta localized in the inner nuclear membrane transports membrane-embedded EGF receptor to the nucleus." J Biol Chem **285**(49): 38720-38729.

Wouters, F. S., P. J. Verveer, et al. (2001). "Imaging biochemistry inside cells." Trends Cell Biol **11**(5): 203-211.

Yang, X. D., X. C. Jia, et al. (2001). "Development of ABX-EGF, a fully human anti-EGF receptor monoclonal antibody, for cancer therapy." Crit Rev Oncol Hematol **38**(1): 17-23.

Yarden, Y. (2001). "The EGFR family and its ligands in human cancer. signalling mechanisms and therapeutic opportunities." Eur J Cancer **37 Suppl 4**: S3-8.

Yeung, M. L., Y. Bennasser, et al. (2005). "siRNA, miRNA and HIV: promises and challenges." Cell Res **15**(11-12): 935-946.

Yezhelyev, M. V., X. Gao, et al. (2006). "Emerging use of nanoparticles in diagnosis and treatment of breast cancer." Lancet Oncol **7**(8): 657-667.

Yoshizaki, H., K. Aoki, et al. (2006). "Regulation of RalA GTPase by phosphatidylinositol 3-kinase as visualized by FRET probes." Biochem Soc Trans **34**(Pt 5): 851-854.

Yoshizaki, H., N. Mochizuki, et al. (2007). "Akt-PDK1 complex mediates epidermal growth factor-induced membrane protrusion through Ral activation." Mol Biol Cell **18**(1): 119-128.

Yoshizaki, H., Y. Ohba, et al. (2003). "Activity of Rho-family GTPases during cell division as visualized with FRET-based probes." J Cell Biol **162**(2): 223-232.

Yuan, F., M. Dellian, et al. (1995). "Vascular permeability in a human tumor xenograft: molecular size dependence and cutoff size." Cancer Res **55**(17): 3752-3756.

Zhang, E. Z., J. G. Laufer, et al. (2009). "In vivo high-resolution 3D photoacoustic imaging of superficial vascular anatomy." Phys Med Biol **54**(4): 1035-1046.

Zhu, K., B. Debreceni, et al. (2000). "Identification of Rho GTPase-dependent sites in the Dbl homology domain of oncogenic Dbl that are required for transformation." J Biol Chem **275**(34): 25993-26001.

Reference for Appendix

---

[i] Christopher A. Hurley, John B. Wong, Jimmy Ho, Michele Writer, Scott A. Irvine, Jayne Lawrence, Stephen L. Hart, Alethea B. Tabor and Helen C. Hailes; *Org. Biomol. Chem.*; 2008; 6; 2554–2559.

[ii] Christopher A. Hurley, John B. Wong, Helen C. Hailes, and Alethea B. Tabor; *J. Org. Chem.*; 2004; 69; 980-983.